DEVELOPMENT OF A SIMPLIFIED MODEL FOR A REINFORCED SQUARE HOLLOW SECTION (SHS) T-JOINT FOR STRESS EVALUATION IN BUS SUPERSTRUCTURES

THANAKORN VICHIENSAMUTH

A THESIS SUBMITTED IN PARTIAL FULFILLMENT

OF THE REQUIREMENT FOR THE DEGREE OF

MASTER OF ENGINEERING IN AUTOMOTIVE ENGINEERING

(INTERNATIONAL PROGRAM)

INTERNATIONAL COLLEGE

KING MONGKUT'S INSTITUTE OF TECHNOLOGY LADKRABANG

2013

KMITL-2013-IC-M-004-004

Thesis Title	Devolopement of a Simplified Model for a Reinforced Square Hollow Section (SHS) T-Joint for Stress Evaluation in Bus Superstructures
Student	Mr. Thanakorn Vichiensamuth
Student ID.	52600910
Degree	Master of Engineering
Program	Automotive Engineering (International Program)
Year	2013
Thesis Advisor	Asst. Prof. Dr. Monsak Pimsarn Prof. Kunio Takahashi Dr. Tanakorn Tantanawat

ABSTRACT

This study aims to create a simplified model of a reinforced square hollow section (SHS) T-joint found in bus superstructures. The approach is to use a combination of one- and two-dimensional finite element models to represent a reference three-dimensional finite element (solid) model of the joint and determine stress correction factors (K_f) as functions of the geometrical variables of the joint. This approach requires the stiffness of the simplified model to be equivalent to the stiffness of the reference solid element model. The stiffness error function was, therefore, defined as an index that represents the deviation of the simplified model's stiffness from the reference model's stiffness. Four types of trial models, namely Model A, Model B, Model C, and Model D were then investigated at various values of SHS beam width and SHS beam thickness, forming a 3-factor Design of Experiment (DOE). The stiffness errors were computed for the experiment. Analysis of Variance (ANOVA) was then applied to evaluate the significance difference of the stiffness errors due to the effect of each factor. The results showed with 95% confidence interval that model type, as well as SHS beam width and SHS beam thickness, had a significant effect on the stiffness error. In addition, when each pair of model types were used in the analysis, it was found that the stiffness errors from Model A were significantly different from those of Model B, Model C, and Model D. However, the stiffness errors from Model B, Model C, and Model D were not significantly different. To complete the

study, Model B, was chosen as a selected geometric model since it provided the minimum average stiffness error. The stress correction factors, relating the maximum stress in the selected geometric model to the maximum stress in the reference solid element model, were then determined under static in-plane load. Since the maximum stress is assumed to be at the weld toe where structural discontinuity exists, the maximum stresses on both selected model and reference solid model were evaluated based on a hot spot stress (HSS) method. The dimension 60-30 mm width and 5-2 mm thickness of SHS were studied. The stress correction factors as functions of the thickness-to-width ratio of the joint were constructed by polynomial regression model for tension, bending, and moment load. The regression equations provide correlation coefficients that show a good relationship between the stress correction factors and the thickness-to-width ratio of the joint. The t score calculated by correlation coefficient ($t > t_{cri}$) confirmed the significance of the relationship. In case of combined load, the stress correction factors and unit load stresses were evaluated as surface fitting in order to evaluate the load-to-stress factors presented as a parametric equations based on superposition concept. The selected model with equivalent stiffness and equivalent stress is called a simplified model. The simplified model provided the stress error less than Model A, which is usually applied in the bus superstructure stress analysis. The resulting simplified model allows the stress evaluation on the bus superstructures to be done more quickly compared to a solid model while maintaining the accuracy of the solutions. Consequently, the designs of bus superstructures can be explored more thoroughly, leading to a better design.

ACKNOWLEDGEMENT

This thesis could not be completed without the assistance of many persons to whom I would like to express my sincere appreciation.

First, I would like to express my gratitude to my advisor, Dr.Tanakorn Tantanawat for the advice and guideline to complete my thesis. I would also like to sincerely thank Asst. Prof. Dr. Monsak Pimsam for kind advising and helping, and Prof.Kunio Takahashi for the suggestion of this thesis.

I would like to thank Thailand Advanced Institute of Science and Technology and Tokyo Institute of Technology (TAIST Tokyo Tech) which is a collaboration of National Science and Technology Development Agency, Thailand (NSTDA), Tokyo Institute of Technology, Japan, and King Mongkut's Institute of Technology Ladkrabang, Thailand, to provide the full scholarship.

Furthermore, I would like to thank staffs in Computer Aided Research Unit (CARU) of NSTDA, Miss. Rattanasuda Naewngerndee for her help, Mr.Sedthawatt Sucharitpwatskul to give me knowledge and suggestions to complete my thesis.

Finally, I would like to thank all of my beloved family, my father, my mother and my sister for all love, caring, understand and motivation throughout my life.

July 4, 2013

Thanakorn Vichiensamuth

TABLE OF CONTENTS

LIST OF TABLES

LIST OF TABLES

Table **Page**

LIST OF FIGURES

Figure **Page**

LIST OF FIGURES

LIST OF FIGURES

Figure **Page**

LIST OF FIGURES

Figure **Page**

CHAPTER 1

INTRODUCTION

1.1 Background and Motivation

Thailand is a country which is famous in tourism. There are a lot of sightseeing places such as waterfalls, beaches, and historical attractions located in many provinces. Both Thai and foreigner tourists are interested in travelling in Thailand to discover new experiences and good memories. As tourism industry grows up rapidly, the number of transportation services increases to support the industry. Bus is one of several choices of transportation services that tourist may choose. Although bus is a huge vehicle, it is economical and easy to access many areas. In addition, a lot of public and private bus services available in many provinces in Thailand. Thus, bus services have become popular for tourists. According to Thailand's department of land transport [1], the numbers of registered buses in year 2010-2012 are plotted in Figure 1.1. It is seen that the number of the registered buses tends to increase in last three years.

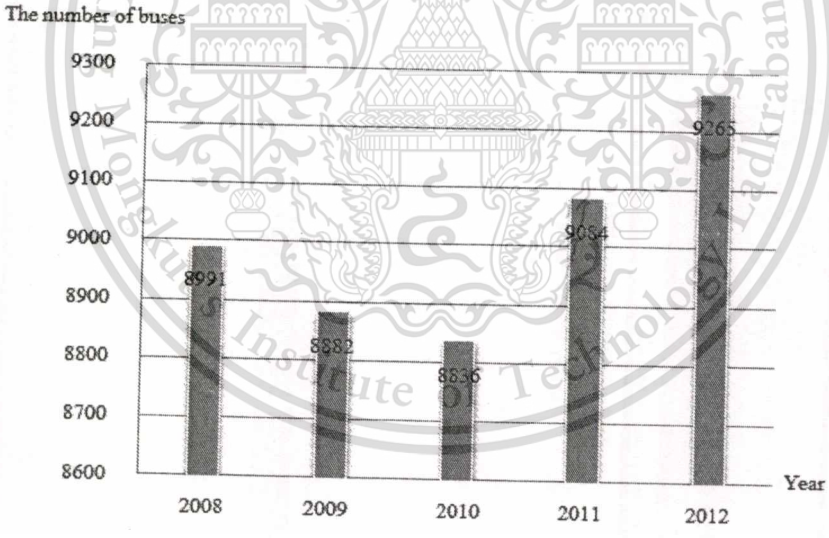

Figure 1.1 The number of registered buses in year 2010-2012.

Most buses in Thailand are assembled in the country although some parts such as chassis, engines are imported from aboard. Because the demand of bus service is increasing, bus making industry is now growing up in Thailand. A number of bus makers are located in different

provinces such as Chonburi, Ratchaburi and Nakornratchasima. Many of them design and build superstructure based on their long experience and expertise. The challenge that all bus makers are facing is to design the superstructure that has sufficient strength in order to ensure the safety of passengers while having minimal weight in order to stay competitive in terms of product cost and fuel consumption.

Bus superstructure needs to be improved in terms of safety and economy, but the experiences without engineering knowledge limit the continuous improvement of the design. Thus, engineering knowledge needs to be applied in order to increase the effectiveness of the bus superstructure design process. Computer Aided Design (CAD) and Computer Aided Engineering (CAE) are ones of the tools that can be used to evaluate stresses on the bus superstructure under several loading conditions. These tools can promote design exploration, leading to continuous improvement of the design.

Different types of joints are used to assemble various forms of structural steels in the bus superstructure. Welding is a jointing technique to assemble those steels. The strength of joint can be decreased because of some defects due to welding process. In case that the effects of weld defects are ignored, the strength of joints can be increased by reinforcements. Those reinforcements are commonly applied to a number of joints in bus superstructures to increase the stiffness of the structure but they are usually ignored in a stress analysis. Joints in bus superstructures may be reinforced by various means. Some joints may be reinforced by steel plates as shown in Figure 1.2.

Figure 1.2 Plate steel reinforcement.

One of interesting means to reinforce the joints is to use a hollow square beam to reinforce square hollow section (SHS) T-joint as shown in Figure 1.3. A hollow square beam is cut to a right angle and then assembled to the SHS T-joint by welding process. Higher load-taking capability is an advantage of this kind of reinforcement over the plate reinforcement. This kind of reinforced joint was found at the rare of the bus superstructure where the primary load is from the bus engine. However, it was found in actual bus superstructure that the failure occurred at the reinforced SHS T-joint. Thus, the reinforced SHS T-joint has to be considered for the stress analysis. Although the current CAD/CAE systems can be applied directly to model this joint, such application leads to intensive computing and resources, making it difficult to explore a number of joint designs. This work aims to create a simplified model to represent the behavior of the reinforced SHS T-joint in the bus superstructure. This simplified model can be applied in the bus superstructure design process and remove its limitation found when applying CAD/CAE system directly.

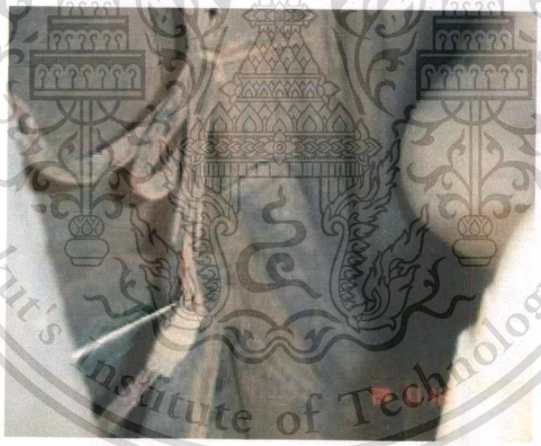

Figure 1.3 Reinforce square hollow section (SHS) T-joint.

1.2 Literature Reviews

Nowadays, Finite element analysis is one of tools for design and analysis of structures in engineering filed. Mohd Aishahruddin Bin Longgo [2] studied bridge decks by using finite element analysis. The behaviors of beam, shell, and solid element model were compared to determine the economical model. The result shows that those beam and shell element models are easier to use and able to provide the necessary parameters for design purpose and more acceptable

results compared to solid element model. Therefore, Manokruang et al. [3] applied a wireframe, which consists of one-dimensional finite elements (beam elements) as shown in Figure 1.4 a) to redesign a bus superstructure under static loading condition. Figure 1.4 b) shows cross-sectional properties of structural beam that have to be specified for beam elements in bus superstructure design process. Finite element analysis using wireframe benefits manufacturing process by reducing cost, fuel consumption, material usage, and product lead time.

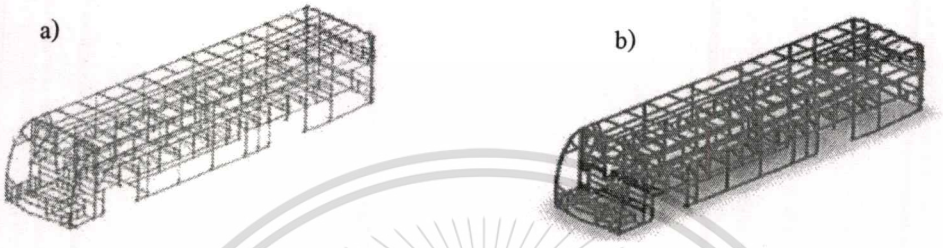

Figure 1.4 a) The bus superstructure modeling using wireframe; b) Applied profile (Manokruang et al., 2009).

The most dangerous bus accident is rollover causing the deformed bus superstructure to penetrate into the passenger compartment. Thus, the strength of the superstructure has to be sufficient in order to ensure the safety of passengers. The reinforcements are applied in order to increase the strength of joints. As a result, the strength of the superstructure increases. The effects of the reinforcement on the bus superstructure are studied. Yu Cheng Lin et al. [4] optimized the bus superstructure including the thicknesses of frame and add some reinforcements under rollover test as shown in Figure 1.5 and Figure1.6. Finite element analysis was applied for the optimization by using shell element model. It was found that the deformation of bus superstructure could be reduced 50% while only increasing 2% of weight by using the optimization analysis method. The applied reinforcements are important to reduce the weight of bus superstructure while the strength is increasing in the designs. Although the reinforcement applied in the model, the computer required more potential and time in the finite element analysis. Thus, those reinforcements are generally not applied in the analysis. In addition, it is complicated to model the reinforcements because they are applied to a number of joints in bus superstructures.

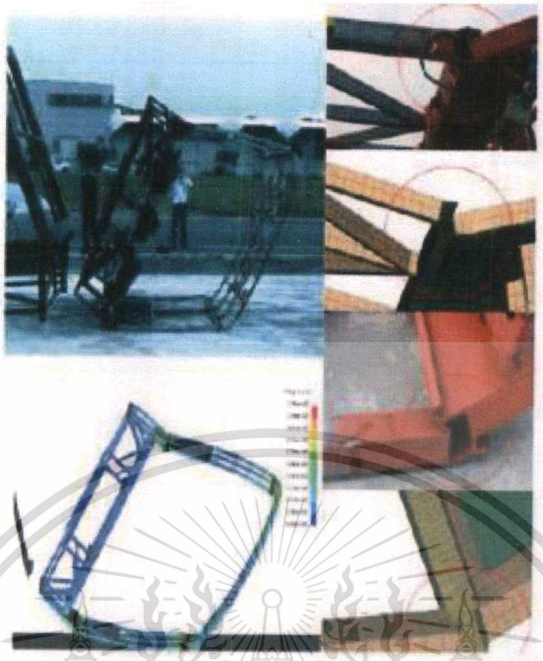

Figure 1.5 The final deformed shape (Yu Cheng Lin et al., 2005).

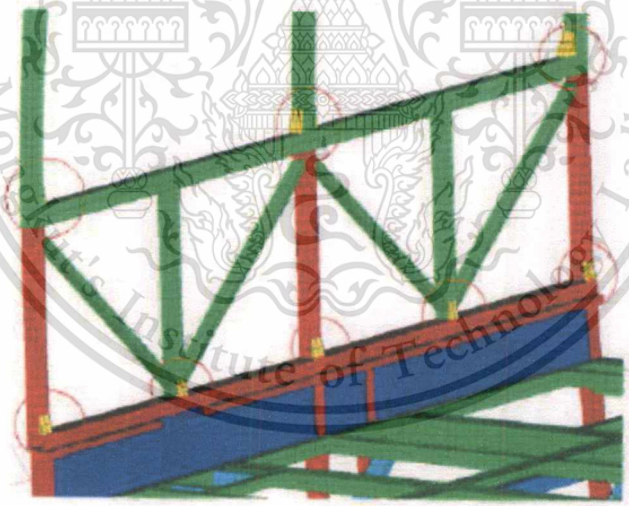

Figure 1.6 The reinforcement applied in the bus structure (Yu Cheng Lin et al., 2005).

Figure 1.7 shows various forms of structural steels, such as hollow square beam, I-beam, C-beam, and plates, normally used in the bus superstructure in order to reduce the bus superstructure weight. The weight reduction helps the bus makers to stay competitive in terms of product cost and fuel consumption. Different types of joints are used to assemble those structural steels.

Welding is the jointing technique widely used in the fabrication of the bus superstructure. Even if the welding process is perfectly controlled, the strength of the structure at welded joint areas are decreased. Radaj [5] shown that peculiarities such as inhomogeneous material, welding residual stress, and weld geometry cause strength reduction in welded joints. Those peculiarities affect on local stress occurred in the welded joints. It is difficult to evaluate stresses of those weld joints on the bus superstructure.

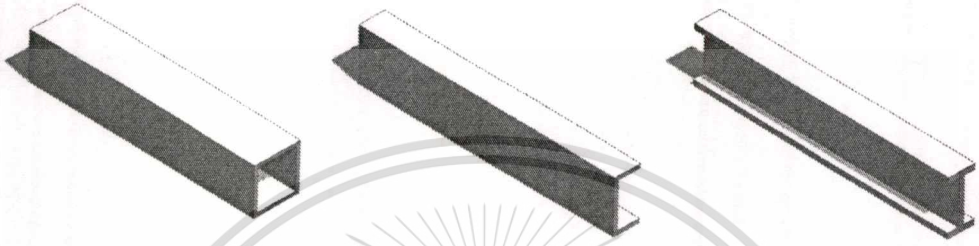

Figure 1.7 Various forms of structural steel.

Welded joints in the bus superstructure are normally ignored for the practical analysis because there are too many joints in the full bus superstructures and it's difficult to model the actual weld geometry. However, there are some studies about the local stress effect due to weld geometry. Kumket B. et al. [6], [7] studied about the effect of stress with different sizes of welded joints, which are difficult to measure the exact dimensions, in a bus superstructure. There are 70 joints that are classified by 11 groups in the body. In their study, wireframe was modeled as a left side frame of the bus superstructure as shown in Figure1.8. The wireframe was analyzed under static load distributed on the beam steel. The joint having maximum stress is selected from the full superstructure model to be studied as a local model with the weld geometry as shown in Figure 1.9. Various types of welded sizes; 2 mm, 3 mm and 4 mm were modeled and analyzed. It was found that the optimum joint design could be the 2 mm welded size or the 3 mm as well as the 4 mm with the safety factor of 2.3. The 2 mm welded size could withstand by 30 kN, whereas the 3 mm and 4 mm welded size could withstand 40 kN. The study shows that the weld geometries should be applied in the model to evaluate the stress because they affect the stress of the joints. Although the suitable weld sizes are evaluated by the analysis, it is difficult to control the weld sizes in the weld process.

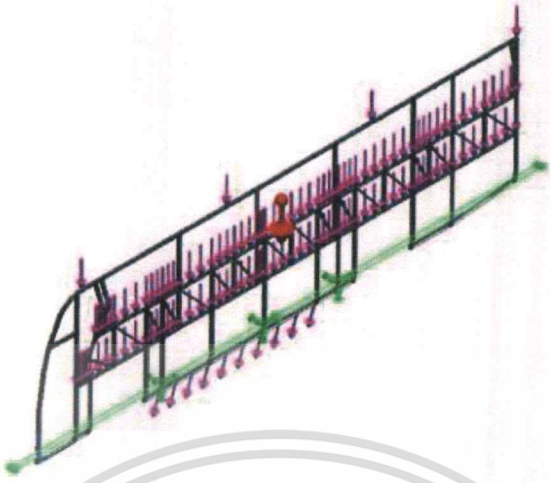

Figure 1.8 Force Action to the bus body frame (Kumket et al., 2010).

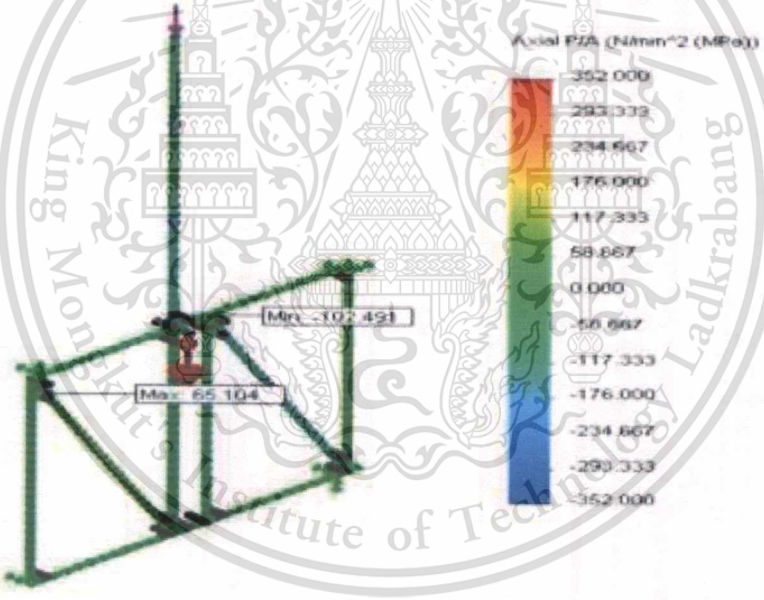

Figure 1.9 Test on 2 mm. welded size (Kumket et al, 2010).

Although the stress of welded joints is difficult to evaluate, the stress evaluation of a welded joints is suggested by many standards such as International Institute of welding (IIW) [8], Eurocode 3 [9], etc. Each standard presents concepts to evaluate the stress of welded joints as shown in Figure 1.10. A global stress concept namely nominal stress method is still prevailing. The application of this method requires the definition of the nominal stress determined by using theories of structural mechanics. However, it is necessary for the application of local concept to

justify the actual stress. Radaj et al. [10] and Hiroyuki et al. [11] presented the local stress concept to evaluate the stress of welded joints. This concept can be assigned to three groups including structural stress method, effective notch stress method, and linear elastic fracture mechanic method (LEFM). Structural stress method sometimes called hot spot stress method is one method based on the local stress concept. This method considers the stress concentration effects of the discontinuity structures, not the weld geometry itself. In case, the effect of non-linear stress due to weld geometry can be considered by effective notch stress method. Effective notch stress method is based on the highest elastic stress at the weld root or weld toe. Furthermore, linear elastic fracture mechanic method subdivided into the stress intensity theory and crack propagation theory is also presented. The accuracy of each stress concept is different. Martinsson [12] presented the relationship between accuracy and structural complexity as shown in Figure 1.11. LEFM provides higher accuracy compared to others concept while the structures are more complex.

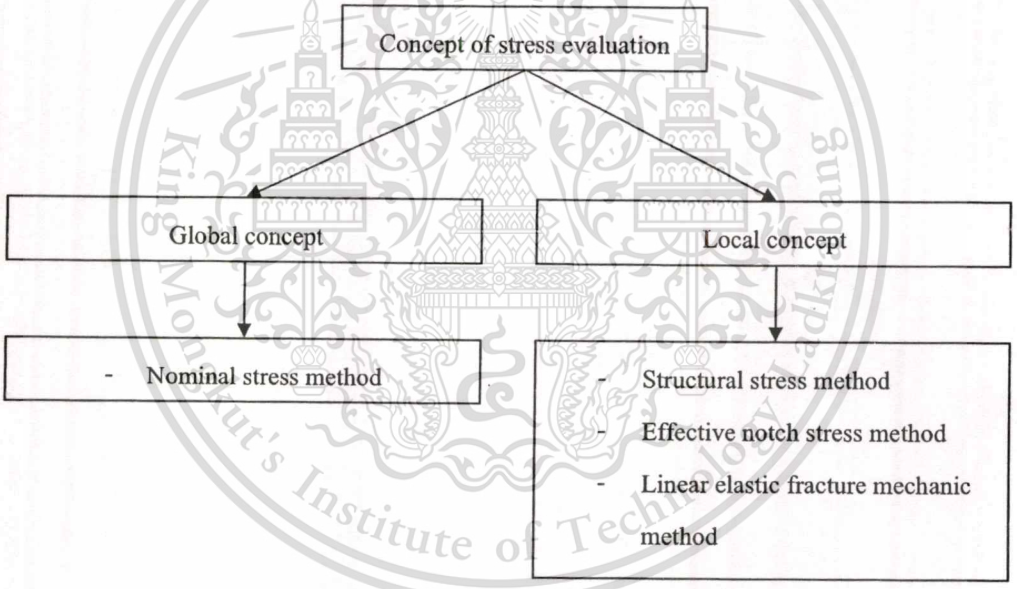

Figure 1.10 Concept of stress evaluation at welded joints.

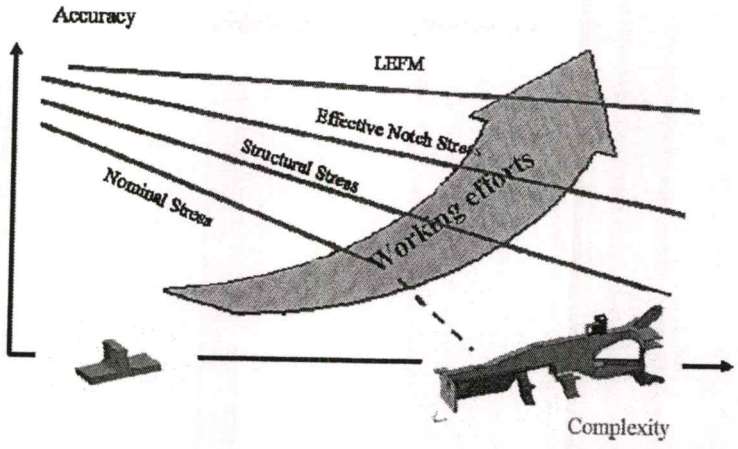

Figure 1.11 Relationship between accuracy and structural complexity for different stress method (Martinsson, 2005).

Structural stress method is simple to apply in superstructures. Thus, there are many approaches to evaluate the stress at welded joints based on structural stress method such as conventional structural stress approach and one millimeter in depth structural stress approach. One millimeter in depth structural stress approach has been proposed by Xiao and Yamada [13]. Furthermore, Aygül [14] summarized 5 techniques for weld modeling to determine the stress of welded joints by using finite element analysis. The calculated stresses are applied to evaluate fatigue life of welded joints.

1) The welds in welded joint can be modeled using oblique shell element that is presented by Niemi [15].
2) Weld modeling technique using rigid links was suggested by Fayard et al. [16].
3) Using shell element with increased thickness in the intersection region of welded joints is suggested by Niemi [17].
4) Weld end modeling, the fourth technique, is presented by Aygül et al [18] .
5) Solid elements are modeled as the weld at the welded joint, which is widely used because of its simplicity in modeling work and its accuracy.

Weld geometry and plate thickness affect the stress of welded joint. Radhi and Barrans [19] were studied the effect of weld toe radius and plate thickness as shown in Figure 1.12 on stress and fatigue life of butt welded joint by using finite element analysis. The weld in weld joint is

modeled using solid elements. Material properties applied in base metal, heat affected zone, and filler metal are different. Weld toe radius and plate thickness contribute stresses leading to the fatigue life calculation. Figure 1.13 shows the relationship between Von-mises equivalent stress and the different thickness with constant weld toe radius. The dimension providing maximum fatigue life is the best geometry. Figure1.14 presents fatigue life of studied dimensions. The best dimension is the plate thicknesses of 4 mm and 6 mm with weld toe radius of 1.2 mm giving maximum fatigue life. The results imply that weld toe radius and plate thickness affect the stress and fatigue life on the welded joint. However, only butt welded joint is studied. Other types of weld joints are applied in the superstructure.

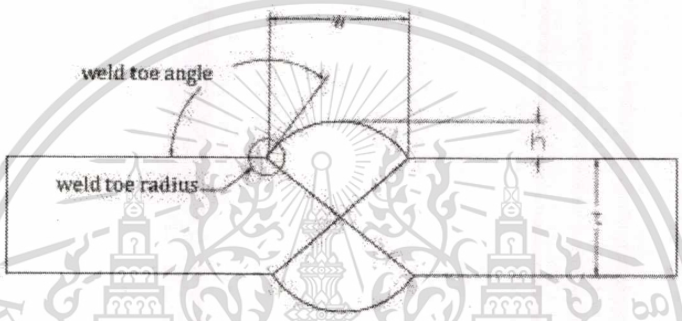

Figure 1.12 Dimension of butt welded joint; weld height h, plate thickness t, weld width W, weld toe radius ρ, and weld toe angle α (Radhi H.E. and Barrans S.M., 2010).

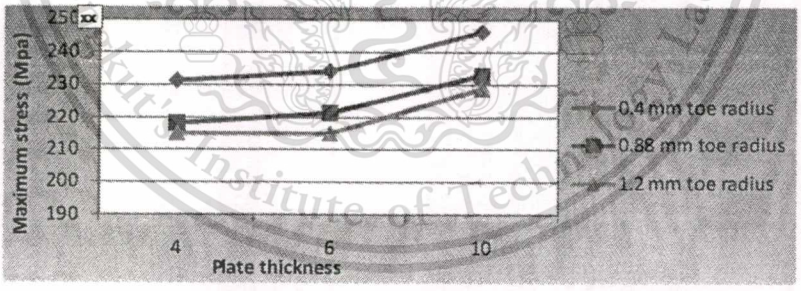

Figure 1.13 Maximum Von-mises equivalent stress (Radhi H.E. and Barrans S.M., 2010).

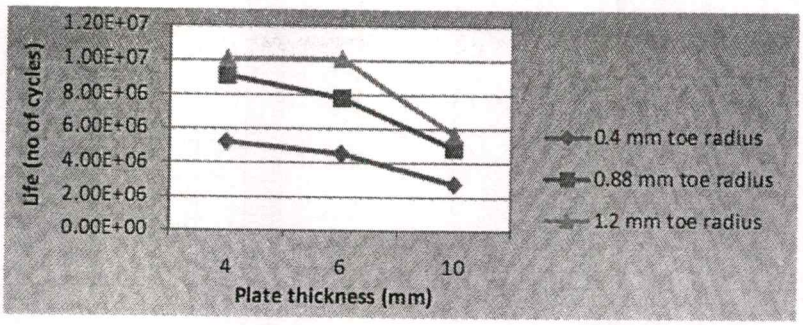

Figure 1.14 Maximum Fatigue life (Radhi H.E. and Barrans S.M., 2010).

Although the welds should be modeled in order to obtain realistic stiffness, they are not modeled because the actual weld geometry is difficult to measure due to some defects occurring during the welding process. It is difficult to model the weld geometry for the analysis. Niemi et al. [18] mention that the welds are not usually modeled for thin shell element as shown in Figure 1.15 a) and b). However, in case of high local bending between two local discontinuities, weld could be modeled by reinforced plate strips as shown in Figure 1.15 (c).

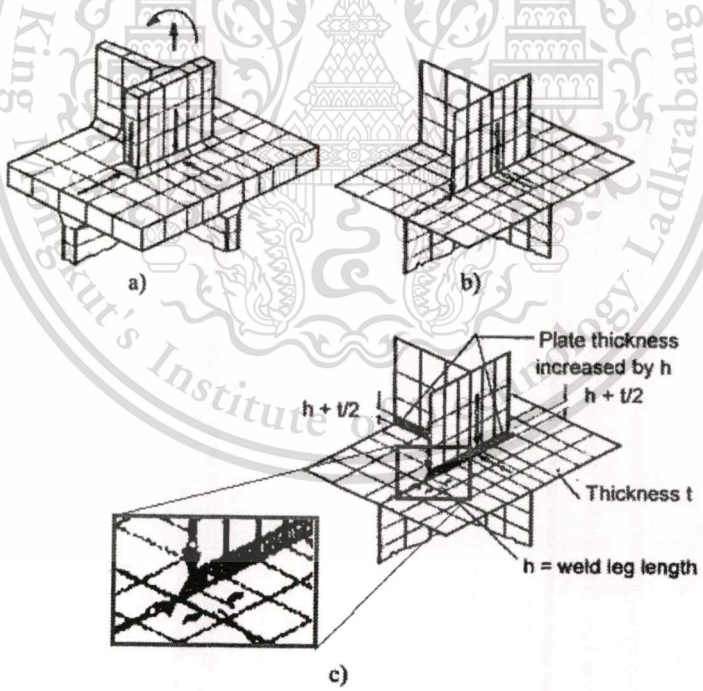

Figure 1.15 a) solid element model with weld modeling; b) shell element model without weld modeling; c) attachment welds modeled with reinforced plate strips (Niemi E. et al.).

In bus superstructures, weight has to be reduced as much as possible to lower the material cost and fuel consumption. Thin-walled hollow square beams are usually used in the bus superstructure design. Hot spot stress (HSS) method can be applied to various applications, particularly to an automotive field. The IIW recommendations for structural hot spot stress method are only applicable to thick structures having a thickness greater than 5 mm. However, various welded joints of thin-walled beams in the bus structure floor were studied by Savaidis [20]. Figure 1.16 shows specimen's geometry and finite element mesh whose size is based on IIW recommendations of hot spot stress method. Moreover, Marin et al [21] studied 3 different specimens using shell elements as a weld geometry as shown in Figure 1.17. HSS method was applied in this study. In the recommendations, coarse meshes are adequate to use in HSS method for the modeling of complex structure in order to reduce a number of elements. Furthermore, Fokilidis et al. [22] studied various fillet welded joints of thin-wall tube by HSS method as shown in Figure 1.18. The IIW recommendations, such as meshing, were also applied in this study. There were good agreements between experiments based on strain gage measurement and finite element analysis using shell elements.

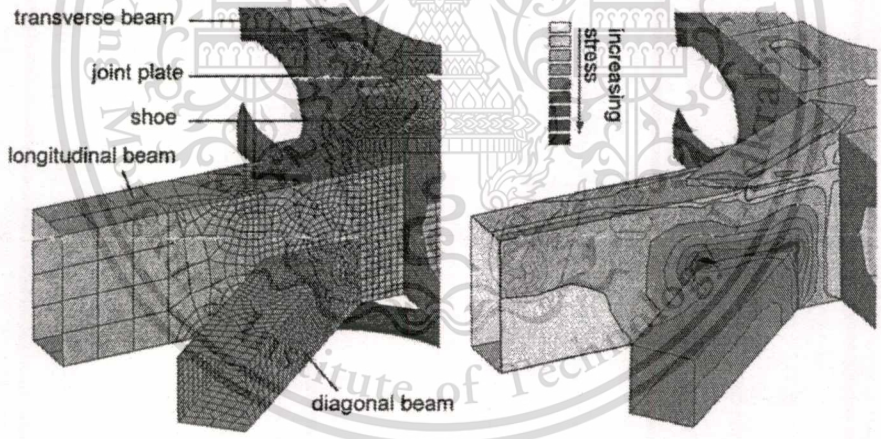

Figure 1.16 Specimen's geometry and finite element mesh detail of weld (Savaidis et al., 2000).

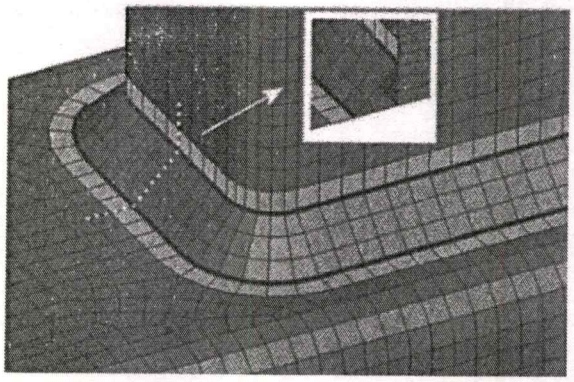

Figure 1.17 Tubular T-Joint conection (Marin et al.)

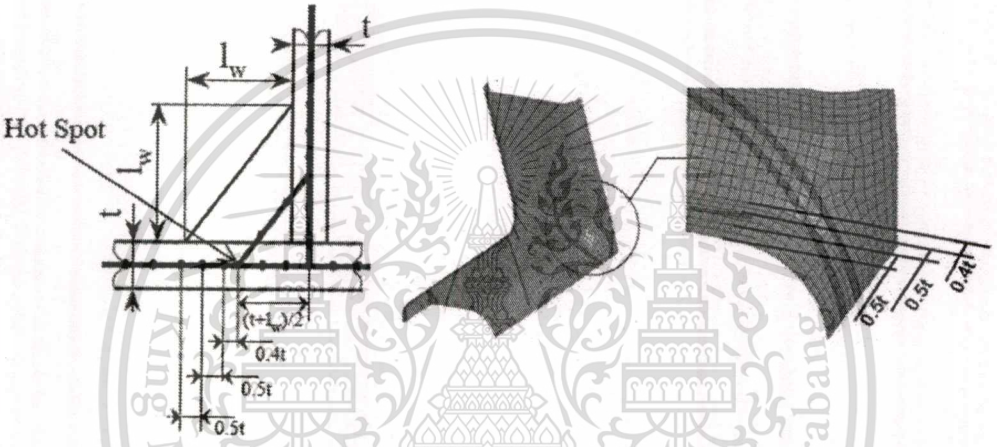

Figure 1.18 Specimen's geometry and finite element mesh detail of weld (Fokilidis et al., 2007).

In IIW recommendation, the hot spot stress is presented in terms of multiplication between stress concentration factor (SCF) and nominal stress. Brennan et al. [23] studied SCFs of welded T-joint and skewed T-joint under tension and pure bending as shown in Figure 1.19. Finite element analysis of linear elastic was applied to evaluate the SCFs using two-dimensional plane stress model as shown in Figure 1.20. The constructed curves were represented as closed-form SCFs in terms of weld geometry parameters such as weldment angle, weld root radius, weld attachment width and plate thickness by using curve fitting. This paper also reports the suitable SCFs from SCF parametric equations compared to SCFs from finite element analysis. However, this study only applies for butt weld but many types of weld is used to joint materials in the superstructure. So, other types of weld should be studied.

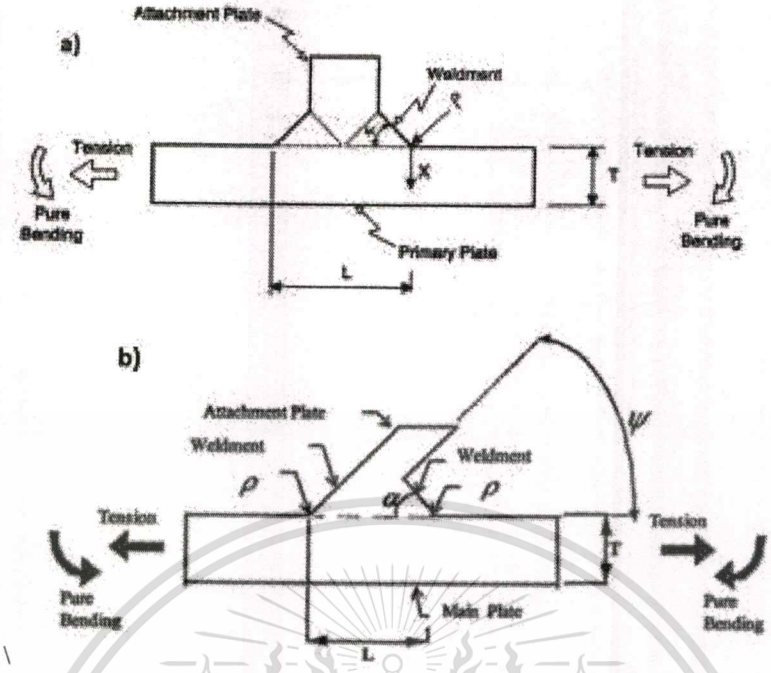

Figure 1.19 a) Geometry of T-butt joint; b) Geometry of skewed T-butt joint (Brennan et al., 2000).

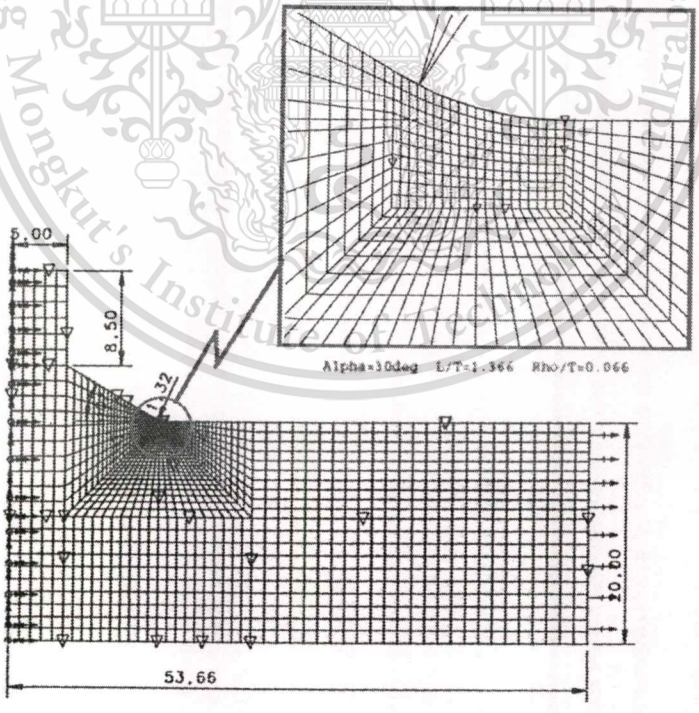

Figure 1.20 Finite element mesh (Brennan et al., 2000).

1.3 Objective

- To create a simplified model that represents a reinforced square hollow section (SHS) T-joint in bus superstructure.

1.4 Scopes

- Square hollow section (SHS) joint found in bus superstructure is studied.
- The valid dimension ranges of square hollow section for the simplified model are width of 30-60 mm and thicknesses of 2.0-5.0 mm.
- The simplified model can be applied in elastic region under in-plane load.
- Only geometry of the joint is considered.
- The weld geometry and residual stress are ignored.

1.5 Thesis Outline

The thesis is organized in 5 Chapters, the contents of which are summarized as followed:

Chapter 1 : Introduction

This chapter introduces the general background of bus production in Thailand, the advantage of reinforcement applied in the bus superstructure. The literature reviews are summarized in this chapter. In additions, the objectives, and the scopes of this study are also presented in this chapter.

Chapter 2 : Hot Spot Stress method

This chapter explains the peculiarities of welded structures affect the stress of welded joints. Many methods of stress determination in welded joint are suggested in this chapter, especially hot stress method. The meaning of hot spot is described. Moreover, many approaches based on hot spot stress method are presented for the stress evaluation.

Chapter 3 : Methodology

This chapter explains the workflow of this study. Actual geometry found in bus superstructure is presented. Finite element models of reference model and trial models are also presented in this chapter. Stiffness matrices of finite element models proposing to evaluate stiffness errors are explained in order to select the simplified model. Furthermore, the stress

correction factors and load-to-stress factors are determined based on hot spot stress method under static in-plane loads.

Chapter 4 : Result

This chapter demonstrates the design experimental results of simplified model such as the stiffness error, the stress correction factor and the load-to stress factor under each loading type. Moreover, computer time for the stress analysis is presented.

Chapter 5 : Conclusion

The obtained results from the previous chapters are concluded in this chapter. The conclusion are included with the stiffness results, model selection, and stress result. Suggestions and future work are also presented.

CHAPTER 2

HOT SPOT STRESS METHOD

2.1 Peculiarities of Welded Structures

Welding is a jointing technique that is widely used in many structures in order to join the material. Welded structures present several peculiarities which make it difficult to determine the stress by local stress approaches. Those peculiarities found in weldments can be subdivided into 3 categories, as stated by Radaj.

1) Inhomogeneous material – This is a characteristic of welded joints. The filler material is generally similar to base material, but special matter is alloyed to attain a higher weld quality. The heat affected zone (HAZ) close to the weld pool shows different microstructures because of the high temperature of welding process. In addition, weld defects sometimes called imperfections such as cracks, porosity, incomplete fusion, undercut, incomplete penetration, and overlaps as shown in Figure 2.1 cause inhomogeneous material within the welded joint.

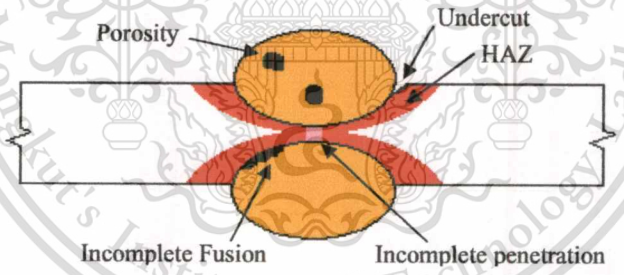

Figure 2.1 Weld defect.

2) Welding residual stresses – Shrinkage because of rapid cooling after welding process produces welding residual stresses via thermal strains and micro structural transformation.

3) Geometry and dimensions of weld – Local stress is difficult to determine because the weld geometry and dimensions vary within a large scatter range due to the nature of welding process. The weld toe geometry as shown in Figure 2.2 may be determined

using external casting techniques. The weld root or nugget edge may be made visible after transverse cutting and polishing.

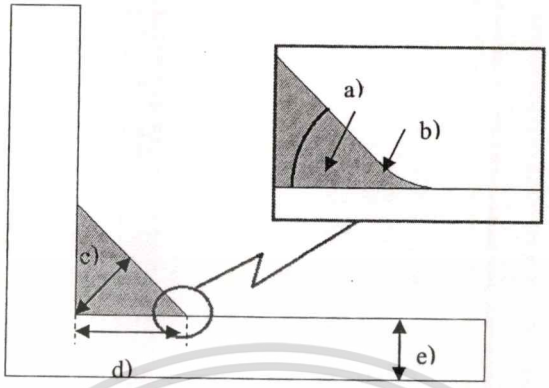

Figure 2.2 a) Weld toe angle; b) Weld toe radius; c) Weld throat; d) Weld length; e) Thickness of base material.

2.2 Stress Evaluation Method of Welded Joints

All of these peculiarities in welded structures can affect the stress of the joint. Generally, the material characteristic values of the base material are used. The effect of residual stresses is only roughly taken into account to evaluate the stress. Weld geometry parameters and weld defect are not considered in the stress analysis because they are difficult to measure in realistic. Many methods in IIW recommendations ignore weld geometry to evaluate the stresses in welded joints. However, the weld geometry modeled in the joints for those methods is assumed to be a perfect weld.

1) Nominal stress method

Nominal stress method is based on global concept. The stresses exclude any stress increased due to the structural detail or the weld geometry as shown in Figure 2.3. The local stress raising effect of weld geometry is ignored. Nominal stress is mostly used in weld component. Nominal stress is determined by using elementary theories of structural mechanics base on linear elastic behavior. Finite element analysis may be applied in this method.

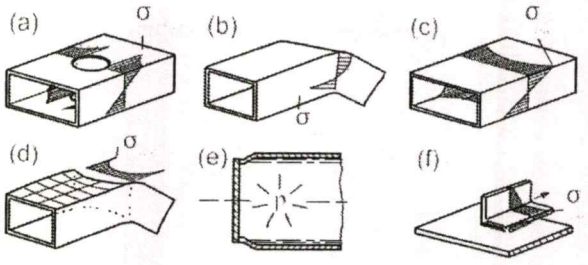

Figure 2.3 Example macro stress rising due to geometry (IIW, 2008).

2) Hot spot stress method

Hot spot assumes that high stress occurs at the weld toe where the cracks are initiated as shown in Figure 2.4. Hot spot stress method includes all stress raising effects of a structural detail excluding all stress rising due to the local weld profile itself. In addition, nonlinear peak stress due to local notch is ignored from hot spot stress method. The hot spot stress method can be applied when the crack initiation occurs at the weld toe as shown in Figure 2.5. This approach is recommended for complicated geometry of welded joints instead of the nominal stress approach. Hot spot stresses are generally applied for plate, shell and tubular structure. One example approach of hot spot stress method is determined by the surface extrapolation.

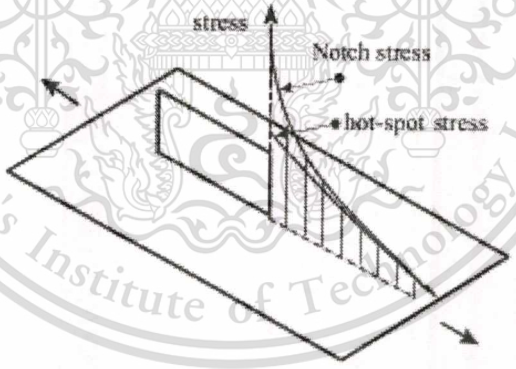

Figure 2.4 Hot spot stress and Notch stress (IIW, 2008).

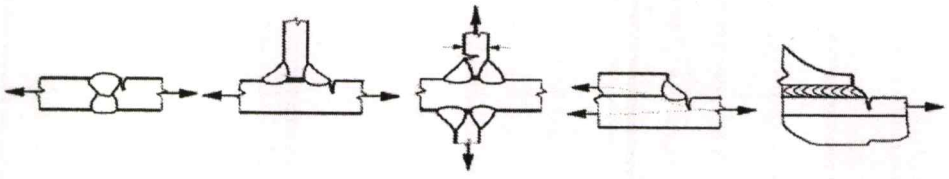

Figure 2.5 Crack initiations at weld toe (IIW, 2008).

3) Effective notch stress method

The stress of effective notch stress method is higher than the stress of hot spot stress method as shown in Figure 2.4 because of the non-linear stress. Effective notch stress method is based on highest elastic stress at weld toe or weld root [24] including nonlinear stress as shown in Figure 2.6. However, this method can be applied in case failure is occurred at weld root or weld toe. Notch radius of r = 1 mm has been verified to give consistent result for structural steels and aluminium alloy as shown in Figure 2.7. Effective notch stress is determined by using finite element analysis. The method is limited to the thickness of base material not greater than 5 mm.

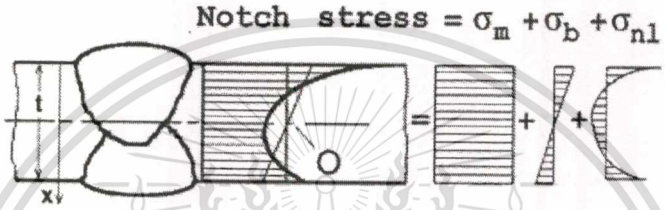

Figure 2.6 Nonlinear stress (IIW, 2008).

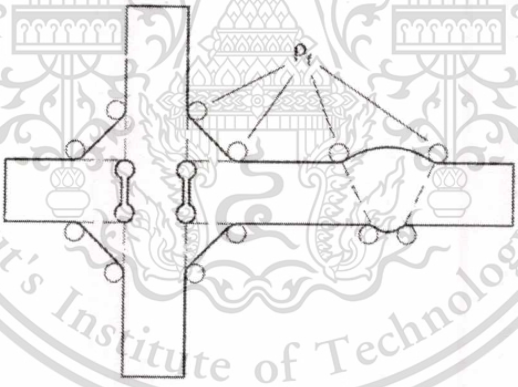

Figure 2.7 Fictitious rounding of weld toes and roots (IIW, 2008).

4) Linear elastic fracture mechanic

Linear elastic fracture mechanic assumes that the material is isotropic and linear elastic. This method is used to assess the behavior of cracks. This method is applied to evaluate the stress based on the equation of crack growth and stress intensity factor rang when the crack initiation was detected in welded joint.

2.3 Hot Spot Stress Method (HSS)

Hot spot stress, sometimes called Geometric stress, has been discussed in [8]. Hot spot is described as a point that high stress is occurred. In welded joint, this point corresponds to the weld toe where discontinuity of structure occurs. Thus, hot spot stress method is limited to the failure location occurring at weld toe in complicated structures. Hot spot stress method includes all stress raising effects of a structural detail excluding all stress concentrations due to the local weld profiles itself. Two types of hot spot stresses are defined according to hot spot stress location as shown in Figure 2.8. For type a), maximum stress occurs at the weld toe on plate surface. When the maximum stress is located at weld toe on plate edge, it is defined as type b).

There are many techniques to evaluate the stress at welded joints based on structural stress concept. For example, conventional structural stress method generally applied for tubular joints determines the hot spot structural stress by the extrapolation on the surface of based material to the weld toe as shown in Figure 2.9. One millimeter in depth approach which is an unconventional structural stress method considers the structural stress calculated 1 mm in depth below the weld toe (on the expected crack path). This approach is proposed by Xiao and Yamada [13] as shown in Figure 2.10.

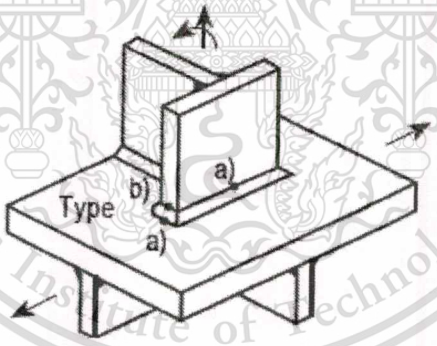

Figure 2.8 Type of hot spot (IIW, 2008).

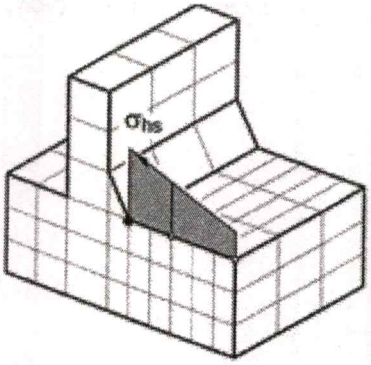

Figure 2.9 Surface extrapolation (IIW, 2008).

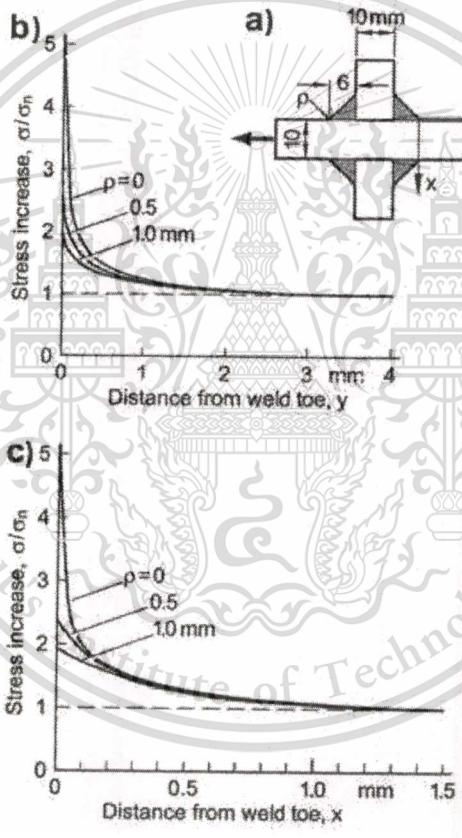

Figure 2.10 Stress distribution (b,c) calculated by the finite element for a reference structural detail (a) with non-linear-carrying fillet welds (double-sided transverse attachment joint; weld toe radius (Xiao and Yamada, 2004).

Aygül [14] summarizes 5 techniques presented for weld modeling to determine the stress for fatigue life calculation using finite element analysis. The first technique was presented by Niemi [15]. The welds in welded joint can be modeled using oblique shell elements. The attached plate should be joined to main plate in the intersection as shown in Figure 2.11. Secondly, weld modeling technique using rigid links as shown in Figure 2.12 was suggested by Fayard et al. [16]. This technique can be used to compute the hot spot stress at the weld toe. Niemi [17] suggested using shell element with increased thickness in the intersection region of welded joints as the third technique as shown in Figure 2.13. Figure 2.14 shows weld end modeling, the fourth technique that is presented by Aygül et al [18]. In some cases, the geometry and shape of welds in a joint may have lager influence than their stiffness. For example, the crack starts at the weld toed at the end of welds. Shell elements can be modeled as the weld at the end where the crack initiates. Finally, solid elements are modeled as the weld at the welded joint as shown in Figure 2.15. This technique is widely used because of its simplicity in modeling work and its accuracy in results. Although the welds should be modeled in order to obtain realistic stiffness, Niemi et al. [17] mentions that the weld are not usually modeled for thin shell element as shown in Figure 2.16 (a-b). However, in case of high local bending between two local discontinuities, weld could be modeled by reinforced plate strips as shown in Figure 2.16 (c).

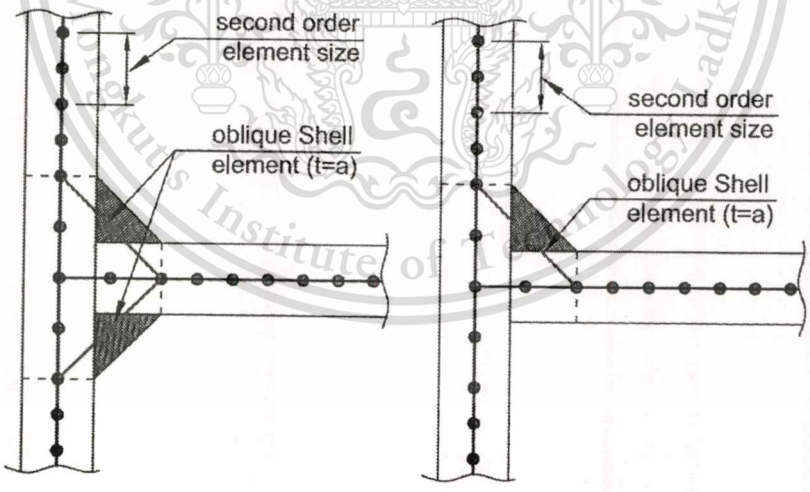

Figure 2.11 Weld modeling using oblique shell elements (Niemi, 1995).

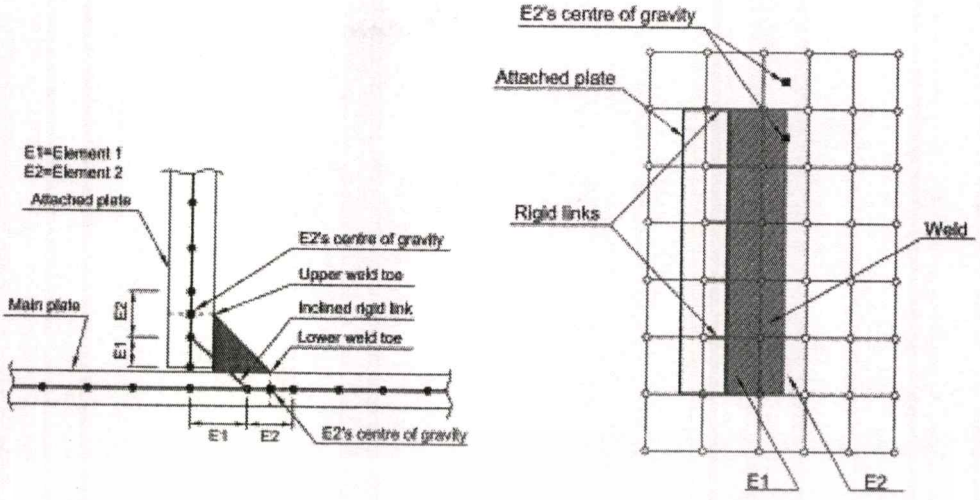

Figure 2.12 Single-side weld modeling with rigid links (Fayard et al., 1996).

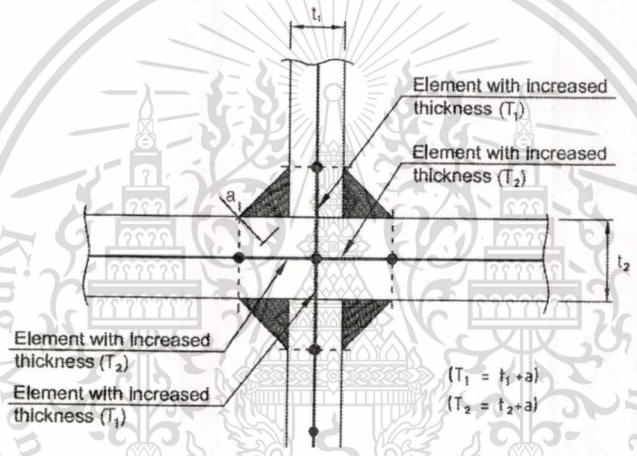

Figure 2.13 Weld modeling using shell elements with increased thickness (Niemi, 1995).

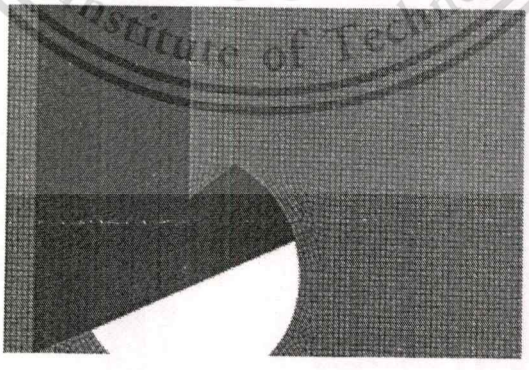

Figure 2.14 Weld end modeling using shell elements (Aygül M. et al, 2011).

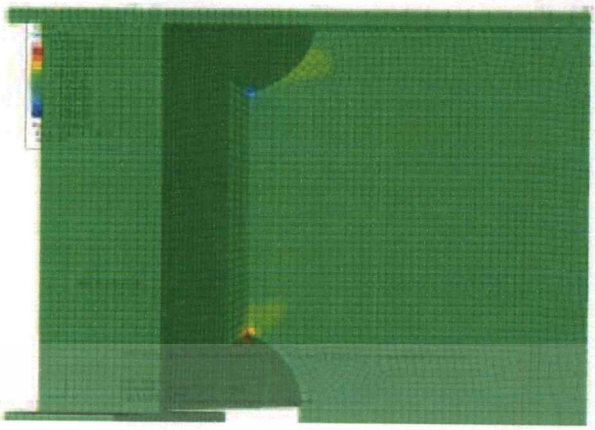

Figure 2.15 Modeling of the welds with solid elements (Mustafa A., 2012).

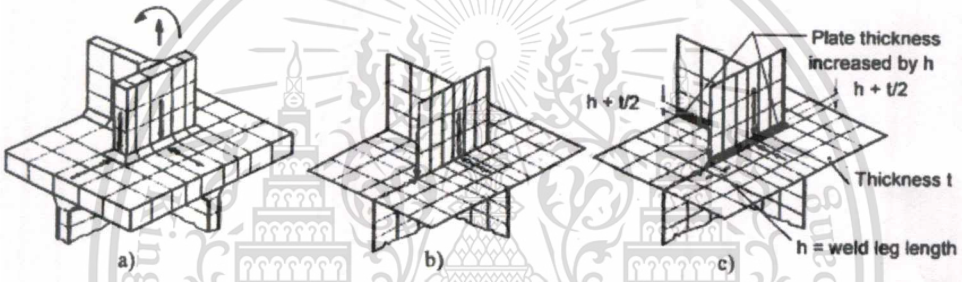

Figure 2.16 a) solid element model with weld modeling; b) shell element model without weld modeling; c) attachment welds modeled with reinforced plate strips (Niemi E. et al.).

2.4 Surface Extrapolation of Hot Spot Stress Method

Hot spot stress can be determined using reference points away from weld toe by extrapolation on surfaces in order to avoid stress singularity. A set of reference points in hot spot stress method depends on thickness of weld components. However, this study focuses on type a) of hot spot stress. Equation (2.1) and Equation (2.2) show the liner and quadratic surface stress extrapolation for find mesh. Both linear extrapolation and quadratic extrapolation shown in Figure 2.17 a) and Figure 2.17 b) can be applied to evaluate the hot spot stress. Surface stresses can be measured experimentally by strain gauges or using finite element analysis.

$$\sigma_{HS,linear} = 1.67\sigma_{0.4t} - 0.67\sigma_{1.0t} \quad (2.1)$$

$$\sigma_{HS,quadratic} = 2.52\sigma_{0.4t} - 2.24\sigma_{0.9t} + 0.72\sigma_{1.4t} \quad (2.2)$$

Where $\sigma_{HS,linear}$ is the linear hot spot stress.

$\sigma_{HS,quadratic}$ is the quadratic hot spot stress.

$\sigma_{0.4t}$ is the surface stress at 0.4t distance away from weld toe.

$\sigma_{0.9t}$ is the surface stress at 0.9t distance away from weld toe.

$\sigma_{1.0t}$ is the surface stress at 1.0t distance away from weld toe.

$\sigma_{1.4t}$ is the surface stress at 1.4t distance away from weld toe.

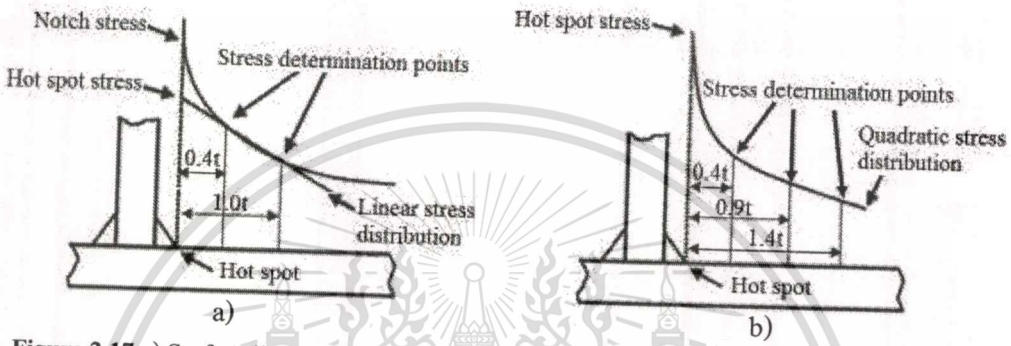

Figure 2.17 a) Surface linear extrapolation; b) Surface quadratic extrapolation (IIW, 2008).

For a thin-walled structure, surface stresses are difficult to be determined by experiment because the distance between reference points are too small to place strain gauges as shown in Figure 2.18. Instead of using experiment, Finite element analysis is suitable to be used to determine surface stresses without any difficulty. Based on a finite element model, it is possible to place nodes on lines where stress must be measured to evaluate hot spot stress as shown in Figure 2.19. Because local weld profiles are excluded in stress raising effects, weld geometry may be modeled or not modeled in finite element analysis.

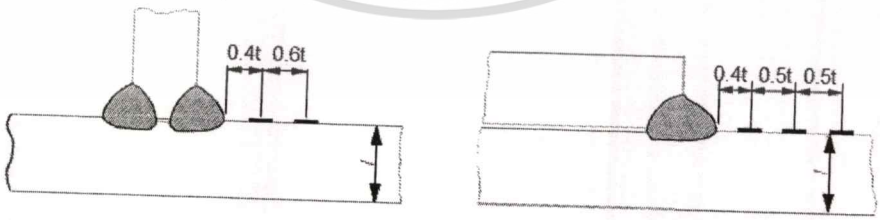

Figure 2.18 Example of strain gauges in plate structures (IIW, 2008).

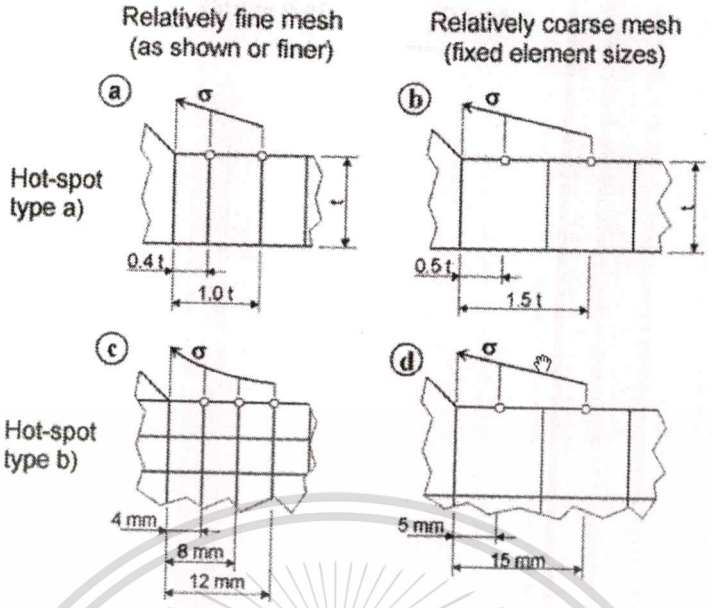

Figure 2.19 Reference points at difference types of meshing (IIW, 2008).

CHAPTER 3

Methodology

3.1 Workflow

Workflow of this study is shown as a diagram in Figure 3.1. After various joints in the bus superstructure had been reviewed, the reinforced square hollow section (SHS) T- joint was found to be an interesting geometry for this study. Computer aided design (CAD) of reference solid element model and trial models without weld geometry were created. Geometry and dimension of the joint are shown in Figure 3.2, where "W" is the width of hollow square beam and "t" is its thickness. The same cross-sectional dimensions of hollow square beams are used for both T-joint and the reinforcement. Width of 30-60 mm and thicknesses of 2.0-5.0 mm are the dimension range of square hollow section commonly sold in the market and, therefore, will be used for the analysis. Table 3.1 summarizes all hollow square beam dimensions that were analyzed by FEA in this study.

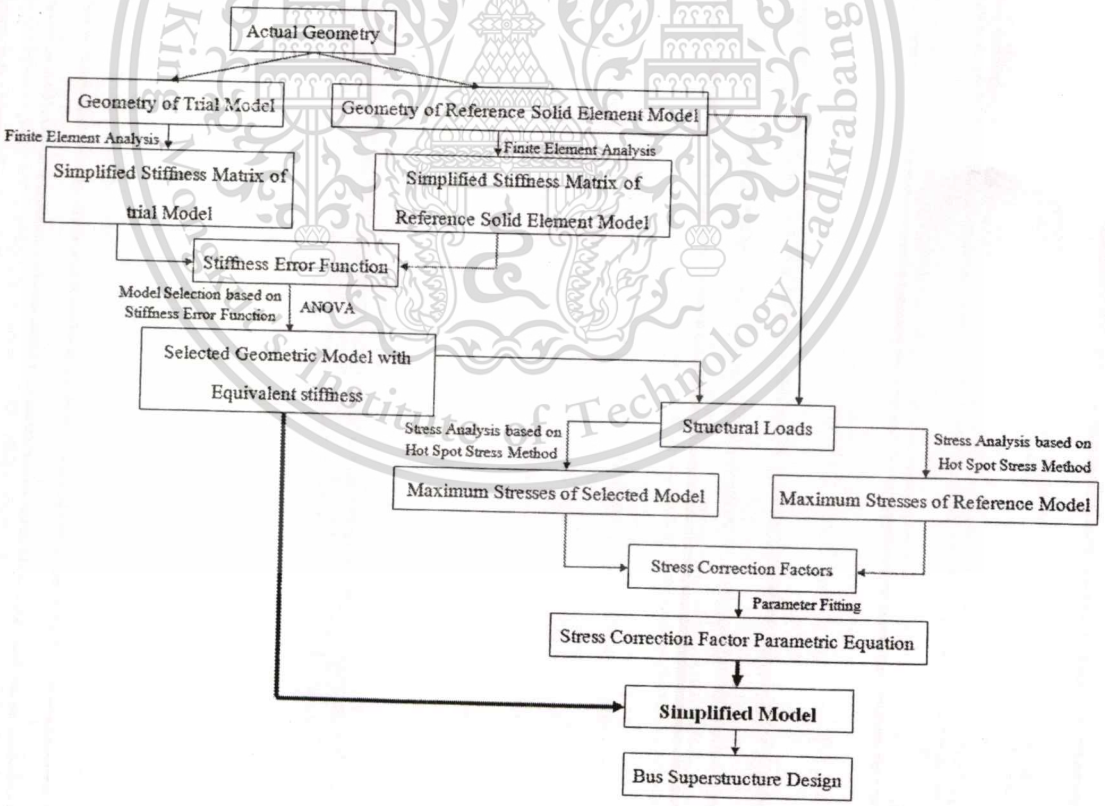

Figure 3. 1 Workflow of the development of a simplified model.

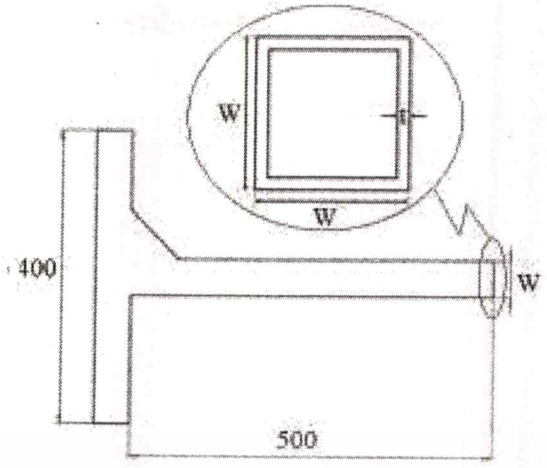

Figure 3.2 Geometry dimension.

Table 3.1 Hollow Square beam dimensions analyzed by FEA

W (mm.)	60	60	60	60	50	50	50	50	40	40	40	40	30	30	30	30
t (mm.)	5	4	3	2	5	4	3	2	5	4	3	2	5	4	3	2

The stiffness matrices of reference solid element model and trial models were evaluated to represent the properties of the joint. The stiffness matrix of trial models were compared to the stiffness matrix of reference solid element model in order to select the best trial model having most equivalent stiffness based on statistical method. After the selection of trial model, the reference solid element model and the selected geometric model were used to determine the maximum stress at the discontinuity of structure based on hot spot stress method under structure loads. The stress correction factors are calculated by determining the relationship between the maximum stress in the selected geometric model and the maximum stress in reference solid element model. The stress correction factors are presented as a function of joint geometries by parameter fitting such as curve and surface fitting in order to apply in bus superstructure stress analysis.

3.2 Actual Geometry

The strength of joints can be increased by reinforcements. Many kinds of reinforcements are applied to a number of joints in bus superstructures such as plate steel. One of interesting joint found in bus superstructure is to use a square hollow beam to reinforce square hollow section T-joint. This kind of joint was selected to be studied. A square hollow beam is cut to be a right angle and then assembled to the square hollow section T-joint as shown in Figure 3.3 by welding process.

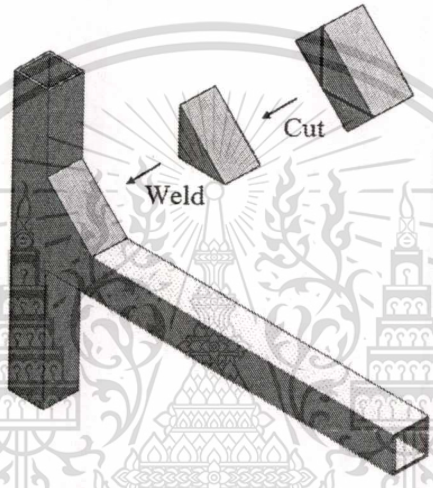

Figure 3.3 Reinforced square hollow sections T-joint assemble.

3.3 Finite Element Model

3.3.1 Finite element analysis

The exact solutions of engineering problems consist of infinite number of variables which are difficult to apply in reality. Finite element analysis (FEA), sometimes called finite element method (FEM), is a computational technique used to obtain approximate solutions of boundary value problems. The concept of finite element analysis is to decrease infinite variables into finite variables. Thus, FEA is nowadays the most general and one of powerful tools for the analysis of structure. General procedure for finite element analysis consists of 6 steps [26].

1) Divide structure into elements with nodes

The structure is divided into small pieces called element as shown in Figure 3.4. One element may consist of one or several nodes.

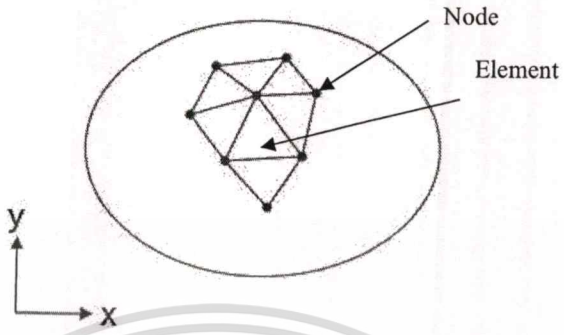

Figure 3.4 Element dividing.

2) Select element interpolation function

Element interpolation function can be selected in many types of function. Figure 3.5 shows triangle element type on Cartesian coordinate consisting of ϕ_1, ϕ_2, and ϕ_3, which are nodal unknowns. The element interpolation functions are defined as Equation (3.1).

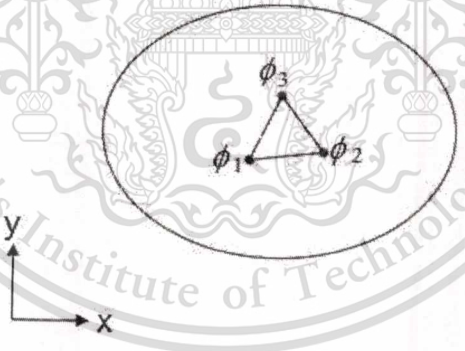

Figure 3.5 Triangle element with node unknowns.

$$\phi(x,y) = N_1(x,y)\phi_1 + N_2(x,y)\phi_2 + N_3(x,y)\phi_3 \tag{3.1}$$

Where $N_i(x,y), i = 1,2,3$ are element interpolation functions.

Moreover, Equation (3.1) can be present as a matrix form in Equation (3.2).

$$\phi(x,y) = [N_1 \quad N_2 \quad N_3]\begin{Bmatrix}\phi_1\\ \phi_2\\ \phi_2\end{Bmatrix}$$

$$= [N]\{\phi\} \tag{3.2}$$

3) Generate element equations

This step is important for finite element analysis. Element equations are generated. For example, Equation (3.3) shows element equation of triangle element in case of static structural problem.

$$\begin{bmatrix}k_{11} & k_{12} & k_{13}\\ k_{21} & k_{22} & k_{23}\\ k_{31} & k_{32} & k_{33}\end{bmatrix}_e \begin{Bmatrix}\phi_1\\ \phi_2\\ \phi_2\end{Bmatrix}_e = \begin{Bmatrix}F_1\\ F_2\\ F_{3_e}\end{Bmatrix}_e \tag{3.3}$$

Equation (3.3) can be abbreviated into Equation (3.4)

$$[K]_e \{\phi\}_e = \{F\}_e \tag{3.4}$$

Where $[K]_e$ is the stiffness matrix of element.

$\{\phi\}_e$ is displacement matrix of element.

$\{F\}_e$ is applied load matrix of element.

4) Form a system of simultaneous equations

Those element equations are summarized in order to form a system of simultaneous equations for the whole structure. The system of simultaneous equations shows in Equation (3.5).

$$[K]_{sys} \{\phi\}_{sys} = \{F\}_{sys} \tag{3. 5}$$

Where $[K]_{sys}$ is the stiffness matrix of system.

$\{\phi\}_{sys}$ is displacement matrix of system.

$\{F\}_{sys}$ is applied load matrix of system.

5) Apply boundary conditions

Boundary conditions are applied in the system of the simultaneous equations in order to determine $\{\phi\}_{sys}$ consisting of nodal unknowns.

6) Calculate for solution results

$\{\phi\}_{sys}$ is used to calculate the solution result. For Example, $\{\phi\}_{sys}$ is displacement in case of static structural problem. $\{\phi\}_{sys}$ is used to evaluate stress, and strain results for finite element analysis.

After reinforced square hollow section T-joint in bus superstructure was selected for this study. Finite element model of reference solid element model and trial models were created in order to evaluate the stiffness and the stress. Table 3.2 show material properties for structural steel used in finite element analysis for both reference solid element model and trial models.

Table 3.2 Structural steel properties.

Property	value
Elastic of modulus (MPa)	2×10^5
Poisson's ratio	0.3

3.3.2 Reference solid element model

Figure 3.6 is a CAD model of square hollow section T-joint with weld geometry which is an actual geometry of the joint. However, it is not clear in IIW recommendations to model or not model weld geometry in CAD model. Hot spot stress includes the stress rising due to structural detail excluding the effect of weld geometry. Therefore, weld geometry was not modeled in this study as shown in Figure 3.7. Reference solid element model from CAD has been transferred to CAE model by meshing. 20-node hexagonal elements with 6 DOFs at each node were used to mesh reference solid element model as shown in Figure 3.8.

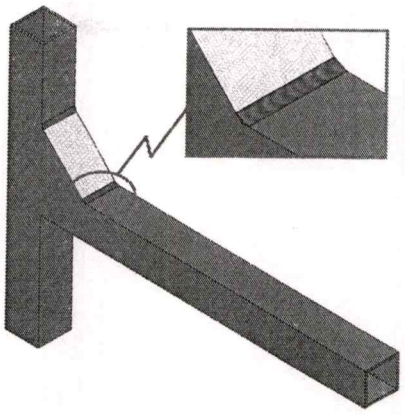

Figure 3.6 CAD model with weld geometry.

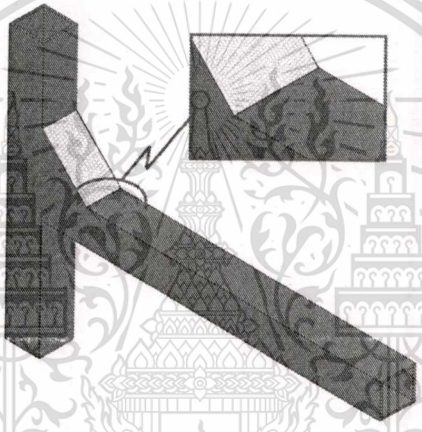

Figure 3.7 CAD model without weld geometry.

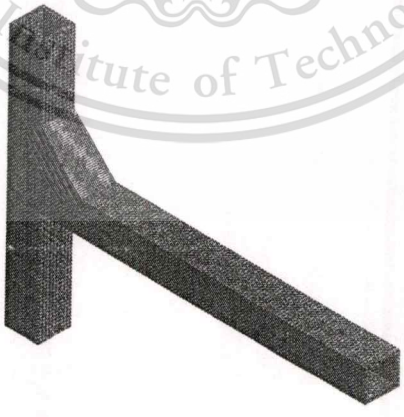

Figure 3.8 Reference solid element model.

3.3.3 Trial model

Four trial model types, namely Model A, Model B, Model C, and Model D are analyzed in this study.

3.3.3.1 Model A

Model A, as shown in Figure 3.9, consists of only 2-node beam elements with 6 DOFs at each node. Width and thickness of a square hollow section (SHS) beam have to be specified as cross-sectional properties for the beam elements. The reinforcement is not modeled in the geometry. This type of model is usually applied in bus superstructure analysis.

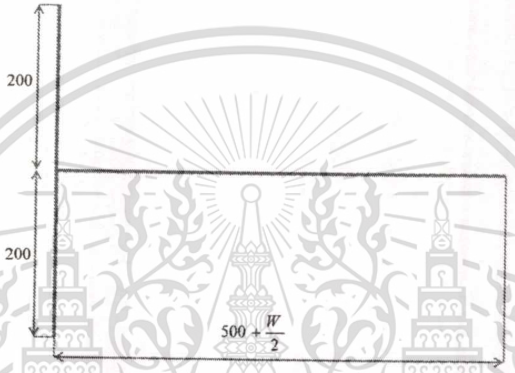

Figure 3.9 Trial model A.

3.3.3.2 Model B

Model B, Model C, and Model D consist of 2 types of element in this study. The first type is 2-node beam element with 6 DOFs at each node. The other type of element is 4-node shell element with 6 DOFs at each node. Shell elements are applied in the model to represent the square hollow section reinforcement. Shell thickness, which is represented by parameter "T", has to be specified to complete the definition of shell elements. Shell dimensional geometry is presented as shell throat shown in Figure 3.10. However, the shell throat and thickness of shell elements are different in each model.

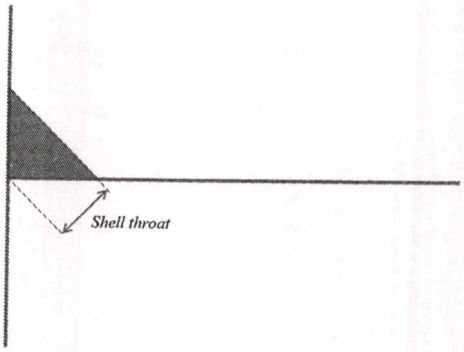

Figure 3.10 Shell throat.

The shell throat and the thickness of shell element in Model B are equal to width of square hollow section as shown in Figure 3.11.

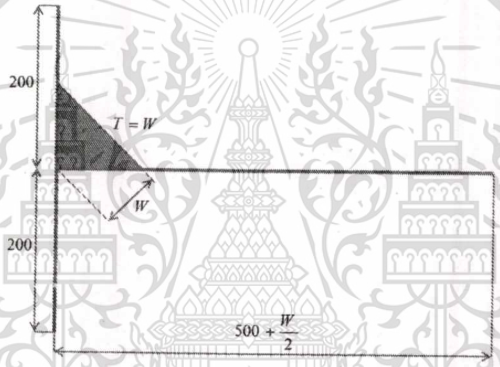

Figure 3.11 Model B.

3.3.3.3 Model C

The shell throat is equal to the width of square hollow section but the thickness of shell element in Model C is twice as much as thickness of square hollow section as shown in Figure 3.12.

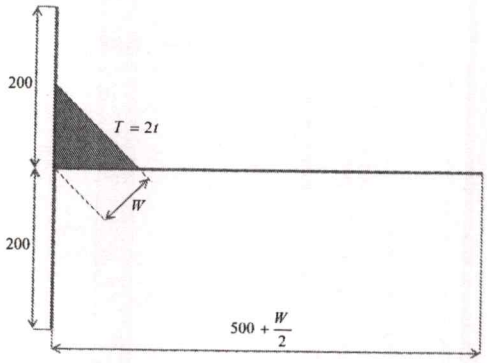

Figure 3.12 Model C.

3.3.3.4 Model D

The thickness of shell element in Model D is equal to the width of square hollow section. The edge of shell element is located along the axis of reinforced square hollow section as shown in Figure 3.12. The shell throat can be written in Equation (3.6).

$$Shell\ throat = \frac{W}{2} + \frac{W}{2\sqrt{2}} \tag{3.6}$$

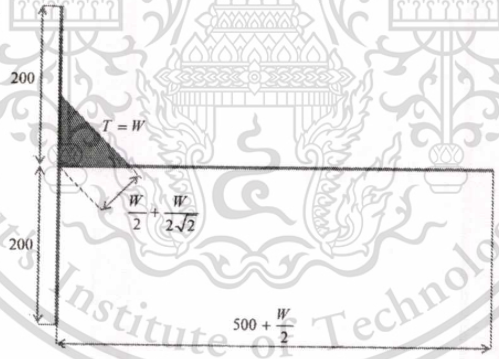

Figure 3.13 Model D.

3.4 Stiffness

3.4.1 Simplified stiffness matrix

Only one trial model from four trial models in the previous section is selected as the selected geometric model. Stiffness is the resistance of deformation in elastic structure to respond to applied loads. Thus, stiffness can be use as an indicator that shows how trial model behaviors

like the reference model. Ideally, the structural behavior of the selected geometric model must be equivalent to that of the reference model as shown in Figure 3.14. However, it is difficult to evaluate the stiffness of all nodes because there are a lot of nodes in the finite element models. Thus, some nodes at the boundary are used to evaluate the simplified stiffness that represents the behavior of the entire model. Only in-plane loads were studied in this work. Equation (3.7) presents the simplified stiffnesses in the stiffness matrix. The simplified stiffness matrices are determined using Equation (3.8) and Equation (3.10) which are basic equations for finite element analysis when displacement and rotation are applied at the boundary of the model. Nine cases of the node translation in x axis, the node translation in y axis, and the node rotation in z axis at the each end of beam were selected to represent the behavior of trial models as shown in Figure 3.15. All simplified stiffnesses of each trial model types and reference model are calculated by using FEA. The simplified stiffnesses of trial models are compared to the simplified stiffness of reference model in order to evaluate the selected geometric model.

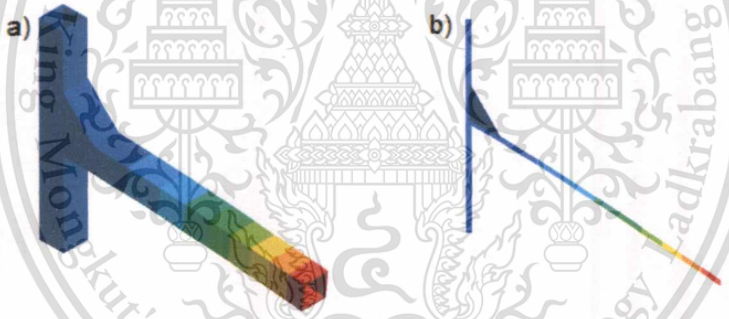

Figure 3.14 a) Solid element model's behavior under bending load;
b) beam element model's behavior under bending load.

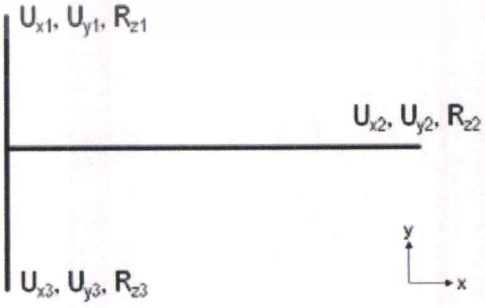

Figure 3.15 Selected nodals at the boundary.

$$[K]=\begin{bmatrix} K_{11} & K_{12} & K_{13} & \cdots & K_{19} \\ K_{21} & & & & \\ K_{31} & & \ddots & & \vdots \\ \vdots & & & & \\ K_{91} & & \cdots & & K_{99} \end{bmatrix} \tag{3.7}$$

$$\begin{bmatrix} F_{x1} \\ F_{y1} \\ M_{z1} \\ F_{x2} \\ F_{y2} \\ M_{z2} \\ F_{x3} \\ F_{y2} \\ M_{z3} \end{bmatrix} = \begin{bmatrix} K_{11} & K_{12} & K_{13} & \cdots & K_{19} \\ K_{21} & & & & \\ K_{31} & & \ddots & & \vdots \\ \vdots & & & & \\ K_{91} & & \cdots & & K_{99} \end{bmatrix} \begin{bmatrix} U_{x1} \\ U_{y1} \\ R_{z1} \\ U_{x2} \\ U_{y2} \\ R_{z2} \\ U_{x3} \\ U_{y2} \\ R_{z3} \end{bmatrix} \tag{3.8}$$

Where $[K]$ is a simplified stiffness matrix.

F is force reaction.

M is moment reaction.

U is displacement apply.

R is rotation apply.

Subscribe of x,y, and z are the direction.

Subscribe of 1, 2, and 3 are the location of the end of beam steel.

Equation (3.8) can be abbreviated into Equation (3.9)

$$[F]=[K][U] \tag{3. 9}$$

$$[K]=[F][U]^{-1} \tag{3.10}$$

Where $[F]$ is a load matrix.

$[U]$ is a displacement matrix.

3.4.2 Stiffness error function

The simplified stiffnesses of trial models were compared to the simplified stiffnesses of reference model by using the stiffness error function. Equation (3.11) is defined to represent the deviation of the node stiffness at the joint boundaries in trial model from those in reference model. The stiffness error represents the summation of node stiffness deviations. The stiffness errors of the joint between reference solid element model and trial models are calculated using Equation (3.12).

$$ERR_{ij} = \frac{K_{s,ij} - K_{t,ij}}{K_{s,ij}} \times 100\,\% \tag{3.11}$$

$$ERR = \frac{\left[\sum \left(ERR_{ij}\right)^2\right]^{1/2}}{n} \tag{3.12}$$

Where $[K]_s$ is stiffness matrix of reference model.

$[K]_t$ is stiffness matrix of trial model.

$K_{s,ij} \in [K]_s$; i, j = 1,2,3,…,9

$K_{s,ij} \in [K]_s$; i, j = 1,2,3,…,9

ERR_{ij} is stiffness error of trail model.

ERR is stiffness error function.

n is number of member of stiffness matrix

3.4.3 Analysis of variance (ANOVA)

Analysis of variance (ANOVA), which is one of statistical methods, has been developed for hypothesis test involving more than two averages. The purpose of ANOVA is to determine the existence of a statistically significant difference among several group means. ANOVA has been applied in many fields such as psychology, business administration, and engineering. ANOVA has also found in many engineering applications such as parameter optimization. In finite element, many parameters applied uncertainly effect to the analysis results. For example, Fazilat H. Dar [26] used ANOVA to determine the factor level of material properties and geometry to minimize the stress results in finite element model of the beam. In this study, ANOVA was applied to detect the significant difference for variance of stiffness error due to the thickness of square hollow section, the width of square hollow section, and trial models.

The Null hypothesis (H_0) says that all the group population means are equal. The hypothesis of equal means implies that the populations have the same normal distribution and equal variance. The alternate hypothesis (H_a) is that at least one pair of means is different.

$$H_0 : \mu_1 = \mu_2 = \mu_3 = \ldots = \mu_k \tag{3.13}$$

H_a : At least two of the group means $\mu_1, \mu_2, \mu_3, \ldots, \mu_k$ are not equal (3.14)

Where $\mu_i, i = 1,2,3,\ldots k$ are the group population means.

To start ANOVA test, degree of freedom (d.f.), sum of square (SS), and mean square (MS) are calculated by the following equations.

$$SS_{between} = \sum_{i=1}^{k} n_i (x_i - \bar{x})^2 \tag{3. 15}$$

$$SS_{within} = \sum_{i=1}^{k} \sum_{j=1}^{n_i} (x_{ij} - \bar{x}_i)^2 \tag{3.16}$$

$$SS_{tot} = \sum_{i=1}^{k} \sum_{j=1}^{n_i} (x_{ij} - \bar{x})^2 \tag{3.17}$$

Where $SS_{between}$ is sum of square representing variation between group means.

SS_{within} is sum of square representing variation within group means.

SS_{tot} is sum of squares total.

$$d.f._{between} = k - 1 \tag{3.18}$$

$$d.f._{within} = n - k \tag{3.19}$$

$$d.f._{tot} = n - 1 \tag{3.20}$$

Where $d.f._{between}$ is the degree of freedom between groups.

$d.f._{within}$ is the degree of freedom within group.

$d.f._{tot}$ is the total degree of freedom. k is number of group.

n is number of sample.

$$MS_{between} = \frac{SS_{between}}{d.f._{between}} \tag{3.21}$$

$$MS_{within} = \frac{SS_{within}}{d.f._{within}} \tag{3.22}$$

Where $MS_{between}$ is the mean square of variance between groups.

MS_{within} is the mean square of variance within group.

The ANOVA test depends on the fact that $MS_{between}$ can be influenced by population differences among means of several groups. Since MS_{within} compares values of each group to its own group mean, the fact that group means might be different does not affect MS_{within}.

The null hypothesis says that all groups are samples from population having same normal distribution the alternative hypothesis says that at least two of the sample groups come from population with different normal distributions. F-statistic has to be estimated to complete the ANOVA test. F is a ratio of $MS_{between}$ and MS_{within} presented in Equation (3.23). If the hypothesis is true, the F-ratio should be approximately equal 1. F-ratio is used to evaluate the probability which is compared to the probability from F-statistic table. Confident interval of 95% (α =95%) is normally used to identify the significant difference among several group means by using F-statistic. The null hypothesis are rejected when the probability is less than 5% , which is the summation of 2.5% on the left side and 2.5% on the right side of the normal distribution, as shown in Figure 3.16. Table 3.3 shows ANOVA summary.

$$F = \frac{MS_{betweem}}{MS_{within}} \tag{3.23}$$

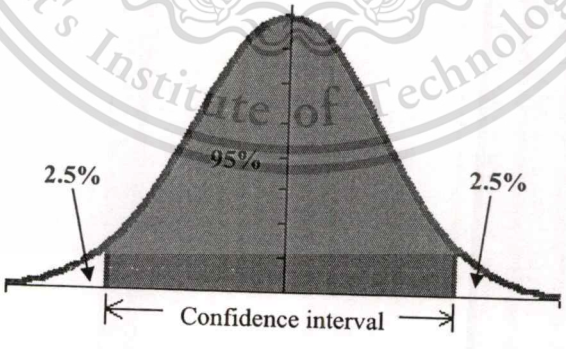

Figure 3.16 Confidence interval of 95%.

Table 3.3 ANOVA summary.

Source	SS	d.f.	MS	F	Prob>F
Between group	$\sum_{i=1}^{k} n_i (x_i - \bar{x})^2$	$k-1$	$\frac{SS_{between}}{d.f._{between}}$	$\frac{MS_{betweem}}{MS_{within}}$	≥1-α
Within Group	$\sum_{i=1}^{k}\sum_{j=1}^{n_i} (x_{ij} - \bar{x}_i)^2$	$n-k$	$\frac{SS_{within}}{d.f._{within}}$		
Total	$\sum_{i=1}^{k}\sum_{j=1}^{n_i} (x_{ij} - \bar{x})^2$	$n-1$			

3.5 Load and Boundary Conditions for Stress Analysis

The stiffness of the selected geometric model is not only are close to the stiffness of the reference solid element model, but the stresses occurred in the selected model must be also equivalent to those in the reference model in order to complete the requirement of the simplified model. The stress correction factor is a factor to correct the stress of the selected model. The stress correction factors were determined by the reference model and the selected model using stress analysis under structural load. Four cases of in-plane loads were applied in this study.

3.5.1 In-plane tension load case

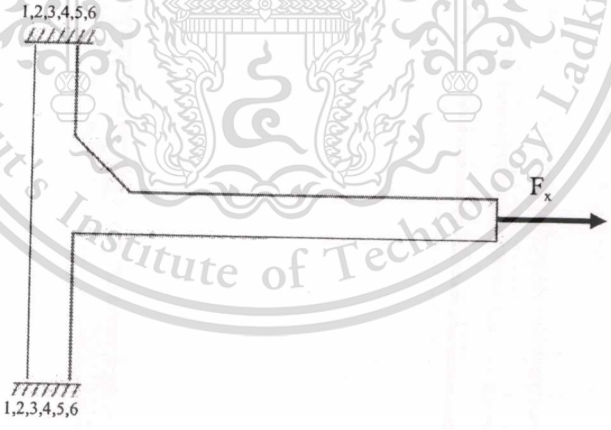

Figure 3.17 In-plane tension load.

Two ends of vertical beam are fix support. Force was applied at the end of horizontal beam as a tension load as shown in Figure 3.17.

3.5.2 In-plane bending load case

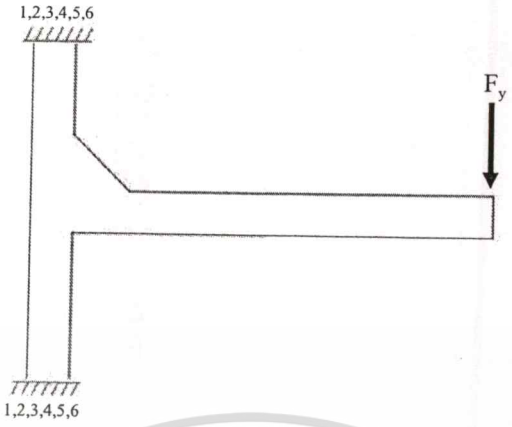

Figure 3.18 In-plane bending load.

Two ends of vertical beam are fix support. Force was applied at the end of horizontal beam as a bending load as shown in Figure 3.18.

3.5.3 In-plane moment load case

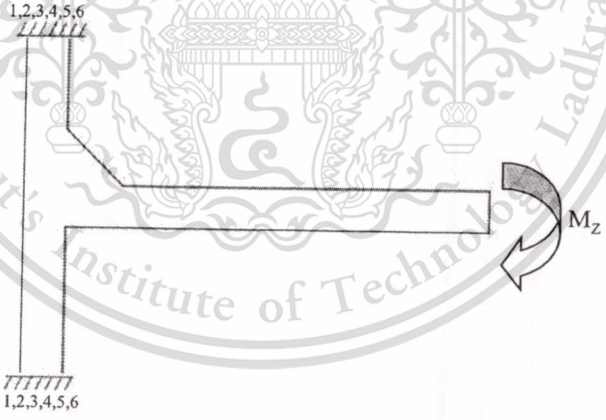

Figure 3.19 In-plane bending load.

Two ends of vertical beam are fix support. Moment was applied at the end of horizontal beam in z-direction as shown in Figure 3.19.

3.5.4 In-plane combined load case

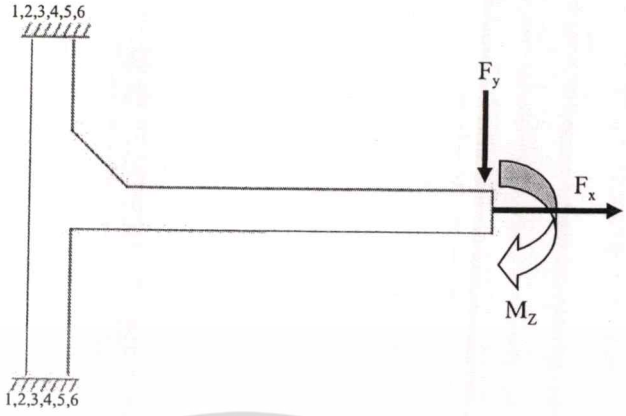

Figure 3.20 In-plane moment load.

Two ends of vertical beam are fix support. Tension load, bending load, and moment were applied at the end of horizontal beam as combined loads as shown in Figure 3.20.

3.6 Principle Stress

The normal and shear stresses depend on the orientation of the planes on which these stresses act. In engineering practice, distribution of the stress field around any points has to be analyzed. It is important to determine the orientation of the planes that causes the maximum and the minimum of normal stress and the orientation of planes that causes the maximum shear stress. These normal stresses are called principle stresses, and the corresponding planes on which they act are called principle planes of stress. The principal stresses of any points are determined by normal and shear stresses in given coordinate system as shown in Figure 3.21. For 2-dimensional stress state, the principal stresses can be determined by using Equation (3.24) to Equation (3.26)

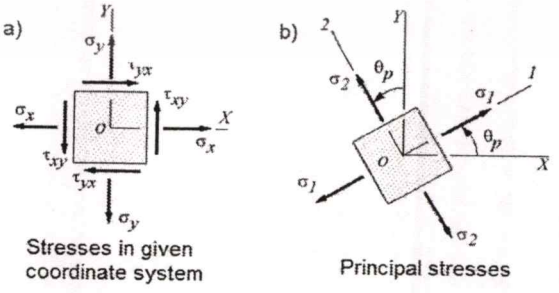

Figure 3.21 a) Normal and shear stresses in given coordinate system; b) Principle stresses

$$\sigma_1 = \left(\frac{\sigma_x + \sigma_y}{2}\right) + \sqrt{\left(\frac{\sigma_x - \sigma_y}{2}\right)^2 + \tau_{xy}^2} \tag{3.24}$$

$$\sigma_2 = \left(\frac{\sigma_x + \sigma_y}{2}\right) - \sqrt{\left(\frac{\sigma_x - \sigma_y}{2}\right)^2 + \tau_{xy}^2} \tag{3.25}$$

$$\tan\varphi = \frac{2\tau_{xy}}{\sigma_x + \sigma_y} \tag{3.26}$$

Where σ_x is a normal stress in x direction.

σ_y is a normal stress in y direction.

τ_{xy} is a shear stress in xy direction.

σ_1 is a first principal stress.

σ_2 is a second principal stress.

φ is the angle between first principal stress and normal stress in x direction.

3.7 Hot Spot Stress Surface Extrapolation

In this study, hot spot stress was determined by quadratic extrapolation because it is generally used for the thin hollow section. In addition, quadratic extrapolation is applied in case of a stiff attachment where steep stress gradient occurred [8]. The crack is initiated when the maximum normal stress exceeds the local yield of the material. According to previous section, the maximum normal stress is first principle stress. The first principal stresses at the reference points were collected to evaluate quadratic hot spot stress extrapolation. The crack was found at intersection between the reinforcement and the horizontal beam in the joint. There are two sides of surface that can be used for the surface extrapolation; reinforcement side and horizontal beam side as shown in Figure 3.22. According to the surface extrapolation, hot spot stress from the surface of reinforcement is higher than the hot spot stress from the surface of horizontal beam. So, hot spot stress was calculated on the surface of reinforcement. Figure 3.23 and Figure 3.24 show finite element meshing for reference model and selected model for the extrapolation.

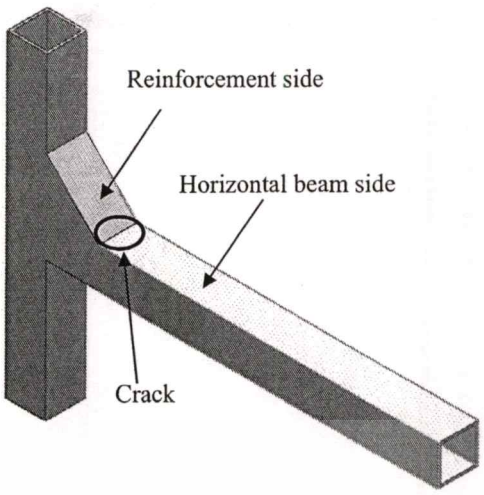

Figure 3.22 Surface extrapolation side.

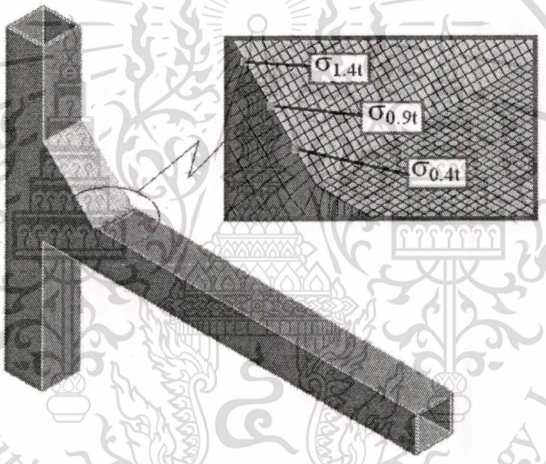

Figure 3.23 Finite element meshing detail of reference solid element model.

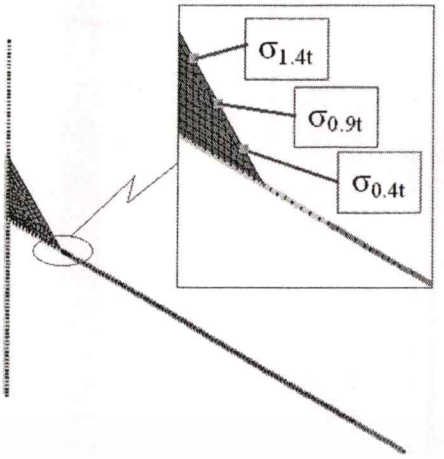

Figure 3.24 Finite element meshing detail of simplified model.

3.8 Stress Correction Factor

At the intersection between the reinforcement and the horizontal beam, high stresses were occurred in finite element analysis and cracks were found in the joint. Thus, the failure was assumed at this location in this study. The maximum stress of reference solid element model and selected geometric model were determined based on hot spot stress method on reinforced structures. The stress correction factors (K_f) are calculated based on maximum stresses of the two models by using Equation (3.27).

$$stress\ \ correction\ \ \ factor = \frac{\sigma_{HS,solid}}{\sigma_{HS,selected}} \tag{3.27}$$

Where $\sigma_{HS,solid}$ is a hot spot stress of reference solid element model.

$\sigma_{HS,simplified}$ is a hot spot stress of selected geometric model.

The stress correction factors can be calculated by the hot spot stresses based on the first principle stresses at reference points. Because the directions of first principle stress are depended on applied loads, the stress correction factors are also different for many cases of applied loads. So, the stress correction factors are calculated for different load cases.

3.8.1 Stress correction factors for single load case

In case when tension, bending, or moment load is applied individually, the directions of first principle stresses for all cases are different. After hot spot stresses of both the reference solid element and the selected model were determined, the stress correction factors of each load case were calculated by the Equation (3.27). Scatter data of SCFs were fit by polynomial regression using least square method.

3.8.2 Load-to-Stress factors for combined load case

In case of combined load, the stresses of all load cases have to be combined to evaluate the stress correction factors but the directions of first principle stresses are difference for each load cases. It causes difficult to combine the stresses. However, finite element analysis results do not only show the first principle stress but also show normal and shear stresses in Cartesian coordinate. The directions of those normal and shear stresses are exactly known that make it easy to combine those stress. Thus, superposition concept was applied to combined normal stresses and shear stresses for the same directions. Superposition concept is the vector sum of individual direction as shown in Figure 3.25.

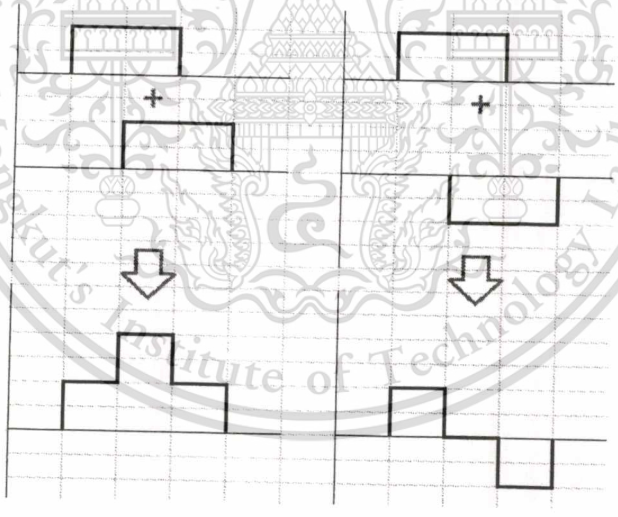

Figure 3.25 Superposition concept.

As shown in Figure 3.26, the normal stresses and shear stresses of selected model and reference solid element model at extrapolation points; 0.4t, 0.9t, and 1.4t, away from weld toe are calculated under one unit load. Those stresses are called unit stresses that are determined under

three unit load cases; tension (f_x), bending (f_y), and moment load (m_z). The stress correction factors are calculated from unit normal stresses and unit shear stresses. The load-to-stress factor (LTS) is defined as stress due to 1 unit load. The load-to-stress factors (LTSs) are determined by using multiplication between those stress correction factors and unit load stresses. The LTS are multiplied by the applied actual load (F_x, F_y, and M_z) to evaluate the normal stresses and shear stresses in the joint as shown in Equation (3.28).

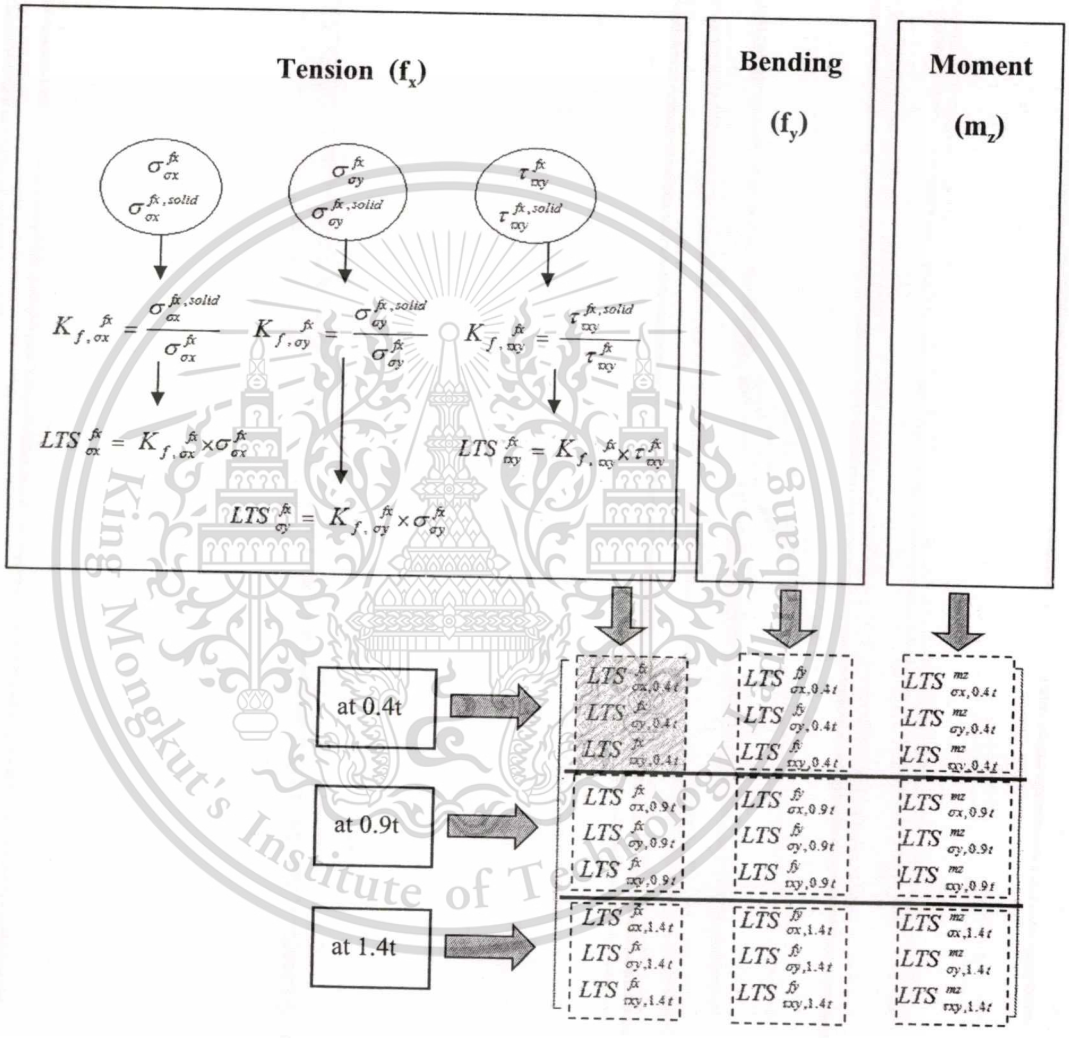

Figure 3.26 Flow work of LTS evaluation.

$$\begin{Bmatrix} \sigma_{x,0.4t} \\ \sigma_{y,0.4t} \\ \tau_{xy,0.4t} \\ \sigma_{x,0.9t} \\ \sigma_{y,0.9t} \\ \tau_{xy,0.9t} \\ \sigma_{x,1.4t} \\ \sigma_{y,1.4t} \\ \tau_{xy,1.4t} \end{Bmatrix} = \begin{bmatrix} LTS^{\ fx}_{\sigma x,0.4t} & LTS^{\ fy}_{\sigma x,0.4t} & LTS^{\ mz}_{\sigma x,0.4t} \\ LTS^{\ fx}_{\sigma y,0.4t} & LTS^{\ fy}_{\sigma y,0.4t} & LTS^{\ mz}_{\sigma y,0.4t} \\ LTS^{\ fx}_{\tau xy,0.4t} & LTS^{\ fy}_{\tau xy,0.4t} & LTS^{\ mz}_{\tau xy,0.4t} \\ LTS^{\ fx}_{\sigma x,0.9t} & LTS^{\ fy}_{\sigma x,0.9t} & LTS^{\ mz}_{\sigma x,0.9t} \\ LTS^{\ fx}_{\sigma y,0.9t} & LTS^{\ fy}_{\sigma y,0.9t} & LTS^{\ mz}_{\sigma y,0.9t} \\ LTS^{\ fx}_{\tau xy,0.9t} & LTS^{\ fy}_{\tau xy,0.9t} & LTS^{\ mz}_{\tau xy,0.9t} \\ LTS^{\ fx}_{\sigma x,1.4t} & LTS^{\ fy}_{\sigma x,1.4t} & LTS^{\ mz}_{\sigma x,1.4t} \\ LTS^{\ fx}_{\sigma y,1.4t} & LTS^{\ fy}_{\sigma y,1.4t} & LTS^{\ mz}_{\sigma y,1.4t} \\ LTS^{\ fx}_{\tau xy,1.4t} & LTS^{\ fy}_{\tau xy,1.4t} & LTS^{\ mz}_{\tau xy,1.4t} \end{bmatrix} \begin{Bmatrix} F_x \\ F_y \\ M_z \end{Bmatrix} \tag{3.28}$$

3.8.3 Curve fitting

Curve fitting is used in many applications such as in engineering. Some engineering data is poorly represented by a straight line; nonlinear curve is suitable to fit the data [27] as shown in Figure 3.27. Polynomial regression fits a nonlinear relationship between the independent variable and the dependent variable using least square method. In general, polynomial regression model of nth order can be described as Equation (3.29). The coefficients of unknowns can be calculated from the observed data.

$$yf_i = a_0 + a_1 x + a_2 x^2 + \ldots + a_n x^n \tag{3.29}$$

Where yf_i is nth-order polynomial curve fitting.

$a_0, a_1, a_2, \ldots, a_n$ are the coefficients of nth-order polynomial curve fitting.

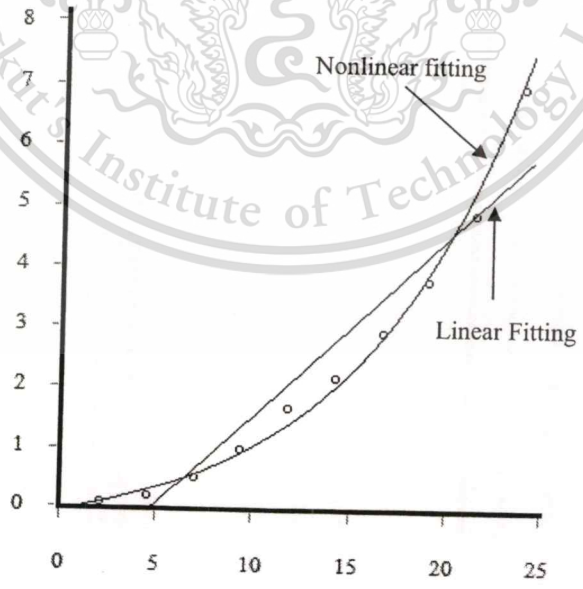

Figure 3.27 Linear fit and nonlinear fit.

The following equation represents 2nd-order [27]. There are three coefficients of the unknowns; a_0, a_1 and $a_2$that can be calculated directly from the observed data.

$$(n)a_0 + \left(\sum x_i\right)a_1 + \left(\sum x_i^2\right)a_2 = \sum y_i \tag{3.30}$$

$$\left(\sum x_i\right)a_0 + \left(\sum x_i^2\right)a_1 + \left(\sum x_i^3\right)a_2 = \sum x_i y_i \tag{3.31}$$

$$\left(\sum x_i^2\right)a_0 + \left(\sum x_i^3\right)a_1 + \left(\sum x_i^4\right)a_2 = \sum x_i^2 y_i \tag{3.32}$$

Where All summations are from i=1 through n.

n is size of sample.

Equation (3.30) to Equation (3.32) can be abbreviated in form of matrix as shown in Equation (3.33)

$$\begin{bmatrix} n & \sum x_i & \sum x_i^2 \\ \sum x_i & \sum x_i^2 & \sum x_i^3 \\ \sum x_i^2 & \sum x_i^3 & \sum x_i^4 \end{bmatrix} \begin{Bmatrix} a_0 \\ a_1 \\ a_2 \end{Bmatrix} = \begin{Bmatrix} \sum y_i \\ \sum x_i y_i \\ \sum x_i^2 y_i \end{Bmatrix} \tag{3.33}$$

However, there are some errors (e) between raw data and curve fitting as shown in Equation (3.34). The correlation coefficient (R) and the coefficient of determination (R^2) indicate the goodness of curve fitting. Correlation coefficient (R) of 1 represents a perfect fit of the scatter data. Sum of square error (S_r) and sum of sum of the squares (S_t) presented in Equation (3.35) and Equation (3.36) are used to calculate correlation coefficient in Equation (3.37). The strong relationship is not enough to conclude the relationship between the variables. T-test has to be used to evaluate the significant of relationship. The t score can be calculated using Equation (3.38) where n is a size of sample. Calculated t score (t) is compared to critical t score (t_{cri}) from the t distribution table where probability is 0.05 and degree of freedom (d.f.) is n-2. The relationship between the variables will be significant when calculated t value is greater than critical t score.

$$y = a_0 + a_1 x + a_2 x^2 + \ldots + a_n x^n + e \tag{3.34}$$

$$S_r = \sum_{i=1}^{n} e^2 = \sum_{i=1}^{n} (y_i - yf_i)^2 \tag{3.35}$$

$$S_t = \sum_{i=1}^{n} \left(y_i - \bar{y}\right)^2 \tag{3.36}$$

$$R = \sqrt{\frac{S_t - S_r}{S_t}} \tag{3.37}$$

$$t = R\sqrt{\frac{n-2}{1-R^2}} \tag{3.38}$$

Curve fitting is use to construct the parametric equations from observed scatter data in case of single load case. The constructed curve fit the data between the ratios of thickness to width of square hollow section and stress correction factors.

3.8.4 Surface fitting

Not only curve fitting, surface fitting are used in many applications. Polynomial surface fitting is applied in case of two independent variables and one dependent variable. Polynomial surface of n^{th}-order polynomial surface is determined by using the method of least square through data points. Equation (3.39) represents the 2^{nd}-order surface fitting as shown in Figure 3.28.

$$z = a_0 + a_2 x + a_3 y + a_4 x^2 + a_5 xy + a_6 y^2 \tag{3.39}$$

Where z is 2^{th} –order polynomial surface fitting.

$a_0, a_1, a_2, \ldots, a_n$ are the coefficients of n^{th}-order polynomial surface fitting.

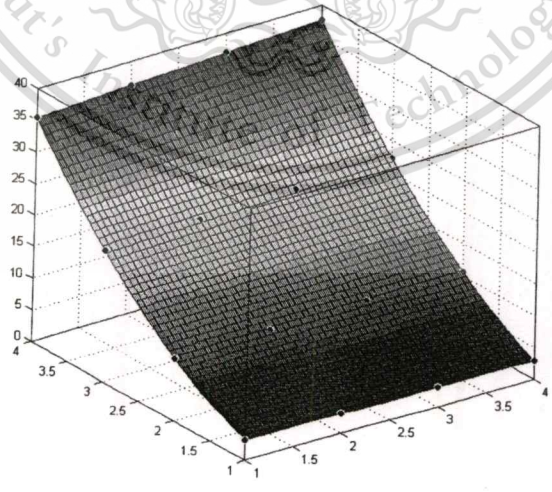

Figure 3.28 Surface fitting.

To define the surface fit, six coefficients; a_0, a_1, a_2, a_3, a_4 ,a_5 ,and a_6 have to be determined with the same process as curve fitting [28] using Equation (3.40).

$$\begin{bmatrix} n+1 & \sum x_i & \sum y_i & \sum x_i^2 & \sum x_i y_i & \sum y_i^2 \\ \sum x_i & \sum x_i^2 & \sum x_i y_i & \sum x_i^3 & \sum x_i^2 y_i & \sum x_i y_i^2 \\ \sum y_i & \sum x_i y_i & \sum y_i^2 & \sum x_i^2 y_i & \sum x_i y_i^2 & \sum y_i^3 \\ \sum x_i^2 & \sum x_i^3 & \sum x_i^2 y_i & \sum x_i^4 & \sum x_i^3 y_i & \sum x_i^2 y_i^2 \\ \sum x_i y_i & \sum x_i^2 y_i & \sum x_i y_i^2 & \sum x_i^3 y_i & \sum x_i^2 y_i^2 & \sum x_i y_i^3 \\ \sum y_i^2 & \sum x_i y_i^2 & \sum y_i^3 & \sum x_i^2 y_i^2 & \sum x_i y_i^3 & \sum y_i^4 \end{bmatrix} \begin{Bmatrix} a_0 \\ a_1 \\ a_2 \\ a_3 \\ a_4 \\ a_5 \end{Bmatrix} = \begin{Bmatrix} \sum z_i \\ \sum x_i z_i \\ \sum y_i z_i \\ \sum x_i^2 z_i \\ \sum x_i y_i z_i \\ \sum y_i^2 z_i \end{Bmatrix} \tag{3.40}$$

Where All the summations for i = 0 to n

CHAPTER 4

RESULT AND DISCUSSION

4.1 Stiffness Result

The Stiffnesses of trial models with various values of square hollow section thickness (t) and width (W) were compared to the stiffness of reference model. The results of stiffness errors, as defined in section 3.4.2, for Model A, Model B, Model C, and Model D are summarized in Table 4.1.

Table 4.1 Stiffness error

W (mm.)	T (mm.)	Stiffness error (%)			
		Model A	Model B	Model C	Model D
60	5	9.237	6.703	6.989	7.676
60	4	13.308	13.162	12.935	13.186
60	3	14.180	12.607	12.954	13.389
60	2	12.000	11.467	11.137	11.285
50	5	8.050	6.894	7.010	7.052
50	4	7.564	6.308	6.472	6.594
50	3	8.183	6.255	5.714	8.408
50	2	13.524	12.087	11.859	12.868
40	5	8.905	4.840	5.637	6.820
40	4	8.329	4.507	5.014	6.196
40	3	9.738	5.949	5.428	6.237
40	2	19.410	16.064	15.480	14.752
30	5	7.243	4.696	5.308	5.776
30	4	7.359	4.671	5.250	5.947
30	3	7.612	4.569	5.154	6.126
30	2	7.964	4.364	5.002	6.201
	sum	162.605	125.143	127.351	138.514
	avg	10.163	7.821	7.959	8.657
	SD	3.308	3.736	3.465	3.122

The statistical method was used to analyze all the stiffness errors. The analysis of variance (ANOVA) is utilized in order to detect significant differences for variance of the stiffness error due to W, t, and model type. The results of ANOVA for stiffness error variation with 95% confidence interval are presented in Table 4.2. The results showed that model type (p-value = 0.0243), as well as SHS beam width (p-value = 2.43×10^{-7}) and SHS beam thickness (p-valve = 2.53×10^{-6}), had a significant effect on the stiffness error. However, the results did not indicate a significant difference in the stiffness error due to different models.

Table 4.2 ANOVA table for Model A, Model B, Model C, and Model D

Source	SS	d.f.	MS	F	Prob>F
W	249.730	3	83.243	15.340	2.43×10^{-7}
t	203.657	3	67.886	12.510	2.53×10^{-6}
Model type	55.232	3	18.411	3.390	0.0243
Error	293.025	54	5.426		
Total	801.644	63			

In order to determine if there is a significant difference in stiffness errors due to different models, ANOVA applied to each pair of models was used in the analysis. It was found in all cases that W and t significantly affect the stiffness error. In addition, the stiffness error of Model A was significantly different from those of Model B, Model C, and Model D as shown in Table 4.3-Table 4.5 (p-value of model < 0.05). However, it was found that there was no significant effect on stiffness error by changing model types among Model B, Model C, and Model D as shown in Table 4.6-Table 4.8 (p-valve of model > 0.05).

Table 4.3 ANOVA table for Model A and Model B

Source	SS	d.f.	MS	F	Prob>F
W	127.891	3	42.631	6.540	0.0022
t	113.971	3	37.991	5.830	0.0039
Model type	43.856	1	43.856	6.730	0.0159
Error	156.509	24	6.521		
Total	442.227	31			

Table 4.4 ANOVA table for Model A and Model C

Source	SS	d.f.	MS	F	Prob>F
W	115.389	3	38.463	6.190	0.0029
t	102.661	3	34.220	5.510	0.0050
Model type	38.839	1	38.839	6.250	0.0196
Error	149.123	24	6.213		
Total	406.012	31			

Table 4.5 ANOVA table for Model A and Model D

Source	SS	d.f.	MS	F	Prob>F
W	98.190	3	98.190	5.700	0.0043
t	55.085	3	55.085	3.200	0.0415
Model type	34.710	1	34.710	6.040	0.0216
Error	137.842	24	5.7434		
Total	325.827	31			

Table 4.6 ANOVA table for Model B and Model C

Source	SS	d.f.	MS	F	Prob>F
W	149.772	3	49.924	7.590	0.0010
t	107.743	3	35.914	5.460	0.0053
Model type	0.152	1	0.152	0.020	0.8804
Error	157.922	24	6.580		
Total	415.589	31			

Table 4.7 ANOVA table for Model B and Model D

Source	SS	d.f.	MS	F	Prob>F
W	143.991	3	47.997	8.400	0.0005
t	58.259	3	19.420	3.400	0.0341
Model type	0.534	1	0.534	0.090	0.7624
Error	137.131	24	5.714		
Total	339.915	31			

Table 4.8 ANOVA table for Model C and Model D

Source	SS	d.f.	MS	F	Prob>F
W	125.608	3	41.870	7.620	0.0010
t	90.489	3	30.163	5.490	0.0051
Model type	3.894	1	3.894	0.710	0.4083
Error	131.944	24	5.498		
Total	351.935	31			

However, from Table 4.1, Model B provides the minimum average stiffness error, which represents the deviation of trial model's stiffness from the reference solid model's stiffness. This model, therefore, is the most suitable for the specified ranges of W and t, to be used for further development of a selected geometric model. This selected model consists of beam elements and shell elements without weld geometry. Beam elements are positioned along neutral axes of hollow square beams. Cross sectional properties of beam steel has to be applied for the analysis. The thickness of shell elements is specified to be equal to the beam width. This is shown in Figure 4.1.

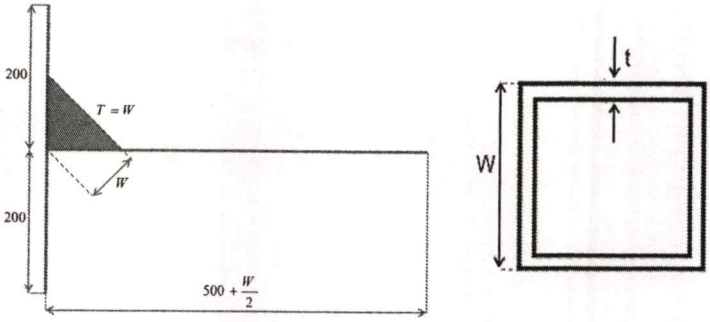

Figure 4.1 The selected geometric model.

4.2 Meshing

The stresses at extrapolation points are used to evaluate the hot spot stress. Meshing is sensitive to the stress results in finite element analysis. However, there is recommendation in IIW for model meshing. The recommendation is applied in this study. Moreover, the convergence of stress solutions for both reference solid element model and simplified model were checked. Meshes were refined at the extrapolation region of the models. Table 4.9 and Table.4.10 show the number of element and maximum first principle stress of reference solid element model and simplified model in case of 30 mm width and 5 mm thickness of square hollow section. In addition, those tables show the difference percentage between the number of element and maximum first principle stress. When the difference percentage is less than 5%, the number of element is suitable for meshing. Figure 4.9 and Figure 4.10 show convergence plot of the maximum first principle stress and number of reference solid element model and simplified model. When the difference percentage is less than 5 %, the data plot tends to be linear. It implies that there is a little difference of stress when the number of element is increased. The convergence plots are applied in every dimension of SHS in this study to select the suitable mesh.

Table 4.9 First principle stress difference of reference solid element model

No. of element	Maximum first principle stress	Difference percentage
175146	0.344	
187538	0.445	29.228%
207564	0.507	13.902%
237792	0.563	11.036%
260816	0.563	0.036%
294694	0.569	1.021%

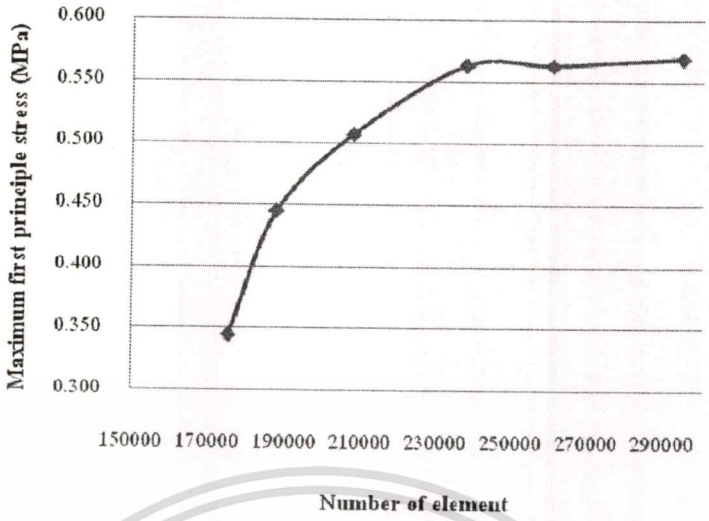

Figure 4.2 Convergence plot of reference solid element model

Table 4.10 First principle stress difference of simplified model

No. of element	Maximum first principle stress	Difference percentage
328	0.24774	
405	0.52129	110.418%
453	0.67455	29.400%
533	0.89878	33.241%
861	0.90227	0.388%

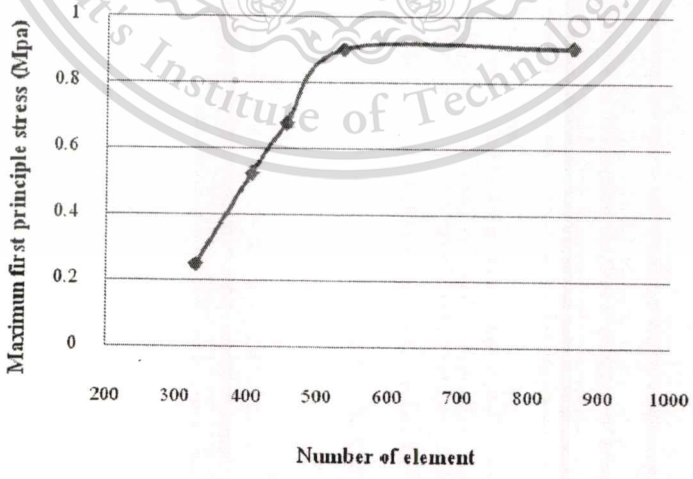

Figure 4.3 Convergence plot of simplified model

4.3 Tension Load

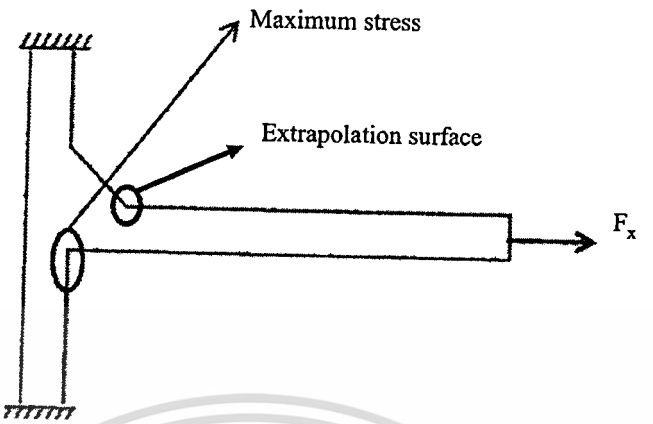

Figure 4.4 Maximum stress due to tension load.

In finite element analysis, the maximum stress is occurred at the intersection between the vertical beam and horizontal beam of the reference model and selected model as shown in Figure 4.4. However, the stress occurred at the intersection between reinforcement and horizontal beam is also high. The crack is also found at this location in reality as shown in section 3.7. Moreover, the maximum stresses are also assumed at the intersection between reinforcement and horizontal beam. Thus, the surface extrapolation hot spot stresses are determined at the reinforcement. Figure 4.5 presents the stress correction factors of square hollow section (SHS) T-joint as a function of thickness (t) for different beam width (W). Different lines represent different width of SHS. When the thickness is increased, the stress correction factor is decreased. Figure 4.6 presents the stress correction factors (K_t) of SHS T-joint a function of beam width (W) for different thickness (t). Different lines represent different thickness of SHS. The stress correction factor is increased while the thickness of the beam is increased. The stress correction factor in case of tension load is less than 1. This means that the stresses of simplified model are less than the stresses of reference solid element model.

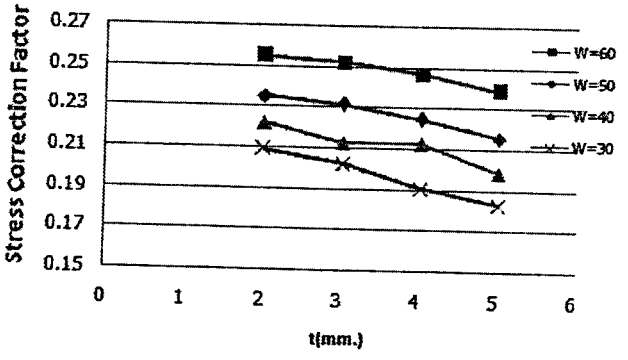

Figure 4.5 The stress correction factor of 2-5 mm thickness with different beam width under tension load.

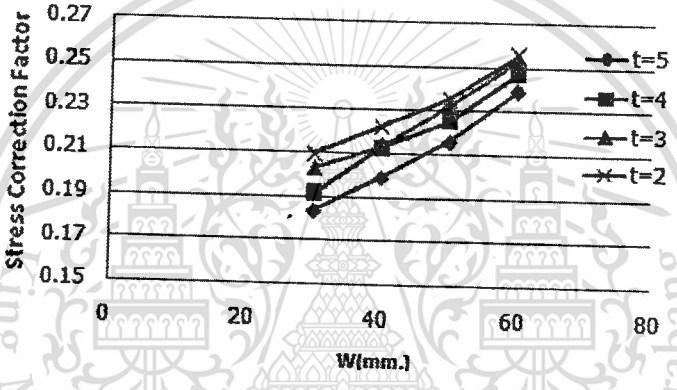

Figure 4.6 The stress correction factor of 50-30 mm beam width with different thickness under tension load.

Thicknesses-to-width ratio of hollow square beam is used to reduce the geometrical parameter to evaluate the stress correction factors (K_t). So, thicknesses to width ratio of hollow square beam are presented as a geometrical parameter of the stress correction factors. The ratio is varied between 1/6 and 1/30. The relationship between the stress correction factors and thicknesses to width ratio of hollow square beam is shown in Figure 4.7. Equation (4.1) presents the curve fitting equation by using regression method. Correlation analysis of the regression equation providing correlation coefficient (R) of 0.723 showed relationship between the stress correction factors and the thickness-to-width ratio of the joint. Moreover, the t score calculated by correlation coefficient is 7.1092, which is greater than critical t score (t_{cri}) of 2.1448. This

indicates the significance of the correlation between the stress correction factors and thickness-to-width ratio of the joint.

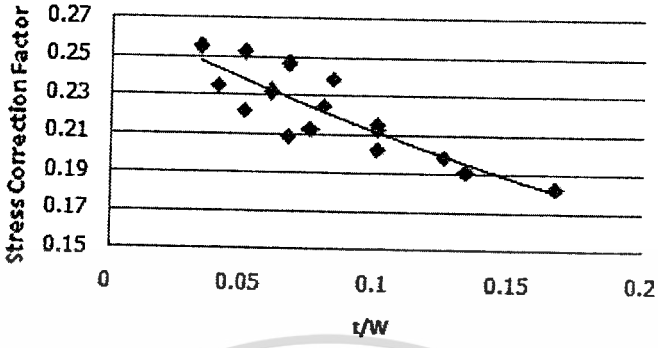

Figure 4.7 The stress correction factor and t/W under tension load.

$$K_{f,t/W}^{fx} = 0.679\left(\frac{t}{W}\right)^2 - 0.634\left(\frac{t}{W}\right) + 0.268 \tag{4.1}$$

4.4 Bending Load

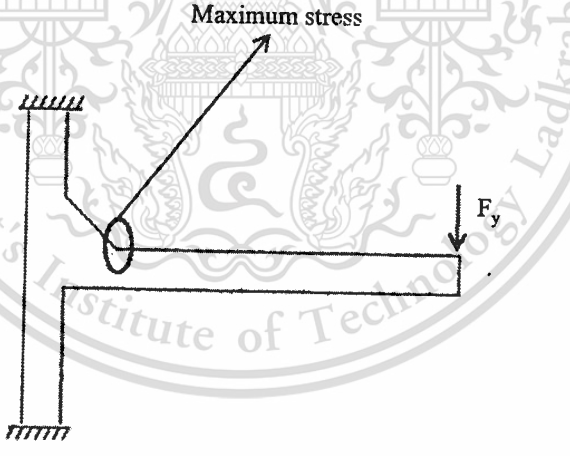

Figure 4.8 Maximum stress due to bending load.

Maximum stress occurs at the intersection between reinforcement and horizontal beam, where the discontinuity points are located on as shown in Figure 4.8. Figure 4.9 presents the stress correction factors (K_f) of square hollow section (SHS) T-joint as a function of thickness (t)

for different beam width (W). Different lines represent different width of SHS. When the thickness of the beam is increased, The stress correction factor is decreased. Figure 4.10 presents The stress correction factor of SHS T-joint as a function beam width (W) of for different thickness (t). Different lines represent different thickness of SHS. The stress correction factors are rapidly increased while the width is deceased.

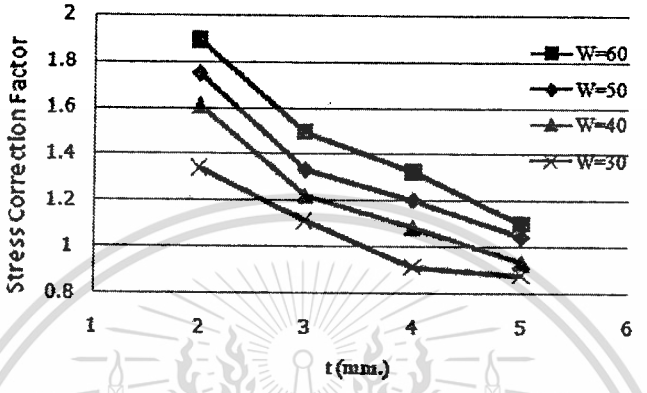

Figure 4.9 The stress correction factor of 2-5 mm thickness with different beam width under bending load.

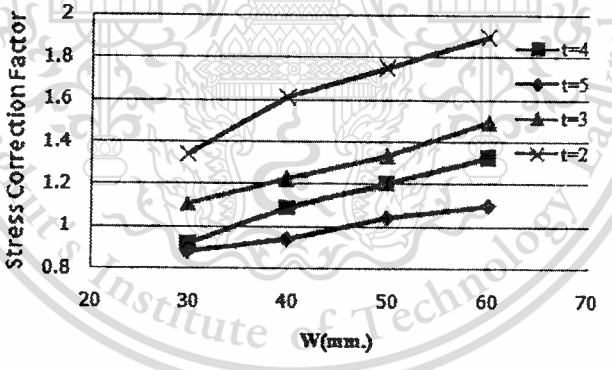

Figure 4.10 The stress correction factor of 50-30 mm beam width with different thickness under bending load.

Thicknesses-to-width ratio of hollow square beam is used to reduce the geometrical parameter to evaluate the stress correction factors (K_t). So, thicknesses to width ratio of hollow square beam are presented as a geometrical parameter of stress correction factors. The ratio is varied between 1/6 and 1/30. The relationship between stress correction factors and thicknesses to

width ratio of hollow square beam is shown in Figure 4.11. Equation (4.2) presents the curve fitting equation by using regression method. Correlation analysis of the regression equation providing correlation coefficient (R) of 0.970 showed relationship between the stress correction factors and the thickness-to-width ratio of the joint. Moreover, the t score calculated by correlation coefficient is 29.512, which is greater than critical t score (t_{cri}) of 2.1448. This indicates the significance of the correlation between the stress correction factors and thickness-to-width ratio of the joint.

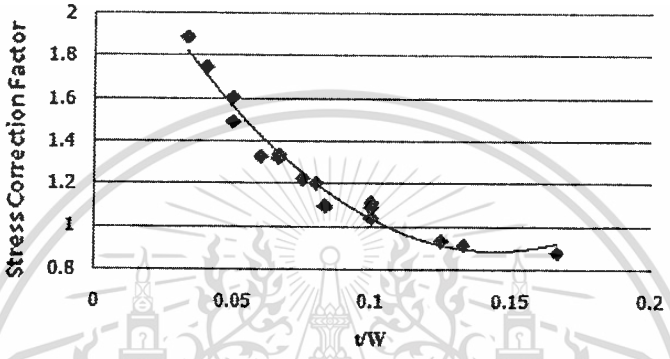

Figure 4.11 The stress correction factor and t/W under bending load.

$$K^{fy}_{f,t/W} = 75.870\left(\frac{t}{W}\right)^2 - 21.960\left(\frac{t}{W}\right) + 2.470 \quad (4.2)$$

4.5 Moment Load

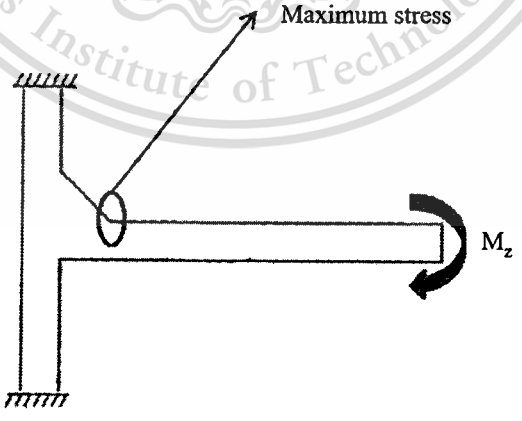

Figure 4.12 Maximum stress due to moment load.

Maximum stress occur the intersection between reinforcement and horizontal beam, where the discontinuity points are located on as shown in Figure 4.12. Figure 4.13 presents the stress correction factors (K_f) of square hollow section (SHS) T-joint as a function of thickness (t) for different beam width (W). Different lines represent different width of SHS. When the thickness is increased, the stress correction factor is decreased. Figure 4.14 presents the stress correction factors of SHS T-joint as a function of width for different beam thickness. Different lines represent different thickness of SHS. The stress correction factors are rapidly increased while the thickness is increased.

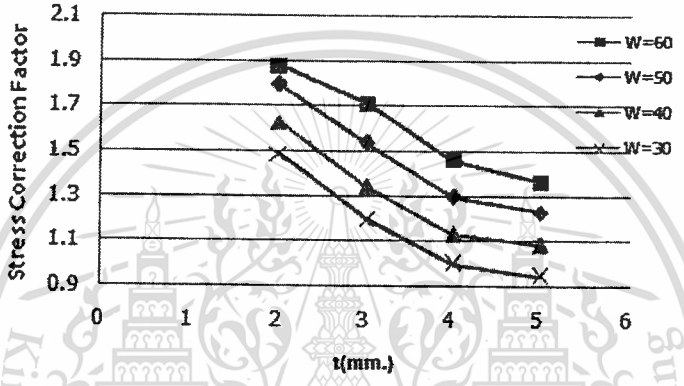

Figure 4.13 The stress correction factor of 2-5 mm thickness with different beam width under moment load.

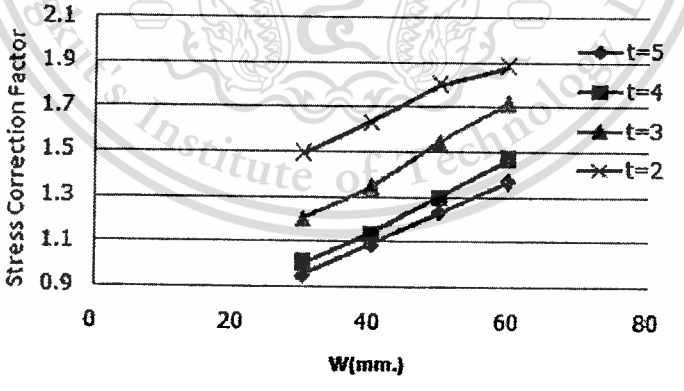

Figure 4.14 The stress correction factor of 50-30 mm beam width with different thickness under moment load.

Thicknesses-to-width ratio of hollow square beam is used to reduce the geometrical parameter to evaluate the SCF. So, thicknesses to width ratio of hollow square beam are presented as a geometrical parameter of SCF. The ratio is varied between 1/6 and 1/30. The relationship between SCFs and thicknesses to width ratio of hollow square beam is shown in Figure 4.15. Equation (4.3) presents the curve fitting equation by using regression method. Correlation analysis of the regression equation providing correlation coefficient (R) of 0.984 showed relationship between the SCFs and the thickness-to-width ratio of the joint. Moreover, the t score calculated by correlation coefficient is 72.3747, which is greater than critical t score (t_{cri}) of 2.1448. This indicates the significance of the correlation between SCFs and thickness-to-width ratio of the joint.

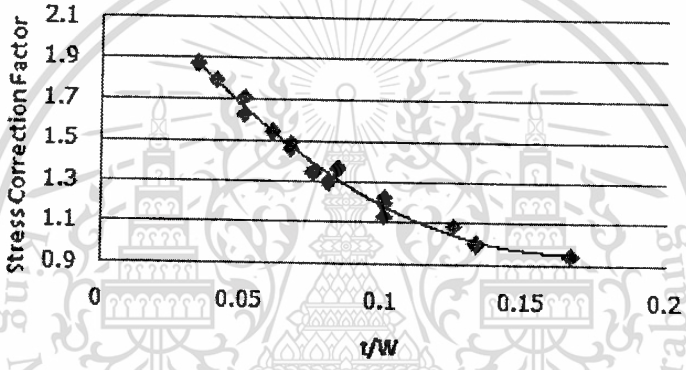

Figure 4.15 The stress correction factor and t/W under moment load.

$$K_{f,t/W}^{mz} = 52.080\left(\frac{t}{W}\right)^2 - 17.310\left(\frac{t}{W}\right) + 2.397 \tag{4.3}$$

4.6 Combined Load Case

4.6.1 σ_x, σ_y, and τ_{xy} of selected model due to unit tension load

In case of combined load, the concept of superposition is used to determine the stresses of selected model because the directions of first principle stress are varied due to applied loads. However, the directions of normal stresses and shear stress in Cartesian coordinate are exactly known. Those normal and shear stresses are plotted with the thickness and width of SHS as a 2nd-order polynomial surface fitting. Figure 4.16 shows the surface fitting of normal stresses in x axis (σ_x) of selected geometric model at the points of 0.4t due to one unit of tension load. All surface

fitting are shown in appendix B-1. All coefficients of determinations (R^2) of surface fitting presented in Table 4.11 are called good correlation, which is greater than 0.85. Moreover, the t scores are presented in Table 4.11 calculated by coefficients of determinations, which are greater than critical t score (t_{cri}) of 2.1448. This indicates the significance of the correlation between stress and studied geometry of square beams.

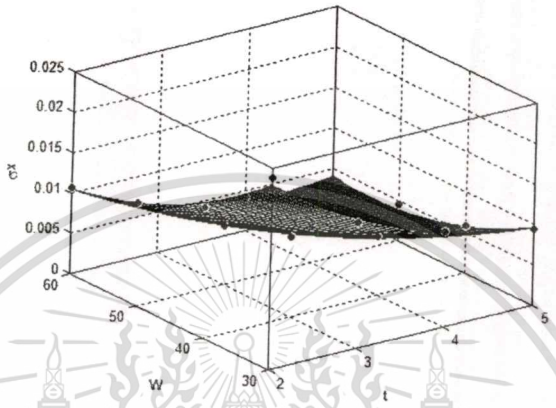

Figure 4.16 σ_x of selected geometric model due to tension load at 0.4t.

Table 4.11 Coefficient of determinations and t scores for unit tension load of surface fitting

Location	Stress	Coefficient of determination (R^2)	t
0.4t	σ_x	0.992	41.303
	σ_y	0.981	27.060
	τ_{xy}	0.987	33.043
0.9t	σ_x	0.981	27.046
	σ_y	0.988	34.230
	τ_{xy}	0.978	24.913
1.4t	σ_x	0.991	39.088
	σ_y	0.986	31.561
	τ_{xy}	0.980	26.020

All surface fitting equations can be shown in form of matrices. Equation (4.4) presents the parametric equation of normal stress and shear stress of selected geometric model due to tension load at the points of extrapolation.

$$\begin{Bmatrix} \sigma^{fx}_{x,0.4t} \\ \sigma^{fx}_{y,0.4t} \\ \tau^{fx}_{xy,.4t} \\ \sigma^{fx}_{x,0.9t} \\ \sigma^{fx}_{y,0.9t} \\ \tau^{fx}_{xy,0.9t} \\ \sigma^{fx}_{x,1.4t} \\ \sigma^{fx}_{y,1.4t} \\ \tau^{fx}_{xy,1.4t} \end{Bmatrix} = 10^{-3} \times \begin{bmatrix} 79.070 & -15.360 & -1.459 & 1.2320 & 0.07609 & 0.009901 \\ 45.310 & -4.810 & -1.143 & 0.3580 & 0.02479 & 0.009090 \\ -45.790 & 6.120 & 1.018 & -0.3935 & -0.03673 & -0.007574 \\ 46.870 & -7.35\ 0 & -1.020 & 0.3958 & 0.06691 & 0.006521 \\ 26.440 & -2.530 & -0.671 & 0.1264 & 0.02150 & 0.005030 \\ -31.430 & 4.030 & 0.760 & -0.2516 & -0.03131 & -0.005600 \\ 26.770 & -3.930 & -0.549 & 0.2013 & 0.03323 & 0.003372 \\ 22.870 & -2.900 & -0.540 & 0.1091 & 0.03444 & 0.003355 \\ -24.380 & 3.130 & 0.584 & -0.1595 & -0.02943 & -0.004083 \end{bmatrix} \begin{Bmatrix} 1 \\ t \\ W \\ t^2 \\ tW \\ W^2 \end{Bmatrix} \quad (4.4)$$

Equation (4.4) can be abbreviated into Equation (4.5).

$$\{\sigma\}_t = [k]_t \{G\} \quad (4.5)$$

Where $\{\sigma\}_t$ is stress matrix of selected model due to 1 unit tension load.

$[k]_t$ is stiffness matrix of selected model due to 1 unit tension load.

$\{G\}$ is geometry matrix.

4.6.2 σ_x, σ_y, and τ_{xy} of selected model due to unit bending load

Figure 4.17 shows the surface fitting of normal stresses in x axis (σ_x) of selected model at the points of 0.4t due to one unit of bending load. All surface fitting are shown in appendix B-2. All coefficients of determinations (R^2) of surface fitting presented in Table 4.12 are called good correlation, which is greater than 0.85. Moreover, the t scores are presented in Table 4.12 calculated by coefficients of determinations, which are greater than critical t score (t_{cri}) of 2.1448. This indicates the significance of the correlation between stress and studied geometry of square beams.

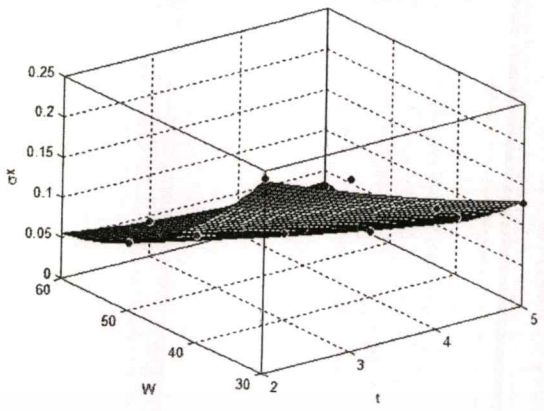

Figure 4.17 σ_x of selected geometric model due to bending load at 0.4t.

Table 4.12 Coefficient of determinations and t scores for unit bending load of surface fitting

Location	Stress	Coefficient of determination	t
0.4t	σ_x	0.986	31.961
	σ_y	0.973	22.479
	τ_{xy}	0.981	27.060
0.9t	σ_x	0.978	25.046
	σ_y	0.986	30.933
	τ_{xy}	0.959	18.048
1.4t	σ_x	0.970	21.215
	σ_y	0.991	39.088
	τ_{xy}	0.979	25.418

All surface fitting equations can be shown in form of matrices. Equation (4.6) presents the parametric equation of normal stress and shear stress of selected geometric model due to bending load at the points of extrapolation.

$$\begin{Bmatrix} \sigma^{fy}_{x,o.4t} \\ \sigma^{fy}_{y,o.4t} \\ \tau^{fy}_{xy,.4t} \\ \sigma^{fy}_{x,o.9t} \\ \sigma^{fy}_{y,o.9t} \\ \tau^{fy}_{xy,o.9t} \\ \sigma^{fy}_{x,1.4t} \\ \sigma^{fy}_{y,1.4t} \\ \tau^{fy}_{xy,1.4t} \end{Bmatrix} = 10^{-3} \times \begin{bmatrix} 885.10 & -86.97 & -23.15 & 3.008 & 0.9877 & 0.16750 \\ 764.30 & -76.98 & -20.84 & 5.577 & 0.5057 & 0.16870 \\ 501.50 & 27.76 & 14.53 & -0.290 & -0.3617 & -0.1148 \\ 642.10 & -67.56 & -16.14 & 0.257 & 1.0690 & 0.10190 \\ 436.00 & -42.91 & -11.15 & 1.872 & 0.4233 & 0.08161 \\ -470.10 & 44.67 & 13.18 & -1.524 & -0.5982 & -0.09661 \\ 594.40 & -91.93 & -13.61 & 3.939 & 1.0360 & 0.08299 \\ 369.20 & -51.79 & -8.39 & 2.607 & 0.5119 & 0.05299 \\ -319.60 & 26.62 & 8.58 & -0.278 & -0.3935 & -0.06076 \end{bmatrix} \begin{Bmatrix} 1 \\ t \\ W \\ t^2 \\ tW \\ W^2 \end{Bmatrix} \quad (4.6)$$

Equation (4.6) can be abbreviated into Equation (4.7).

$$\{\sigma\}_b = [k]_b \{G\} \quad (4.7)$$

Where $\{\sigma\}_b$ is stress matrix of selected model due to unit bending load.

$[k]_b$ is stiffness matrix of selected model due to unit bending load.

$\{G\}$ is geometry matrix.

4.6.3 σ_x, σ_y, and τ_{xy} of selected model due to unit moment load

Figure 4.18 shows the surface fitting of normal stresses in x axis (σ_x) of selected model at the points of 0.4t due to one unit of moment load. All surface fitting are shown in appendix B-3. All coefficients of determinations (R^2) of surface fitting presented in Table 4.13 are called good correlation, which is greater than 0.85. Moreover, the t scores are presented in Table 4.13 calculated by coefficients of determinations, which are greater than critical t score (t_{cri}) of 2.1448. This indicates the significance of the correlation between stress and studied geometry of square beams.

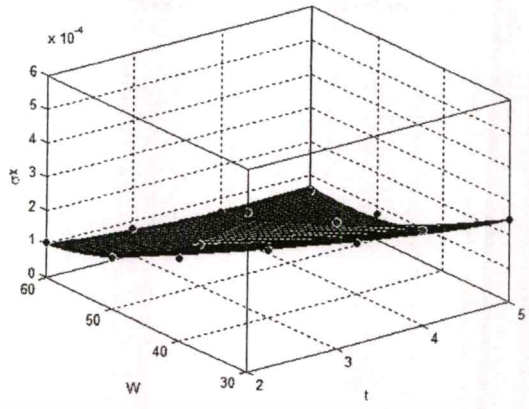

Figure 4.18 σ_x of selected geometric model due to moment load at 0.4t.

Table 4.13 Coefficient of determinations and t scores for unit moment load of surface fitting

Location	Stress (σ)	Coefficient of determination (R^2)	t
0.4t	σ_x	0.989	35.692
	σ_y	0.972	22.176
	τ_{xy}	0.978	24.953
0.9t	σ_x	0.976	23.871
	σ_y	0.962	18.888
	τ_{xy}	0.956	17.375
1.4t	σ_x	0.986	31.689
	σ_y	0.981	27.090
	τ_{xy}	0.969	20.996

All surface fitting equations can be shown in form of matrices. Equation (4.8) presents the parametric equation of normal stress and shear stress of selected geometric model due to moment load at the points of extrapolation.

$$\begin{Bmatrix} \sigma^{mz}_{x,o.4t} \\ \sigma^{mz}_{y,o.4t} \\ \tau^{mz}_{xy,.4t} \\ \sigma^{mz}_{x,o.9t} \\ \sigma^{mz}_{y,o.9t} \\ \tau^{mz}_{xy,o.9t} \\ \sigma^{mz}_{x,1.4t} \\ \sigma^{mz}_{y,1.4t} \\ \tau^{mz}_{xy,1.4t} \end{Bmatrix} = 10^{-4} \times \begin{bmatrix} 17.110 & -1.823 & -0.4424 & 0.0784 & 0.01947 & 0.003178 \\ 12.490 & -0.969 & -0.3507 & 0.0743 & 0.00447 & 0.002943 \\ -9.757 & 0.637 & 0.2800 & -0.0196 & -0.00716 & -0.002209 \\ 12.730 & -1.486 & -0.3163 & 0.0261 & 0.02152 & 0.001985 \\ 6.612 & -0.484 & -0.1680 & 0.0115 & 0.00528 & 0.001210 \\ -8.066 & 0.701 & 0.2267 & -0.0218 & -0.00964 & -0.001659 \\ 8.185 & -1.074 & -0.1824 & 0.0393 & 0.01152 & 0.001127 \\ 6.299 & -0.860 & -0.1407 & 0.0424 & 0.00851 & 0.008665 \\ -6.416 & 0.606 & 0.1715 & -0.0146 & -0.00829 & -0.001211 \end{bmatrix} \begin{Bmatrix} 1 \\ t \\ W \\ t^2 \\ tW \\ W^2 \end{Bmatrix} \tag{4.8}$$

Equation (4.8) can be abbreviated into Equation (4.9).

$$\{\sigma\}_m = [k]_m \{G\} \tag{4.9}$$

Where $\{\sigma\}_m$ is stress matrix of selected model due to 1 unit moment load.

$[k]_m$ is stiffness matrix of selected model due to 1 unit moment load.

$\{G\}$ is geometry matrix.

4.6.4 Stress correction factors due to tension load

The stress correction factors (K_t), as defined in 3.8, were determined by the normal and shear stresses of reference model and selected geometric model. Figure 4.19 shows surface fitting of stress concentration factors at the points the points of 0.4t due to tension load. All surface fitting are shown in appendix B-4. All coefficients of determinations (R^2) of surface fitting presented in Table 4.14 are called good correlation, which is greater than 0.85. Moreover, the t scores are presented in Table 4.14 calculated by coefficients of determinations, which are greater than critical t score (t_{cri}) of 2.1448. This indicates the significance of the correlation between stress and studied geometry of square beams.

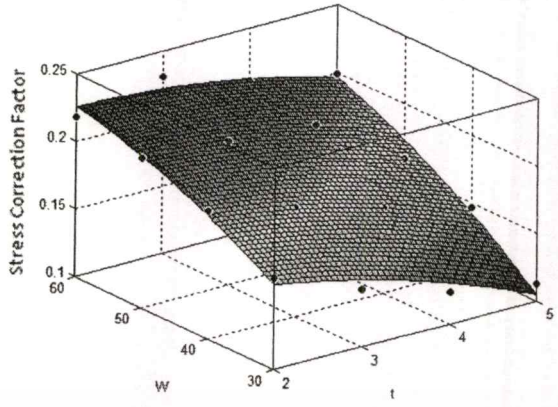

Figure 4.19 $K_{f,x}$ due to tension load at 0.4t.

Table 4.14 Coefficient of determinations and t scores for K_f of surface fitting due to tension load

Location	Stress correction factor (K_f)	Coefficient of determination (R^2)	t
0.4t	$K_{f,x}$	0.966	19.889
	$K_{f,y}$	0.992	42.700
	$K_{f,xy}$	0.975	23.492
0.9t	$K_{f,x}$	0.988	33.557
	$K_{f,y}$	0.982	27.420
	$K_{f,xy}$	0.984	29.158
1.4t	$K_{f,x}$	0.973	22.522
	$K_{f,y}$	0.964	19.469
	$K_{f,xy}$	0.990	37.572

All surface fitting equations can be shown in form of matrices. Equation (4.10) presents the parametric equation of stress correction factors (K_f) of selected model due to tension load at the points of extrapolation.

$$\begin{Bmatrix} K_{f_{x,o.4t}}^{fx} \\ K_{f_{y,o.4t}}^{fx} \\ K_{f_{xy,o.4t}}^{fx} \\ K_{f_{x,o.9t}}^{fx} \\ K_{f_{y,o.9t}}^{fx} \\ K_{f_{xy,o.9t}}^{fx} \\ K_{f_{x,1.4t}}^{fx} \\ K_{f_{y,1.4t}}^{fx} \\ K_{f_{xy,1.4t}}^{fx} \end{Bmatrix} = \begin{bmatrix} 0.0653 & -0.0075 & 0.0046 & -0.0031 & 0.000329 & -3.54\times10^{-5} \\ 0.1640 & -0.1001 & 0.0115 & 0.0061 & -0.000050 & -2.82\times10^{-5} \\ 0.3051 & -0.1599 & 0.0092 & 0.0140 & 0.000611 & -7.21\times10^{-5} \\ 0.1274 & 0.0687 & 0.0089 & 0.0090 & -0.000857 & -2.03\times10^{-5} \\ 0.2641 & -0.1831 & 0.0182 & 0.0221 & -0.001689 & -2.09\times10^{-5} \\ 0.1688 & -0.1548 & 0.0191 & 0.0158 & -0.000865 & -7.27\times10^{-5} \\ 0.4051 & -0.1239 & 0.0022 & 0.0117 & -0.000368 & 6.75\times10^{-5} \\ 0.359 & -0.2323 & 0.0149 & 0.0499 & -0.005712 & 23.13\times10^{-5} \\ 0.2067 & -0.2014 & 0.0211 & 0.0260 & -0.001756 & -4.70\times10^{-5} \end{bmatrix} \begin{Bmatrix} 1 \\ t \\ W \\ t^2 \\ tW \\ W^2 \end{Bmatrix} \quad (4.10)$$

Equation (4.10) can be abbreviated into Equation (4.11).

$$\{K_f\}_t = [K]_t \{G\} \quad (4.11)$$

Where $\{K_f\}_t$ is matrix of stress correction factor due to tension load.

$[K]_t$ is stiffness matrix of stress correction factor due to tension load.

$\{G\}$ is geometry matrix.

4.6.5 Stress correction factor due to bending load

Figure 4.20 shows surface fitting of stress correction factors (K_f) at the points the points of 0.4t due to bending load. All surface fitting are shown in appendix B-5. All coefficients of determinations (R^2) of surface fitting presented in Table 4.15 are called good correlation, which is greater than 0.85. Moreover, the t scores are presented in Table 4.15 calculated by coefficients of determinations, which are greater than critical t score (t_{cri}) of 2.1448. This indicates the significance of the correlation between stress and studied geometry of square beams.

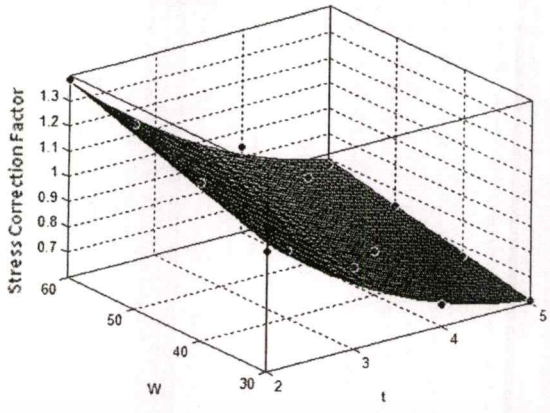

Figure 4.20 $K_{f,x}$ due to bending load at 0.4t.

Table 4.15 Coefficient of determinations and t scores for K_f of surface fitting due to bending load

Location	Stress correction factor (K_f)	Coefficient of determination (R^2)	t
0.4t	$K_{f,x}$	0.961	18.453
	$K_{f,y}$	0.926	13.200
	$K_{f,xy}$	0.947	15.800
0.9t	$K_{f,x}$	0.956	17.363
	$K_{f,y}$	0.883	10.292
	$K_{f,xy}$	0.969	20.944
1.4t	$K_{f,x}$	0.929	13.579
	$K_{f,y}$	0.897	11.056
	$K_{f,xy}$	0.923	12.959

All surface fitting equations can be shown in form of matrices. Equation (4.12) presents the parametric equation of stress correction factors (K_f) of selected geometric model due to bending load at the points of extrapolation.

$$\begin{Bmatrix} K_{f\,x,o.4t}^{fy} \\ K_{f\,y,o.4t}^{fy} \\ K_{f\,xy,o.4t}^{fy} \\ K_{f\,x,o.9t}^{fy} \\ K_{f\,y,o.9t}^{fy} \\ K_{f\,xy,o.9t}^{fy} \\ K_{f\,x,1.4t}^{fy} \\ K_{f\,y,1.4t}^{fy} \\ K_{f\,xy,1.4t}^{fy} \end{Bmatrix} = \begin{bmatrix} 1.5220 & -0.4295 & 0.0113 & 0.0414 & -0.000890 & -0.07\times10^{-4} \\ 0.5965 & -0.3382 & 0.0564 & 0.0095 & 0.001230 & -5.00\times10^{-4} \\ 2.3960 & -1.3260 & 0.0653 & 0.1528 & -0.002253 & -4.10\times10^{-4} \\ 1.8870 & -0.6184 & 0.0116 & 0.0983 & -0.006312 & 2.10\times10^{-4} \\ 2.1110 & -0.7698 & 0.0340 & 0.0775 & -0.001424 & -1.91\times10^{-4} \\ 0.6108 & -1.2010 & 0.1415 & 0.2207 & -0.020470 & -3.29\times10^{-4} \\ 0.9935 & -0.2875 & 0.0268 & 0.0587 & -0.006258 & 0.53\times10^{-4} \\ 1.7320 & -0.5956 & 0.0351 & 0.0798 & -0.005290 & 0.13\times10^{-4} \\ 2.3130 & -1.4220 & 0.0849 & 0.1931 & -0.008038 & -3.9\times10^{-4} \end{bmatrix} \begin{Bmatrix} 1 \\ t \\ W \\ t^2 \\ tW \\ W^2 \end{Bmatrix} \quad (4.12)$$

Equation (4.12) can be abbreviated into Equation (4.13)

$$\{K_f\}_b = \lfloor K \rfloor_b \{G\} \quad (4.13)$$

Where $\{K_f\}_b$ is matrix of stress correction factors due to bending load.

$\lfloor K \rfloor_b$ is stiffness matrix of stress correction factors due to bending load.

$\{G\}$ is geometry matrix.

4.6.6 Stress correction Factor due to moment load

Figure 4.21 shows surface fitting of stress correction factors (K_f) at the points the points of 0.4t due to moment load. All surface fitting are shown in appendix B-6. All coefficients of determinations (R^2) of surface fitting presented in Table 4.16 are called good correlation, which is greater than 0.85. Moreover, the t scores are presented in Table 4.16 calculated by coefficients of determinations, which are greater than critical t score (t_{cri}) of 2.1448. This indicates the significance of the correlation between stress and studied geometry of square beams.

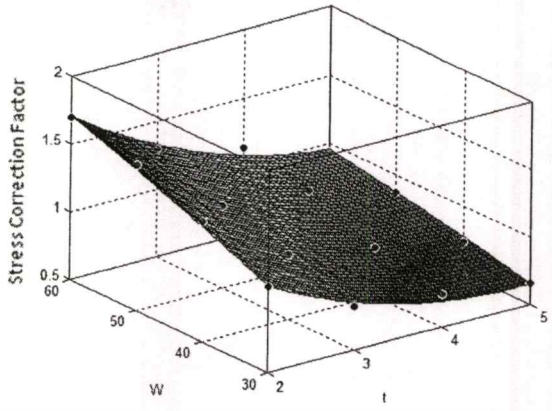

Figure 4.21 $K_{f,x}$ due to moment load at 0.4t.

Table 4.16 Coefficient of determinations and t scores for SCFs of surface fitting due to moment load

Location	Stress correction factor (K_f)	Coefficient of determination (R^2)	t
0.4t	$K_{f,x}$	0.978	24.994
	$K_{f,y}$	0.950	16.268
	$K_{f,xy}$	0.968	20.656
0.9t	$K_{f,x}$	0.963	19.129
	$K_{f,y}$	0.874	9.855
	$K_{f,xy}$	0.966	19.953
1.4t	$K_{f,x}$	0.859	9.251
	$K_{f,y}$	0.902	11.354
	$K_{f,xy}$	0.966	19.869

All surface fitting equations can be shown in form of matrices. Equation (4.14) presents the parametric equation of stress correction factors (K_f) of selected geometric model due to moment load at the points of extrapolation.

$$\begin{Bmatrix} K_{f\,x,o.4t}^{mz} \\ K_{f\,y,o.4t}^{mz} \\ K_{f\,xy,o.4t}^{mz} \\ K_{f\,x,o.9t}^{mz} \\ K_{f\,y,o.9t}^{mz} \\ K_{f\,xy,o.9t}^{mz} \\ K_{f\,x,1.4t}^{mz} \\ K_{f\,y,1.4t}^{mz} \\ K_{f\,xy,1.4t}^{mz} \end{Bmatrix} = \begin{bmatrix} 1.224 & -0.5217 & 0.0323 & 0.0632 & -0.002852 & -0.91\times10^{-4} \\ 1.569 & -0.6354 & 0.0432 & 0.0305 & 0.003632 & -3.96\times10^{-4} \\ 2.790 & -1.3590 & 0.0595 & 0.1555 & -0.003420 & -2.17\times10^{-4} \\ 1.593 & -0.6714 & 0.0302 & 0.1199 & -0.009321 & 1.96\times10^{-4} \\ 4.311 & -1.1490 & -0.0236 & 0.1094 & -0.000018 & 4.07\times10^{-4} \\ 2.109 & -1.3780 & 0.1008 & 0.2473 & -0.023840 & 3.46\times10^{-4} \\ 2.562 & -0.6482 & -0.0061 & 0.0714 & -0.001026 & 2.08\times10^{-4} \\ 3.281 & -0.7168 & -0.0130 & 0.0859 & -0.005383 & 5.80\times10^{-4} \\ 2.532 & -1.4080 & 0.0868 & 0.1976 & -0.011350 & -2.07\times10^{-4} \end{bmatrix} \begin{Bmatrix} 1 \\ t \\ W \\ t^2 \\ tW \\ W^2 \end{Bmatrix} \tag{4.14}$$

Equation (4.14) can be abbreviated into Equation (4.15).

$$\{K_f\}_m = [K]_m \{G\} \tag{4.15}$$

Where $\{K_f\}_m$ is matrix of stress correction factors due to moment load.

$[K]_m$ is stiffness matrix of stress correction factor due to moment load.

$\{G\}$ is geometry matrix.

4.6.7 Load-to-stress factor (LTS)

A matrix has m rows and n columns, which is called mxn order matrix. The items in a matrix are called elements of matrix. The matrices below, $[A]$, $[B]$ and $[C]$ are three matrices with same order.

$$[A] = \begin{bmatrix} A_{11} & A_{12} & \cdots & A_{1n} \\ A_{21} & A_{22} & \cdots & A_{2n} \\ \vdots & \vdots & \ddots & \vdots \\ A_{m1} & A_{m2} & \cdots & A_{mn} \end{bmatrix} \tag{4.16}$$

$$[B] = \begin{bmatrix} B_{11} & B_{12} & \cdots & B_{1n} \\ B_{21} & B_{22} & \cdots & B_{2n} \\ \vdots & \vdots & \ddots & \vdots \\ B_{m1} & B_{m2} & \cdots & B_{mn} \end{bmatrix} \tag{4.17}$$

$$[C] = \begin{bmatrix} C_{11} & C_{12} & \cdots & C_{1n} \\ C_{21} & C_{22} & \cdots & C_{2n} \\ \vdots & \vdots & \ddots & \vdots \\ C_{m1} & C_{m2} & \cdots & C_{mn} \end{bmatrix} \tag{4.18}$$

Where m,n = 1, 2, 3, ...

When $[C]$ is a matrix which is calculated by the operation between $[A]$ and $[B]$ as shown in Equation (4.19).

$$[C] = [A] \otimes [B] \tag{4.19}$$

Then, the elements of $[C]$ are defined by the multiplication between the elements of $[A]$ and $[B]$ as shown in Equation (4.20). This operation is defined as "elemental multiplication".

$$C_{mn} = A_{mn} \times B_{mn} \tag{4.20}$$

Load-to-stress factors (LTSs) are calculated by the multiplication between stress correction factors (K_f) and unit load stresses. However, all stress correction factors and unit load stresses have to be written in form of matrices. The unit stresses in Equation (4.4), (4.6), and (4.8) are rewritten the summation matrix of stresses as shown in Equation 4.21. Moreover, the stress correction factors in Equation (4.8), (4.10), and (4.12) are rewritten the summation matrix of stress correction factors as shown in Equation (4.22). The matrix of LTSs is calculated by the operation between the summation matrix of unit stress and the summation matrix of stress correction factor as shown in Equation (4.23).

$$[\sigma_u] = \begin{bmatrix} \sigma^{fx}_{\sigma x,0.4t} & \sigma^{fy}_{\sigma x,0.4t} & \sigma^{mz}_{\sigma x,0.4t} \\ \sigma^{fx}_{\sigma y,0.4t} & \sigma^{fy}_{\sigma y,0.4t} & \sigma^{mz}_{\sigma y,0.4t} \\ \tau^{fx}_{\tau xy,0.4t} & \tau^{fy}_{\tau xy,0.4t} & \tau^{mz}_{\tau xy,0.4t} \\ \sigma^{fx}_{\sigma x,0.9t} & \sigma^{fy}_{\sigma x,0.9t} & \sigma^{mz}_{\sigma x,0.9t} \\ \sigma^{fx}_{\sigma y,0.9t} & \sigma^{fy}_{\sigma y,0.9t} & \sigma^{mz}_{\sigma y,0.9t} \\ \tau^{fx}_{\tau xy,0.9t} & \tau^{fy}_{\tau xy,0.9t} & \tau^{mz}_{\tau xy,0.9t} \\ \sigma^{fx}_{\sigma x,1.4t} & \sigma^{fy}_{\sigma x,1.4t} & \sigma^{mz}_{\sigma x,1.4t} \\ \sigma^{fx}_{\sigma y,1.4t} & \sigma^{fy}_{\sigma y,1.4t} & \sigma^{mz}_{\sigma y,1.4t} \\ \tau^{fx}_{\tau xy,1.4t} & \tau^{fy}_{\tau xy,1.4t} & \tau^{mz}_{\tau xy,1.4t} \end{bmatrix} \tag{4.21}$$

$$[K_f]=\begin{bmatrix} K_{f\sigma x,0.4t}^{fx} & K_{f\sigma x,0.4t}^{fy} & K_{f\sigma x,0.4t}^{mz} \\ K_{f\sigma y,0.4t}^{fx} & K_{f\sigma y,0.4t}^{fy} & K_{f\sigma y,0.4t}^{mz} \\ K_{f\tau xy,0.4t}^{fx} & K_{f\tau xy,0.4t}^{fy} & K_{f\tau xy,0.4t}^{mz} \\ K_{f\sigma x,0.9t}^{fx} & K_{f\sigma x,0.9t}^{fy} & K_{f\sigma x,0.9t}^{mz} \\ K_{f\sigma y,0.9t}^{fx} & K_{f\sigma y,0.9t}^{fy} & K_{f\sigma y,0.9t}^{mz} \\ K_{f\tau xy,0.9t}^{fx} & K_{f\tau xy,0.9t}^{fy} & K_{f\tau xy,0.9t}^{mz} \\ K_{f\sigma x,1.4t}^{fx} & K_{f\sigma x,1.4t}^{fy} & K_{f\sigma x,1.4t}^{mz} \\ K_{f\sigma y,1.4t}^{fx} & K_{f\sigma y,1.4t}^{fy} & K_{f\sigma y,1.4t}^{mz} \\ K_{f\tau xy,1.4t}^{fx} & K_{f\tau xy,1.4t}^{fy} & K_{f\tau xy,1.4t}^{mz} \end{bmatrix} \tag{4.22}$$

$$[LTS]=[\sigma_u]\otimes[K_f] \tag{4.23}$$

The matrix of Load-to-stress factors is used to determine the normal stresses and shear stress at the extrapolation points shown in Equation (4.24). Those stresses are used to determine to evaluate the first principle stresses at the each point of extrapolation by using Equation (4.26). The first principle stresses at the each extrapolation point are used to calculate the hot spot stresses of models by Equation (4.27).

$$\begin{Bmatrix} \sigma_{x,0.4t} \\ \sigma_{y,0.4t} \\ \tau_{xy,0.4t} \\ \sigma_{x,0.9t} \\ \sigma_{y,0.9t} \\ \tau_{xy,0.9t} \\ \sigma_{x,1.4t} \\ \sigma_{y,1.4t} \\ \tau_{xy,1.4t} \end{Bmatrix} = \begin{bmatrix} LTS_{\sigma x,0.4t}^{fx} & LTS_{\sigma x,0.4t}^{fy} & LTS_{\sigma x,0.4t}^{mz} \\ LTS_{\sigma y,0.4t}^{fx} & LTS_{\sigma y,0.4t}^{fy} & LTS_{\sigma y,0.4t}^{mz} \\ LTS_{\tau xy,0.4t}^{fx} & LTS_{\tau xy,0.4t}^{fy} & LTS_{\tau xy,0.4t}^{mz} \\ LTS_{\sigma x,0.9t}^{fx} & LTS_{\sigma x,0.9t}^{fy} & LTS_{\sigma x,0.9t}^{mz} \\ LTS_{\sigma y,0.9t}^{fx} & LTS_{\sigma y,0.9t}^{fy} & LTS_{\sigma y,0.9t}^{mz} \\ LTS_{\tau xy,0.9t}^{fx} & LTS_{\tau xy,0.9t}^{fy} & LTS_{\tau xy,0.9t}^{mz} \\ LTS_{\sigma x,1.4t}^{fx} & LTS_{\sigma x,1.4t}^{fy} & LTS_{\sigma x,1.4t}^{mz} \\ LTS_{\sigma y,1.4t}^{fx} & LTS_{\sigma y,1.4t}^{fy} & LTS_{\sigma y,1.4t}^{mz} \\ LTS_{\tau xy,1.4t}^{fx} & LTS_{\tau xy,1.4t}^{fy} & LTS_{\tau xy,1.4t}^{mz} \end{bmatrix} \begin{Bmatrix} F_x \\ F_y \\ M_z \end{Bmatrix} \tag{4.24}$$

Equation (4.24) can be abbreviated into Equation (4.25)

$$\{\sigma\}=[LTS]\{F\} \tag{4.25}$$

Where $\{\sigma\}$ is a stress matrix of extrapolation points.

$[LTS]$ is a matrix of load-to-stress factors.

$\{F\}$ is a matrix of applied load..

$$\sigma_1 = \left(\frac{\sigma_x + \sigma_y}{2}\right) + \sqrt{\left(\frac{\sigma_x - \sigma_y}{2}\right)^2 + \tau_{xy}^2} \tag{4.26}$$

$$\sigma_{HS,quadratic} = 2.52\sigma_{0.4t} - 2.24\sigma_{0.9t} + 0.72\sigma_{1.4t} \tag{4.27}$$

4.7 The Application of Simplified Model

It is difficult to use solid elements in the bus superstructure model because of the limit of computer potential. Thus, beam elements were applied but the model with beam elements is too simple to maintain the accuracy of the results compared to solid elements. However, the modified model, which is presented in this study, is applied in the bus superstructure model for more accurate results. The modified model that is called simplified model consists of two parts, the model of stiffness equivalence and the load-to-stress as shown in Figure 4.22. The stiffness and stress of the simplified model have to be equivalent to the reference solid element model in order to represent the reference model in the finite element analysis. Moreover, the diagram in Figure 4.22 also shows how to use the simplified model in order to evaluate the hot spot stress of a reinforced SHS T-joint.

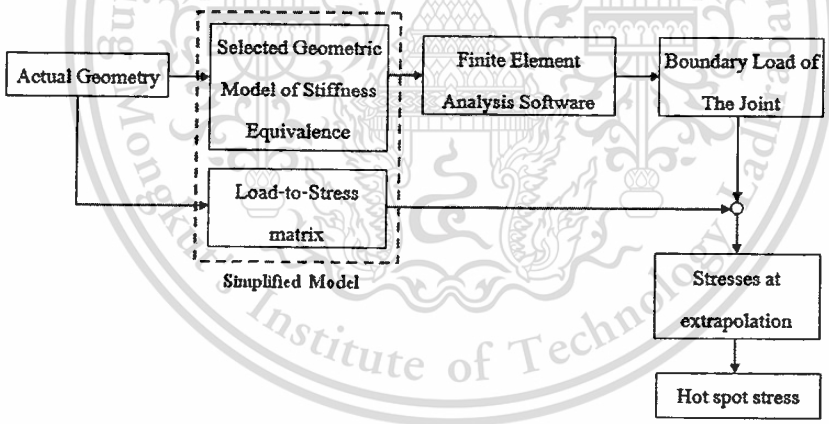

Figure 4.22 Simplified model.

Beam elements are applied in the bus superstructure analysis as shown in Figure 4.23 a). Only beam elements provide lack of accurate results. Thus, the simplified model providing stiffness equivalence is applied in the superstructure for stress analysis as shown in Figure 4.23 b). The simplified model consists of two types of element such as beam elements and shell elements. Figure 4.24 shows the all dimensions of simplified model to apply in the superstructure.

The full model of bus superstructure with simplified model is analyzed. Then, the boundary loads of the simplified model at the boundary nodes were calculated by using finite element analysis.

The cross-sectional properties of square hollow section beam used as reinforcement were used to evaluate the unit stresses and stress correction factors, as defined in section 4.6.1-4.6.6. Then, those unit stresses and stress correction factors were used to evaluate the matrix of load-to-stress factors (LTSs), as defined in section 4.6.7.

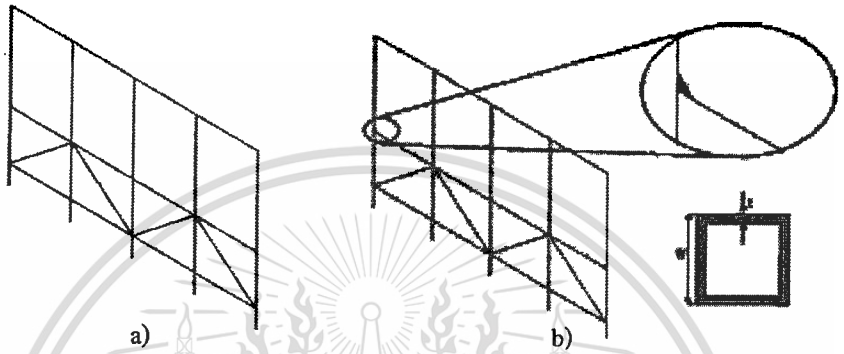

Figure 4.23 a) Beam elements of bus superstructure model; b) Bus superstructure model with simplified model.

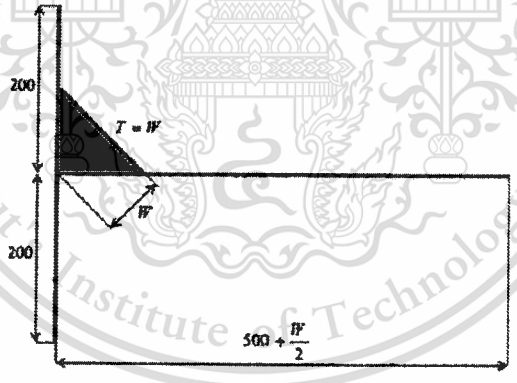

Figure 4.24 Dimension of simplified model.

The boundary loads and the matrix of LTSs are used to evaluate the stresses at the extrapolation points by using Equation (4.24). Then, the first principle stresses at those points are determined by Equation (4.25). Equation (4.26) and first principle stress at the extrapolation points are used to calculate the hot spot stress of the reinforcement.

4.8 Comparison of Simplified Model to Other Models

4.8.1 Comparison of simplified model to other models in case of tension, bending and moment load

Some dimensions of square hollow sections that are sold in the market were used to be evaluated the stress by using stress correction factor parametric equations. The stresses were determined under tension, bending and moment load. Table 4.17 to Table 4.19 show the stress error between Model A and simplified model to reference solid element model for 5 cross-sectional dimensions of square hollow section. The stress errors of simplified model calculated by Equation (4.28) tends to decrease compare to Model A.

$$\frac{\left(\sigma_{hs,solid} - \sigma_{hs,simplified}\right)}{\sigma_{hs,solid}} \times 100\,\% \tag{4.28}$$

Table 4.17 The stress error between Model A and simplified model compared to reference solid element model under tension load

t (mm.)	W (mm.)	t/W	Model A	Simplified model
2.3	50	0.046	-19.000%	-5.016%
3.2	32	0.100	-138.500%	-20.490%
3.2	38	0.084	-89.080%	-10.820%
3.2	40	0.080	-76.300%	-3.690%
3.2	50	0.064	-31.160%	-13.100%

Table 4.18 The stress error between Model A and simplified model compared to reference solid element model under bending load

t (mm.)	W (mm.)	t/W	Model A	Simplified model
2.3	50	0.046	63.510%	24.690%
3.2	32	0.100	45.450%	15.120%
3.2	38	0.084	50.090%	16.250%
3.2	40	0.080	51.400%	18.270%
3.2	50	0.064	56.450%	-17.780%

Table 4.19 The stress error between Model A and simplified model compared to reference solid element model under moment load

t (mm.)	W (mm.)	t/W	Model A	Simplified model
2.3	50	0.046	67.160%	11.040%
3.2	32	0.100	49.380%	-20.450%
3.2	38	0.084	56.520%	-13.110%
3.2	40	0.080	55.470%	-12.610%
3.2	50	0.064	60.740%	-48.200%

4.6.2 Comparison of simplified model to other models in case of combination load

Table 4.20 shows the average stress error between Model A and simplified model using LTS to the reference solid element model under combined load for studied geometries of square hollow section. It shows that the stress error of simplified model is substantially decreased compared to the error of Model A. This means the simplified model with LTS is effective to represent the reference solid element model.

Table 4.20 The average stress error between Model A and simplified model compared to reference solid element model under combined load

Tension (F_x)	Bending (F_y)	Moment (M_z)	Model A	Simplified model
1	0	0	-77.510%	0.770%
0	-1	0	50.950%	-5.170%
0	0	-1	54.200%	1.320%
1	-1	0	-50.860%	-5.020%
1	0	-1	61.310%	0.730%
0	-1	-1	-50.990%	-5.150%
1	-1	-1	-50.870%	-5.010%
2	-4	-6	-50.930%	-5.070%

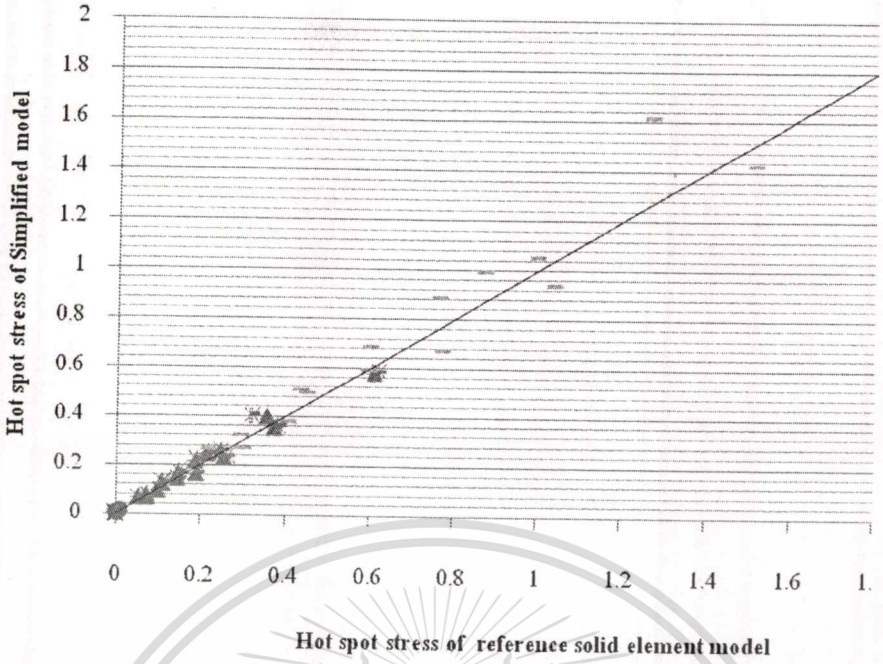

Figure 4.25 Scatter diagram showing errors of HSS of simplified model using LTS and reference solid element model

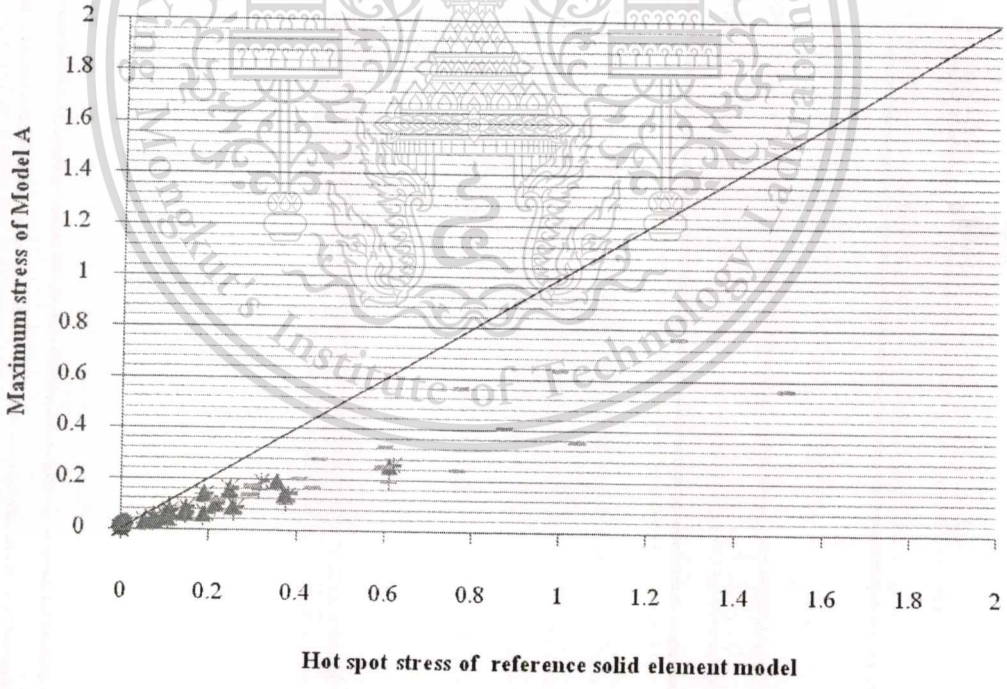

Figure 4.26 Scatter diagram showing errors of HSS of simplified model using LTS and Model A

Scatter diagrams showing stresses for the tension, bending, moment and combination load cases are given in Figure 4.25 and Figure 9.26, respectively, from which a considerable improvement in accuracy is apparent over the HSS of simplified model using LTS and maximum stress from Model A. This is evident from the scatter data of hot spot stress of simplified model close to symmetric line. The scatter data of maximum stress of Model A are lower than symmetric line. Therefore, the simplified model tends to provide more accuracy stress result compared to Model A which is normally applied in stress analysis of bus superstructure.

4.9 Computer Time

Finite element analysis of the reference solid model and the simplified model for various values of W and t were performed on personal computer with Intel Core i7 CPU and 8GB of RAM.

Table 4.21 Computer time of reference solid element model and simplified model

W×t (mm)	Computer time (s)	
	Reference solid element model	Simplified model
60×5	154.94	1.342
60×4	191.226	1.170
60×3	311.472	1.529
60×2	581.446	1.030
50×5	116.844	1.310
50×4	164.394	1.326
50×3	270.194	1.279
50×2	428.004	1.186
40×5	89.294	1.544
40×4	119.06	1.357
40×3	220.242	1.357
40×2	310.878	1.186
30×5	49.140	1.357
30×4	91.042	1.326
30×3	144.676	1.357
30×2	245.420	1.373

The results showed that computer time used for the reference solid element model is significantly longer than computer time used for the simplified model as show in Table 4.21. This demonstrated shows that the simplified model can be used to reduce computing time for the stress analysis of the bus superstructure.

4.10 Summary of Result

The stiffness and stress of the simplified model have to be equivalent to the reference solid element model in order to represent the reference model in the finite element analysis. Firstly, this chapter presents the ANOVA tables in order to indicate significant difference of W, t and model type by using ANOVA. Then, one of the trail models was selected by using the minimum stiffness error between reference model and all trial models. After the model selection, the reference solid element model and selected geometric model were used to evaluate the stress by following IIW recommendation for hot spot stress meshing. The suitable number of element for each mode's meshing is presented as a convergence plot to evaluate the stresses. Those stresses are used to calculate for the stress correction factors presented as a function of thickness-to-width of square hollow section joint under in-plane tension, bending, and moment load case. In case of in-plane combined load, the stress correction factors and unit loads at the extrapolation points are evaluated and presented as parametric equations with surface fitting. After that, load-to-stress factors (LTSs) calculated by the multiplication between stress correction factors and unit loads are also presented. The LTSs are presented as a parametric matrix. The simplified model, which is consists of equivalent stiffness and LTSs matrix, is summarized. Then, it shows how to apply the simplified model in the bus superstructure for the stress analysis. Moreover, the comparison between the stress from simplified model and model A to reference model of some square hollow sections using SCFs in case of in-plane tension, bending, and moment load are shown. Finally, the stress of simplified model using LTSs and model A in case of in-plane combined load are compared to reference model. It was found that the simplified model tends to provide more accuracy stress result compared to Model A. Moreover, Computer time using for reference solid element model is longer than computer time using for simplified model.

CHAPTER 5

CONCLUSION

5.1 Conclusion

In bus superstructure production, the structures are designed by the long experiences of the experts. The design of the bus structure has to ensure the safety of the passengers while the bus weight has to be minimal for the bus maker to stay competitive in terms of production cost and fuel consumption. However, these experiences pose a limitation to improve the bus superstructure design. Therefore, engineering knowledge needs to be applied in order to increase the effectiveness of the design process. Computer Aided Design (CAD) and Computer Aided Engineering (CAE) are ones of the tools that can be used to evaluate stresses on the bus superstructure under several loading conditions.

The bus superstructures consist of many kinds of steel such as I-beam, square beam, and plate steel. Welding process is applied to assemble those steels. There are many kinds of joints in the bus superstructure. Although the welding process is under well controlled, it is difficult to evaluate the stress at the weld joint due to peculiarities. To increase the stiffness of the structure, the reinforcements are applied in the joints. Joints in bus superstructures may be reinforced by various means. Some joints may be reinforced by steel plates. However, those reinforcements are ignored in the stress analysis using CAE. One of interesting means to reinforce the joints is to use a hollow square beam to reinforce square hollow section (SHS)

The reinforcement of square hollow section (SHS) T-joints, usually ignored in bus superstructure analysis, was considered carefully in this study. Trial models namely Model A, Model B, Model C, and Model D were investigated to evaluate the stiffness error functions, which represent the deviations of trial model's stiffnesses from the reference solid element model's stiffness. The results showed with confidence interval of 95% that model type, as well as SHS beam width and SHS beam thickness, had a significant effect on the stiffness error. Each pair of model type was analyzed to indicate the significant relationship of stiffness error function. It was found that the stiffness errors from Model A were significantly different from those from Model B, Model C, and Model D. However, the stiffness errors from Model B, Model C, and Model D were not significantly different. To complete this study, Model B providing the minimum average stiffness error, was selected as a selected geometric model. Finite element

analysis (FEA) was then used to evaluate hot spot stress (HSS) of both reference model and selected model in order to determine the stress correction factor (K_f) under in-plane load.

Beam elements applied in the model of bus superstructure are too simple to maintain the accuracy of the results compared to solid element. Therefore, the simplified model, which is studied in this study, is applied to the joints in the bus superstructure for more accurate results as defined in section 4.7. The simplified model consists of two parts, the equivalent stiffness and the equivalent stress. The stress correction factors are factor to correct the stress. The cross-sectional properties of square hollow section are used to evaluate the unit stresses and stress correction factors in order to determine the hot spot stress.

The stress correction factors (K_f) of reinforced SHS T-joint in bus superstructure without weld geometry were presented as a function of thickness-to-width ratio of hollow section beam using polynomial regression. The direction of first principle stresses in case of single load does not change. So, the hot spot stress of the simplified model can be corrected by using the stress correction factor in each single load case. Equation (5.1) to Equation (5.3) is presented the curve fitting of the stress correction factor under tension, bending, and moment load. The stress correction factors are valid for ratio of width and thickness of SHS T-joints varying between 1/6 - 1/30 and having thickness less than 5 mm.

$$K_{f,t/W}^{fx} = 0.679\left(\frac{t}{W}\right)^2 - 0.634\left(\frac{t}{W}\right) + 0.268 \tag{5.1}$$

$$K_{f,t/W}^{fy} = 75.870\left(\frac{t}{W}\right)^2 - 21.960\left(\frac{t}{W}\right) + 2.470 \tag{5.2}$$

$$K_{f,t/W}^{mz} = 52.080\left(\frac{t}{W}\right)^2 - 17.310\left(\frac{t}{W}\right) + 2.397 \tag{5.3}$$

In case of combined in-plane load, it is difficult to evaluate the direction of the first principle stress. Thus, the stresses in given coordinate are easier to determine by using the load-to-stress factors (LTS) as a function of SHS geometry. The LTS matrix calculated by the elemental multiplication in section 4.6.7 between unit stresses matrix and stress correction factor matrix as shown in Equation (5.4). The LTSs are applied for the SHS width of 60-30mm and thickness of 5-2 mm. The LTS matrix and boundary load matrix are applied in Equation (5.5) to calculate the normal stresses and shear stresses at extrapolation points. Equation (5.6) is applied to evaluate the

first principle stress at each extrapolation point. Then, the quadratic hot spot stress is determined by using Equation (5.7) as shown in section 4.6.7.

$$[LTS] = [\sigma_u] \otimes [K_f] \tag{5.4}$$

$$\begin{Bmatrix} \sigma_{x,0.4t} \\ \sigma_{y,0.4t} \\ \tau_{xy,0.4t} \\ \sigma_{x,0.9t} \\ \sigma_{y,0.9t} \\ \tau_{xy,0.9t} \\ \sigma_{x,1.4t} \\ \sigma_{y,1.4t} \\ \tau_{xy,1.4t} \end{Bmatrix} = \begin{bmatrix} LTS^{fx}_{\sigma x,0.4t} & LTS^{fy}_{\sigma x,0.4t} & LTS^{mz}_{\sigma x,0.4t} \\ LTS^{fx}_{\sigma y,0.4t} & LTS^{fy}_{\sigma y,0.4t} & LTS^{mz}_{\sigma y,0.4t} \\ LTS^{fx}_{\tau xy,0.4t} & LTS^{fy}_{\tau xy,0.4t} & LTS^{mz}_{\tau xy,0.4t} \\ LTS^{fx}_{\sigma x,0.9t} & LTS^{fy}_{\sigma x,0.9t} & LTS^{mz}_{\sigma x,0.9t} \\ LTS^{fx}_{\sigma y,0.9t} & LTS^{fy}_{\sigma y,0.9t} & LTS^{mz}_{\sigma y,0.9t} \\ LTS^{fx}_{\tau xy,0.9t} & LTS^{fy}_{\tau xy,0.9t} & LTS^{mz}_{\tau xy,0.9t} \\ LTS^{fx}_{\sigma x,1.4t} & LTS^{fy}_{\sigma x,1.4t} & LTS^{mz}_{\sigma x,1.4t} \\ LTS^{fx}_{\sigma y,1.4t} & LTS^{fy}_{\sigma y,1.4t} & LTS^{mz}_{\sigma y,1.4t} \\ LTS^{fx}_{\tau xy,1.4t} & LTS^{fy}_{\tau xy,1.4t} & LTS^{mz}_{\tau xy,1.4t} \end{bmatrix} \begin{Bmatrix} F_x \\ F_y \\ M_z \end{Bmatrix} \tag{5.5}$$

$$\sigma_1 = \left(\frac{\sigma_x + \sigma_y}{2}\right) + \sqrt{\left(\frac{\sigma_x - \sigma_y}{2}\right)^2 + \tau_{xy}^2} \tag{5.6}$$

$$\sigma_{HS,quadratic} = 2.520\,\sigma_{0.4t} - 2.240\,\sigma_{0.9t} + 0.720\,\sigma_{1.4t} \tag{5.7}$$

Reinforced square hollow section T-joints found in the bus superstructure were studied by using the simplified model. The simplified model is valid for the SHS width of 60-30mm and thickness of 5-2 mm, which are commonly sold in the market, under elastic region of the material. The weld geometry and residual stress are ignored in this model. The simplified model consisting of two equivalent parts, the equivalent stiffness and the equivalent stress, was compared to reference model. In addition, the simplified model is valid for 2-dimensional loads. The simplified model provided less stress error compared to reference solid element model than Model A did. It implies that the stresses of the simplified model are close to the stress of the reference solid element model compared to model A which is normally applied in bus superstructure. However, the simplified model has to be modified based on the presented methodology in order to improve the accuracy results of the bus superstructure where 3 dimensional loads are applied for the further study. According to section 4.9, the computer time used for the simplified model is less the computer time used for reference solid model. This

simplified model allows the stress evaluation on the bus superstructure to be done more quickly compared to reference solid model while the accuracy of the solution is maintained.

5.2 Suggestion and Future Work

Framework for developing simplified model has been demonstrated in this study. However this framework can be repeated to develop the effective simplified model. This simplified model is valid only for the 2 dimensional load cases and a dimension range of square hollow section. Future study can be carried out to improve the accuracy of the results. There are some suggestions to the work for further study as follow:

- Study the simplified model with applied load of opposite direction
- Modify the simplified model based on the methodology presented in this work in order to extend the application to 3 dimensional load
- Improve the model by varying finite element parameters of shell throat and shell thickness in order to represent more accurate stiffness of the joint
- Extent scope of the model for other load types may occur in reality to maintain the accuracy of the stress results

REFERENCES

1. Department of Land Transport, Ministries of Transport and Communications, " สถิติการขนส่งประจำไตรมาสที่ 2 ปีงบประมาณ 2556 (มกราคม-มีนาคม 2556)"
2. Mohd, A.B.L. 2008, "Comparison of Brodge Decks Modeling Between Beam ans Shell and 3D Solid Finite Element Models", **Universiti Teknologi Malaysia**, Malaysia
3. Manokruang, S., Butdee ,S. 2009, "Methodology of Bus-Body Structural Redesign for Lightweight Productivity Improvement", **Asia International Journal of Science and Technology in Production and Manufacturing Engineering.** 2(2) : 79-87.
4. Yu, C.L., Hong, C.N. 2005, "Structural Design Optimization of the Body Section Using the Finite Element Method", **SEA Standard**
5. Radaj, D. 1996, "Review of fatigue strength assessment of nonwelded and welded structures based on local parameters", **Int. Journal of Fatigue.** 18(3) : 153-170.
6. Kumket, S., Jongprasitphon, S., Butdee ,S. 2010, "Welding Joint Analysis using FEM together with Physical Experiment for a Bus Body Structure based on the Standard No. 1", **Asia International Journal of Science and Technology in Production and Manufacturing Engineering.** 3(2) : 49-55.
7. Kumket, S. 2010, "Design and Analysis of Bus Body Structure (Standard No.1)", **Master Thesis, King Mongkut's University of Technology North Bangkok**, Thailand.
8. Hobbacher, A. 2008, "Recommendations for fatigue design of welded joints and components", doc XIII-2151r4-07/XV-1254r4-07, **Int. Institute of Welding**.
9. European Committee for Standardization. 1993, "Eurocode 3, Design of steel structures. Part 1-1: General rules for buildings ENV"
10. Radaj, D., Sonsino, C.M., Fricke, W. 2009, "Recently Developments in Local Concepts of Fatigue Assessment of Welded Joints", **Int. Journal of Fatigue.** 31(1) : 2-12.
11. Hiroyuki, Y., Kengo, A. "Local Stress Approach for Fatigue Assessment", **Kochi University of Technology**, Japan.

REFERENCES (CONT.)

12. Martinsson, J. 2005, "Fatigue Assessment of Complex Welded Steel Structures" **KTH Royal Institute of Technology**, Sweden.

13. Xiao, Z.G., Yamada, K. 2004, "A Method of Determining Geometric Stress for Fatigue Strength Evaluation of Steel Welded joints", **Int. Journal of Fatigue.** 26(12) : 77-93.

14. Aygül, M. 2012, "Fatigue Analysis of Welded Structures Using the Finite element Method", **Chalmers University of Technology**. Sweden.

15. Niemi, E. 1995, "Stress Determination for Fatigue Analysis of Welded Components", doc IIS/IIW-1221-93, **Int. Institute of Welding.**

16. Fayard, J., Bignonnet, A., Dand, V.K. 1996, "Fatigue Design Criterion for Welded structures", **Fatigue & Fracture of Engineering Materials & Structures.** 19(6) : 723-729.

17. Aygül, M., Al-Emrani, M. Urushadze, S. 2012, "Modelling and Fatigue life Assessment of orthotropic Bridge Deck Detail Using FEM", **Int. Journal of Fatigue.** 40 : 129-142.

18. Niemi, E., Fricke, W., Maddox, S.J. 2004, "Fatigue Analysis of Welded Conponent : Design's Guide to the Structural Hot-Spot Stress Approach", IIW-1430-00 **Int. Institute of Welding.**

19. Radhi, H.E., Barrans, S.M. 2010, "Finite Element Analysis of Effect of Weld Toe radius and Plate Thickness on Fatigue of Butt welded Joint", **Computing and Engineering Researchers' Conference.** 60-64.

20. Savaidis, G., Vormwald, M. 2000, "Hot-Spot Evaluation of Fatigue in welded Structural Connections Supportes by Finite Element Analysis", **Int. Journal of Fatigue.** 22(2) : 85-91.

21. Fokilidis, A., Savaidis, G. 2007, "Experimental Investigation of Fatigue of Thin-Walled edled Structures of Commercial Vehicle Frames", **Int. Conference of Diagnosis and Prediction in Mechanical Engineering System.** 2 : 34-38.

REFERENCES (CONT.)

22. Marin, T., Niciletto., G. "Fatigue Design of Welded Joints using the Finite element Method and The 2007 ASME Div. 2 Master curve", **University of Parma,** Italy

23. Brennan, F.B., Peleties, P., Hellier, A.K. 2000, "Prediction Weld Toe Stress concentration Factors for Y and Skewed T-Joint palate Connections", **Int. Journal of Fatigue.** 22(7) : 573-584.

24. Fricke, W. 2010, "Guideline for the Fatigue Assessment by Notch Stress Analysis for Welded Structures", IIW-Doc. XIII-2240r2-08/XV-1289r2-08., **Int. Institute of Welding.**

25. Dechaumphai, P. 2010, **Finite Element method Fundamentals and applications,** Alpha Science International Limited.

26. Fozilat, H.D, Judith, R., Meakin, Richard, M.A. 2002, "Statistical methods in finite element analysis", **Int. Journal Biomechanics.** 35 : 1155-1161.

27. Chapra, S.C., Cannale, R.P 2006, **Numerical Method for Engineering,** Mcgraw-Hill Fifth edition. 338-339.

28. Lancaster, P., Salkauskas, K. 1986, **Curve and Surface Fitting: An Introduction,** Academic press. 148.

APPENDIX A

M-FILE

Appendix A-1: M-file for ANOVA

This appendix is m-file for ANOVA to evaluate the significant of the stiffness error of all models.

```
clear;
format long;
ABCD = [  60  5  9.236842896 ;
  60 4  13.30802468 ;
  60 3  14.18004625 ;
  60 2  12.00027442 ;
  50 5  8.049586682 ;
  50 4  7.563969561 ;
  50 3  8.183191777 ;
  50 2  13.52392656 ;
  40 5  8.904582919 ;
  40 4  8.329097429 ;
  40 3  9.737479913 ;
  40 2  19.40948774 ;
  30 5  7.243264146 ;
  30 4  7.359280242 ;
  30 3  7.611485462 ;
  30 2  7.964289183 ;
  60 5  6.703366088 ;
  60 4  13.16188082 ;
  60 3  12.60707344 ;
  60 2  11.46731143 ;
  50 5  6.893795875 ;
```

50 4 6.307940925 ;

50 3 6.254704065 ;

50 2 12.08688594 ;

40 5 4.840421303 ;

40 4 4.507271935 ;

40 3 5.949052877 ;

40 2 16.06431946 ;

30 5 4.695710528 ;

30 4 4.670814524 ;

30 3 4.568650396 ;

30 2 4.363941488 ;

60 5 6.989614125 ;

60 4 12.93507461 ;

60 3 12.95423388 ;

60 2 11.1372578 ;

50 5 7.010493085 ;

50 4 6.47291997 ;

50 3 5.714661804 ;

50 2 11.85976146 ;

40 5 5.637499766 ;

40 4 5.014427597 ;

40 3 5.428391545 ;

40 2 15.48040405 ;

30 5 5.308449978 ;

30 4 5.250620918 ;

30 3 5.15453375 ;

30 2 5.002342106 ;

60 5 7.675906887 ;

60 4 13.1858934 ;

60 3 13.38904205 ;

60 2 11.28487673 ;

50 5 7.051457451 ;

```
    50 4  6.594353889 ;
    50 3  8.408314947 ;
    50 2  12.8683611  ;
    40 5  6.819563805 ;
    40 4  6.196133517 ;
    40 3  6.237084156 ;
    40 2  14.75244905 ;
    30 5  5.776293787 ;
    30 4  5.947290589 ;
    30 3  6.12589577  ;
    30 2  6.20127732  ];
y  = ABCD(:,3);
g1 = ABCD(:,1);
g2 = ABCD(:,2);
g3 = ['A';'A';'A';'A';'A';'A';'A';'A';'A';'A';'A';'A';'A';'A';'A';
      'B';'B';'B';'B';'B';'B';'B';'B';'B';'B';'B';'B';'B';'B';'B';
      'C';'C';'C';'C';'C';'C';'C';'C';'C';'C';'C';'C';'C';'C';'C';
      'D';'D';'D';'D';'D';'D';'D';'D';'D';'D';'D';'D';'D';'D';'D'];
[PABCD,table,stats]= anovan(y,{g1 g2 g3},'model','linear')

data = [
   60 5  9.236842896 9.236842896 9.236842896 6.703366088 6.703366088 6.989614125 ;
   60 4  13.30802468 13.30802468 13.30802468 13.16188082 13.16188082 12.93507461 ;
   60 3  14.18004625 14.18004625 14.18004625 12.60707344 12.60707344 12.95423388 ;
   60 2  12.00027442 12.00027442 12.00027442 11.46731143 11.46731143 11.1372578  ;
   50 5  8.049586682 8.049586682 8.049586682 6.893795875 6.893795875 7.010493085 ;
   50 4  7.563969561 7.563969561 7.563969561 6.307940925 6.307940925 6.47291997  ;
   50 3  8.183191777 8.183191777 8.183191777 6.254704065 6.254704065 5.714661804 ;
   50 2  13.52392656 13.52392656 13.52392656 12.08688594 12.08688594 11.85976146 ;
   40 5  8.904582919 8.904582919 8.904582919 4.840421303 4.840421303 5.637499766 ;
   40 4  8.329097429 8.329097429 8.329097429 4.507271935 4.507271935 5.014427597 ;
   40 3  9.737479913 9.737479913 9.737479913 5.949052877 5.949052877 5.428391545 ;
```

```
40 2  19.40948774 19.40948774 19.40948774 16.06431946 16.06431946 15.48040405 ;
30 5  7.243264146 7.243264146 7.243264146 4.695710528 4.695710528 5.308449978 ;
30 4  7.359280242 7.359280242 7.359280242 4.670814524 4.670814524 5.250620918 ;
30 3  7.611485462 7.611485462 7.611485462 4.568650396 4.568650396 5.15453375  ;
30 2  7.964289183 7.964289183 7.964289183 4.363941488 4.363941488 5.002342106 ;
60 5  6.703366088 6.989614125 7.675906887 6.989614125 7.675906887 7.675906887 ;
60 4  13.16188082 12.93507461 12.68054832 12.93507461 12.68054832 13.1858934  ;
60 3  12.60707344 12.95423388 13.38904205 12.95423388 13.38904205 13.38904205 ;
60 2  11.46731143 11.1372578  11.28487673 11.1372578  11.28487673 11.28487673 ;
50 5  6.893795875 7.010493085 7.051457451 7.010493085 7.051457451 7.051457451 ;
50 4  6.307940925 6.47291997  6.594353889 6.47291997  6.594353889 6.594353889 ;
50 3  6.254704065 5.714661804 8.408314947 5.714661804 8.408314947 8.408314947 ;
50 2  12.08688594 11.85976146 12.8683611  11.85976146 12.8683611  12.8683611  ;
40 5  4.840421303 5.637499766 6.819563805 5.637499766 6.819563805 6.819563805 ;
40 4  4.507271935 5.014427597 6.196133517 5.014427597 6.196133517 6.196133517 ;
40 3  5.949052877 5.428391545 6.237084156 5.428391545 6.237084156 6.237084156 ;
40 2  16.06431946 15.48040405 6.021063034 15.48040405 6.021063034 14.75244905 ;
30 5  4.695710528 5.308449978 5.776293787 5.308449978 5.776293787 5.776293787 ;
30 4  4.670814524 5.250620918 5.947290589 5.250620918 5.947290589 5.947290589 ;
30 3  4.568650396 5.15453375  6.12589577  5.15453375  6.12589577  6.12589577  ;
30 2  4.363941488 5.002342106 6.20127732  5.002342106 6.20127732  6.20127732  ];

 y  = data(:,3);
g1 = data(:,1);
g2 = data(:,2);
g3 = ['A';'A';'A';'A';'A';'A';'A';'A';'A';'A';'A';'A';'A';'A';'A';'A';
      'B';'B';'B';'B';'B';'B';'B';'B';'B';'B';'B';'B';'B';'B';'B';'B'];
[PAB,table,stats]= anovan(y,{g1 g2 g3},'model','linear')

y  = data(:,4);
g1 = data(:,1);
g2 = data(:,2);
```

```
g3 = ['A';'A';'A';'A';'A';'A';'A';'A';'A';'A';'A';'A';'A';'A';'A';'A';
      'C';'C';'C';'C';'C';'C';'C';'C';'C';'C';'C';'C';'C';'C';'C';'C'];
[PAC,table,stats]= anovan(y,{g1 g2 g3},'model','linear')

y  = data(:,5);
g1 = data(:,1);
g2 = data(:,2);
g3 = ['A';'A';'A';'A';'A';'A';'A';'A';'A';'A';'A';'A';'A';'A';'A';'A';
      'D';'D';'D';'D';'D';'D';'D';'D';'D';'D';'D';'D';'D';'D';'D';'D'];
[PAD,table,stats]= anovan(y,{g1 g2 g3},'model','linear')

y  = data(:,6);
g1 = data(:,1);
g2 = data(:,2);
g3 = ['B';'B';'B';'B';'B';'B';'B';'B';'B';'B';'B';'B';'B';'B';'B';'B';
      'C';'C';'C';'C';'C';'C';'C';'C';'C';'C';'C';'C';'C';'C';'C';'C'];
[PBC,table,stats]= anovan(y,{g1 g2 g3},'model','linear')

y  = data(:,7);
g1 = data(:,1);
g2 = data(:,2);
g3 = ['B';'B';'B';'B';'B';'B';'B';'B';'B';'B';'B';'B';'B';'B';'B';'B';
      'D';'D';'D';'D';'D';'D';'D';'D';'D';'D';'D';'D';'D';'D';'D';'D'];
[PBD,table,stats]= anovan(y,{g1 g2 g3},'model','linear')

y  = data(:,8);
g1 = data(:,1);
g2 = data(:,2);
g3 = ['C';'C';'C';'C';'C';'C';'C';'C';'C';'C';'C';'C';'C';'C';'C';'C';
      'D';'D';'D';'D';'D';'D';'D';'D';'D';'D';'D';'D';'D';'D';'D';'D'];
[PCD,table,stats]= anovan(y,{g1 g2 g3},'model','linear')
```

Appendix A-2: An example of m-file for normal stresses and shear stress

This appendix is an example m-file to fit surface of the normal stresses and shear stress due to tension load at 0.4t, 0.9t and 1.4t away from discontinuity structure.

```
%sigmax, sigmay, and tauxy due to fx at 0.4t, 0.9t and 1.4t
clear;
data = [
60 5 0.0031836 0.0016588 -0.0019103 0.0016947 0.0012635 -0.001183 0.0011763
0.00084546 -0.00093605;
60 4 0.0041504 0.0019161 -0.0025047 0.0021141 0.0012827 -0.0013276 0.0013513
0.00093171 -0.0010686;
60 3 0.005696 0.0025891 -0.0038473 0.0027878 0.0017244 -0.0018929 0.0018822
0.0012714 -0.0014435;
60 2 0.010748 0.0041207 -0.0056552 0.0043003 0.0023591 -0.0027474 0.0031588
0.0013181 -0.0020354;
50 5 0.004523 0.0023746 -0.0024828 0.0025815 0.0016478 -0.0016401 0.0017355
0.0012201 -0.0012047;
50 4 0.0049472 0.0028364 -0.0037638 0.0029018 0.0019165 -0.0021594 0.0022415
0.0017111 -0.0017198;
50 3 0.0072822 0.0036767 -0.004677 0.0038968 0.0024609 -0.0023933 0.0027122
0.0017077 -0.0019278;
50 2 0.012741 0.0054804 -0.0069376 0.0055892 0.0031672 -0.0035445 0.0038995
0.0021502 -0.0026468;
40 5 0.0057839 0.0036501 -0.0036638 0.003284 0.002486 -0.0023724 0.0022772
0.0018548 -0.0018457;
40 4 0.0072291 0.0041566 -0.0044782 0.0041144 0.0025104 -0.0029574 0.0029094
0.0020625 -0.0023415;
40 3 0.009881 0.005337 -0.0062878 0.0056973 0.0036575 -0.0035746 0.0040011
0.0029209 -0.0028448;
40 2 0.016263 0.0079596 -0.0091691 0.0078347 0.004843 -0.0048568 0.0057331
0.0039983 -0.0038867;
```

```
30 5 0.0093547 0.0076469 -0.00673 0.0051374 0.0045582 -0.0045083 0.0035655
0.0031682 -0.0032284;
30 4 0.011857 0.0097952 -0.0087536 0.0067765 0.0054075 -0.0052907 0.0047818
0.003737 -0.0040615;
30 3 0.015674 0.0095765 -0.010059 0.0096607 0.0067473 -0.0063734 0.0067172
0.0050946 -0.0050003;
30 2 0.023828 0.012721 -0.014119 0.013861 0.0074042 -0.009143 0.008272
0.0066278 -0.0071768];

datat=transpose(data)
W = data(:,1);
t = data(:,2);

figure(1)
  sx0_4 = data(:,3);
  [fsx0_4,stasx0_4] = fit( [t, W], sx0_4, 'poly22' )
  plot(fsx0_4 , [t, W], sx0_4)
  xlabel('t')
  ylabel('W')
  zlabel('\sigmax')

figure(2)
  sy0_4 = data(:,4);
  [fsy0_4,stasy0_4] = fit( [t, W], sy0_4, 'poly22' )
  plot(fsy0_4 , [t, W], sy0_4)
  xlabel('t')
  ylabel('W')
  zlabel('\sigmay')

figure(3)
  sxy0_4 = data(:,5);
  [fsxy0_4,stasxy0_4] = fit( [t, W], sxy0_4, 'poly22' )
```

```
plot(fsxy0_4, [t, W], sxy0_4)
xlabel('t')
ylabel('W')
zlabel('\tauxy')

figure(4)
sx0_9 = data(:,6);
[fsx0_9,stasx0_9] = fit( [t, W], sx0_9, 'poly22' )
plot(fsx0_9, [t, W], sx0_9)
xlabel('t')
ylabel('W')
zlabel('\sigmax')

figure(5)
sy0_9 = data(:,7);
[fsy0_9,stasy0_9]= fit( [t, W], sy0_9, 'poly22' )
plot(fsy0_9 , [t, W], sy0_9)
xlabel('t')
ylabel('W')
zlabel('\sigmay')

figure(6)
sxy0_9 = data(:,8);
[fsxy0_9,stasxy0_9]= fit( [t, W], sxy0_9, 'poly22' )
plot(fsxy0_9 , [t, W], sxy0_9)
xlabel('t')
ylabel('W')
zlabel('\tauxy')

figure(7)
sx1_4 = data(:,9);
[fsx1_4,stasx1_4]= fit( [t, W], sx1_4, 'poly22' )
```

```
    plot(fsx1_4, [t, W], sx1_4)
    xlabel('t')
    ylabel('W')
    zlabel('\sigmax')

figure(8)
    sy1_4 = data(:,10);
    [fsy1_4,stasy1_4] = fit( [t, W], sy1_4, 'poly22' )
    plot(fsy1_4 , [t, W], sy1_4)
    xlabel('t')
    ylabel('W')
    zlabel('\sigmay')

figure(9)
    sxy1_4 = data(:,11);
    [fsxy1_4,stasxy1_4]= fit( [t, W], sxy1_4, 'poly22' )
    plot(fsxy1_4 , [t, W], sxy1_4)
    xlabel('t')
    ylabel('W')
    zlabel('\tauxy')
```

Appendix A-3: An example m-file for stress correction factor

This appendix is an example m-file to fit surface of all stress correction factors due to tension load at 0.4t, 0.9t and 1.4t away from discontinuity structure.

```
%stress concentration factors due to fx at 0.4t, 0.9t and 1.4t
clear;
data = [
60 5 0.0031836 0.0016588 -0.0019103 0.0016947 0.0012635 -0.001183 0.0011763
0.00084546 -0.0009360;
60 4 0.0041504 0.0019161 -0.0025047 0.0021141 0.0012827 -0.0013276 0.0013513
0.00093171 -0.0010686;
60 3 0.005696 0.0025891 -0.0038473 0.0027878 0.0017244 -0.0018929 0.0018822
0.0012714 -0.0014435;
60 2 0.010748 0.0041207 -0.0056552 0.0043003 0.0023591 -0.0027474 0.0031588
0.0013181 -0.0020354;
50 5 0.004523 0.0023746 -0.0024828 0.0025815 0.0016478 -0.0016401 0.0017355
0.0012201 -0.0012047;
50 4 0.0049472 0.0028364 -0.0037638 0.0029018 0.0019165 -0.0021594 0.0022415
0.0017111 -0.0017198;
50 3 0.0072822 0.0036767 -0.004677 0.0038968 0.0024609 -0.0023933 0.0027122
0.0017077 -0.0019278;
50 2 0.012741 0.0054804 -0.0069376 0.0055892 0.0031672 -0.0035445 0.0038995
0.0021502 -0.0026468;
40 5 0.0057839 0.0036501 -0.0036638 0.003284 0.002486 -0.0023724 0.0022772
0.0018548 -0.0018457;
40 4 0.0072291 0.0041566 -0.0044782 0.0041144 0.0025104 -0.0029574 0.0029094
0.0020625 -0.0023415;
40 3 0.009881 0.005337 -0.0062878 0.0056973 0.0036575 -0.0035746 0.0040011
0.0029209 -0.0028448;
40 2 0.016263 0.0079596 -0.0091691 0.0078347 0.004843 -0.0048568 0.0057331
0.0039983 -0.0038867;
```

```
30  5   0.0093547  0.0076469  -0.00673   0.0051374   0.0045582  0.0045083  0.0035655
0.0031682      -0.0032284;
30  4   0.011857   0.0097952  -0.0087536  0.0067765  0.0054075  -0.0052907  0.0047818
0.003737       -0.0040615;
30  3   0.015674   0.0095765  -0.010059   0.0096607  0.0067473  -0.0063734  0.0067172
0.0050946      -0.0050003;
30  2   0.023828   0.012721   -0.014119   0.013861   0.0074042  -0.009143   0.008272
0.0066278      -0.0071768];

datat=transpose(data)
W = data(:,1);
t = data(:,2);

figure(1)
        scfx0_4 = data(:,3);
        [fscfx0_4,stascfx0_4] = fit( [t, W], scfx0_4, 'poly22' )
        plot(fscfx0_4 , [t, W], scfx0_4)
        xlabel('t')
        ylabel('W')
        zlabel('\sigmax')

figure(2)
        scfy0_4 = data(:,4);
        [fscf0_4,stascfy0_4] = fit( [t, W], scfy0_4, 'poly22' )
        plot(fscfy0_4 , [t, W], scfy0_4)
        xlabel('t')
        ylabel('W')
        zlabel('\sigmay')

figure(3)
        scfxy0_4 = data(:,5);
        [fscfxy0_4,stascfxy0_4] = fit( [t, W], scfxy0_4, 'poly22' )
```

```
plot(fscfxy0_4, [t, W], scfxy0_4)
xlabel('t')
ylabel('W')
zlabel('\tauxy')

figure(4)
scfx0_9 = data(:,6);
[fscfx0_9,stascfx0_9] = fit( [t, W], scfx0_9, 'poly22' )
plot(fsx0_9, [t, W], scfx0_9)
xlabel('t')
ylabel('W')
zlabel('\sigmax')

figure(5)
scfy0_9 = data(:,7);
[fscfy0_9,stascfy0_9]= fit( [t, W], scfy0_9, 'poly22' )
plot(fscfy0_9 , [t, W], scfy0_9)
xlabel('t')
ylabel('W')
zlabel('\sigmay')

figure(6)
scfxy0_9 = data(:,8);
[fscfxy0_9,stascfxy0_9]= fit( [t, W], scfxy0_9, 'poly22' )
plot(fscfxy0_9 , [t, W], scfxy0_9)
xlabel('t')
ylabel('W')
zlabel('\tauxy')

figure(7)
scfx1_4 = data(:,9);
[fscfx1_4,stascfx1_4]= fit( [t, W], scfx1_4, 'poly22' )
```

```
plot(fscfx1_4, [t, W], scfx1_4)
xlabel('t')
ylabel('W')
zlabel('\sigmax')

figure(8)
  scfy1_4 = data(:,10);
    [fscfy1_4,stascfy1_4] = fit( [t, W], scfy1_4, 'poly22' )
    plot(fscfy1_4 , [t, W], scfy1_4)
    xlabel('t')
    ylabel('W')
    zlabel('\sigmay')

figure(9)
  scfxy1_4 = data(:,11);
    [fscfxy1_4,stascfxy1_4]= fit( [t, W], scfxy1_4, 'poly22' )
    plot(fscfxy1_4 , [t, W], scfxy1_4)
    xlabel('t')
    ylabel('W')
    zlabel('\tauxy')
```

Appendix A-4: M-file for load-to-stress factor

This appendix is an example m-to evaluate LTS parametric equations due to tension load at 0.4t, 0.9t and 1.4t away from discontinuity structure.

```
clear;
syms t
syms W
 %format long;

   %%%%% fx %%%%%&
fxt=[
0.07907      0.04531      -0.04579      0.04687      0.02644      -0.03143      0.02677
0.02287      -0.02438   ;
-0.01536   -0.004805      0.006124      -0.007352      -0.002528      0.004027      -
0.003928      -0.002903      0.003131   ;
-0.001459   -0.001143      0.001018      -0.00102      -0.0006706      0.0007603      -
0.0005489      -0.0005396      0.0005839   ;
 0.001232   0.000358      -0.0003935      0.0003958      0.0001264      -0.0002516
0.0002013      0.0001091      -0.0001595   ;
7.609e-005      0.00002479      -0.00003673      0.00006691      0.00002156      -0.00003131
0.00003323      0.00003444      -0.00002943 ;
9.901e-006      0.000009096      -0.000007574      0.000006521      0.000005036      -0.000005605
0.000003372      0.000003355      -0.000004083   ];

fx=transpose(fxt);
para=[1;t;W;t*t;t*W;W*W];
FX=[fx*para];

   %%%%%% SCFfx %%%%%%%
SCFfxt=[
0.0653      0.164      0.3051      0.1274      0.2641      0.1688      0.4051
0.359      0.2067   ;
```

```
-0.00754    -0.1001    -0.1599    -0.06868    -0.1831    -0.1548    -0.1239    -
0.2323    -0.2014    ;
0.004598    0.01147    0.00923    0.00889    0.01818    0.01906    0.002208
0.01489    0.02114    ;
-0.003134    0.006139    0.01395    0.009009    0.02212    0.01582    0.01173
0.04986    0.02604    ;
0.0003293    -0.00005003    0.0006111    -0.0008565    -0.001689    -0.0008652    -
0.0003681    -0.005712    -0.001756  ;
-0.0000354    -0.00002824    -0.00007213    -0.000002028    -0.00002093    -0.00007274
0.00006747    0.0002313    -0.00004703 ];

SCFfx=transpose(SCFfxt);
SCFFX=[SCFfx*para];

  %%%%%%load to factor for fx%%%%%%
LTSFX=[
FX(1,1)*SCFFX(1,1);
FX(2,1)*SCFFX(2,1);
FX(3,1)*SCFFX(3,1);
FX(4,1)*SCFFX(4,1);
FX(5,1)*SCFFX(5,1);
FX(6,1)*SCFFX(6,1);
FX(7,1)*SCFFX(7,1);
FX(8,1)*SCFFX(8,1);
FX(9,1)*SCFFX(9,1)]

%%%%%%%%%%%%%%%%%%%%%%%%%%%%%%%%%%%%%%%%

  %%%%%% fy %%%%%%
fyt=[
0.8851    0.7643    -0.5015    0.6421    0.436    -0.4701    0.5944    0.3692
-0.3196    ;
```

```
-0.08697  -0.07698  0.02776  -0.06756  -0.04291  0.04467  -0.09193  -0.05179
0.02662  ;
-0.02315  -0.02084  0.01453  -0.01614  -0.01115  0.01318  -0.01361  -0.008389
0.008578  ;
0.003008  0.005577  -0.0002896 0.0002526 0.001872  -0.001524 0.003939  0.002607  -
0.0002781 ;
9.88E-04  5.06E-04  -3.62E-04 1.07E-03  4.23E-04  -5.98E-04 1.04E-03  5.12E-04  -
3.94E-04  ;
1.68E-04  1.69E-04  -1.15E-04 1.02E-04  8.16E-05  -9.66E-05 8.30E-05  5.30E-05  -
6.08E-05  ];

fy=transpose(fyt);
para=[1;t;W;t*t;t*W;W*W];
FY=[fy*para];

  %%%%%% SCFfy %%%%%%
SCFfyt=[
1.522      0.5965    2.396     1.887     2.111     0.6108    0.9935    1.732
2.313    ;
-0.4295    -0.3382   -1.326    -0.6184   -0.7698   -1.201    -0.2875   -0.5956
-1.422   ;
0.01133    0.05637   0.06533   0.01161   0.03395   0.1415    0.0268    0.0351
0.08491  ;
0.04144    0.009467  0.1528    0.09834   0.07751   0.2207    0.05872
0.07981    0.1931   ;
-0.0008903  0.00123   -0.002253  -0.006312  -0.001424  -0.02047  -0.006258  -0.00529
-0.008038  ;
-0.000006818  -0.0005002  -0.0004101  0.0002101  -0.0001905 -0.000329  0.00005324
0.00001302 -0.0003935 ];

SCFfy=transpose(SCFfyt);
SCFFY=[SCFfy*para];
```

```
%%%%%%%load to factor for fy%%%%%%
LTSFY=[
FY(1,1)*SCFFY(1,1);
FY(2,1)*SCFFY(2,1);
FY(3,1)*SCFFY(3,1);
FY(4,1)*SCFFY(4,1);
FY(5,1)*SCFFY(5,1);
FY(6,1)*SCFFY(6,1);
FY(7,1)*SCFFY(7,1);
FY(8,1)*SCFFY(8,1);
FY(9,1)*SCFFY(9,1)]

%%%%%%%%%%%%%%%%%%%%%%%%%%%%%%%%%%%%%%%%%%%%

%%%%%% mz %%%%%%

mzt=[
0.001711    0.001249    -0.0009757    0.001273    0.0006612    -0.0008066
0.0008185    0.0006299    -0.0006416 ;
-0.0001823    -0.00009692    0.00006365    -0.0001486    -0.00004839    0.00007005    -
0.0001074    -0.00008595    0.0000606 ;
-0.00004424    -0.00003507    0.000028    -0.00003163    -0.0000168    0.00002267    -
0.00001824    -0.00001407    0.00001715 ;
0.000007837    0.000007434    -0.000001963    0.000002607    0.000001148    -0.00000218
0.00000393    0.000004242    -0.000001463    ;
0.000001947    4.471E-07    -7.156E-07    0.000002152    5.279E-07    -0.000000964
0.000001152    0.000000851    -8.292E-07 ;
3.178E-07    2.943E-07    -2.209E-07    1.985E-07    0.000000121    -1.659E-07
1.127E-07    8.665E-08    -1.211E-07 ];
```

```
mz=transpose(mzt);
para=[1;t;W;t*t;t*W;W*W];
MZ=[mz*para];

   %%%%%% SCFfy %%%%%%%
SCFmzt=[
1.224     1.569     2.79      1.593     4.311     2.109     2.562     3.281
 2.532     ;
-0.5217   -0.6354   -1.359    -0.6714   -1.149    -1.378    -0.6482   -0.7168
-1.408    ;
0.03233   0.0432    0.05946   0.03016   -0.02355  0.1008    -0.00613  -0.01296
 0.08681  ;
0.06319   0.03047   0.1555    0.1199    0.1094    0.2473    0.07139   0.08595
0.1976    ;
-0.002852 0.003632  -0.00342  -0.009321 -0.00001829 -0.02384  -0.001026 -0.005383
-0.01135  ;
-0.00009079 -0.0003961 -0.0002169 0.000196  0.0004071  0.0003461  0.0002077
0.0005795  -0.0002073 ];

SCFmz=transpose(SCFmzt);
SCFMZ=[SCFmz*para];

   %%%%%%%load to factor for mz%%%%%%%

LTSMZ=[
MZ(1,1)*SCFMZ(1,1);
MZ(2,1)*SCFMZ(2,1);
MZ(3,1)*SCFMZ(3,1);
MZ(4,1)*SCFMZ(4,1);
MZ(5,1)*SCFMZ(5,1);
MZ(6,1)*SCFMZ(6,1);
MZ(7,1)*SCFMZ(7,1);
```

```
MZ(8,1)*SCFMZ(8,1);
MZ(9,1)*SCFMZ(9,1)]

%%%%%%%%%%%%%%%%%%%%%%%%%%%%%%%%%%%%%%%%%%%%

  %%%%%% load to factor matrix %%%%%%
LTSmatrix=[LTSFX LTSFY LTSMZ]

  %%%%%%%%%%%%%%%%%%%%%%%%%%%%%%%%%%%%%%%%%%%%
```

APPENDIX B

SURFACE FITTING

Appendix B-1: σ_x, σ_y, and τ_{xy} of selected parametric model due to 1 unit tension load

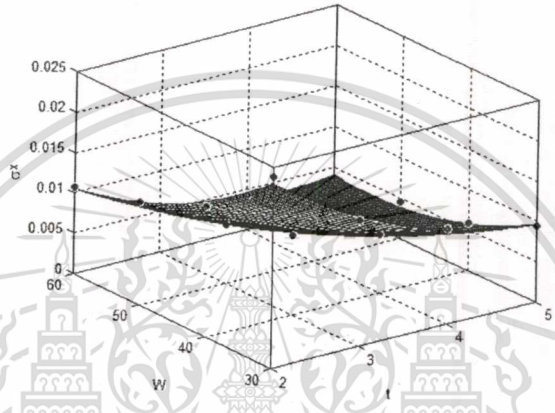

Figure B-1.1 σ_x of selected parametric model due to tension load at 0.4t

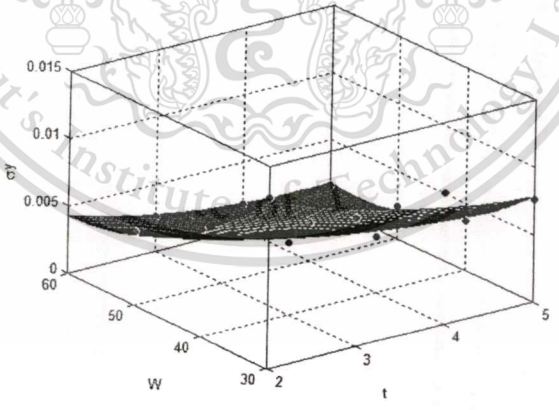

Figure B-1.2 σ_y of selected parametric model due to tension load at 0.4t

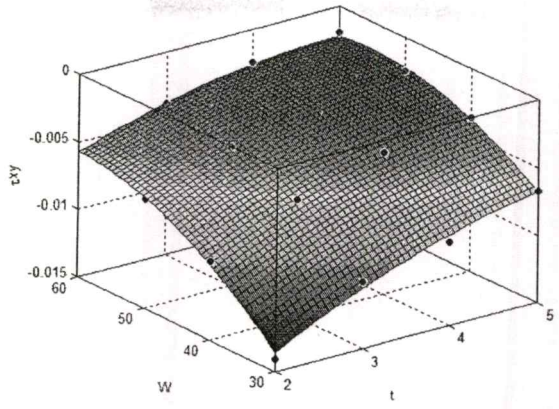

Figure B-1.3 τ_{xy} of selected parametric model due to tension load at 0.4t

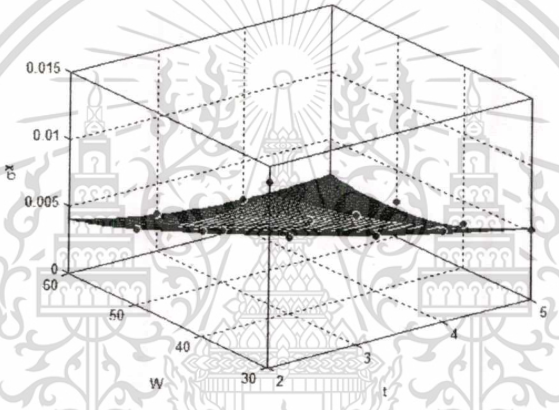

Figure B-1.4 σ_x of selected parametric model due to tension load at 0.9t

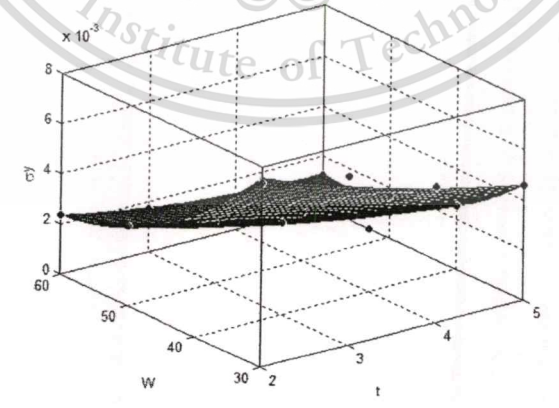

Figure B-1.5 σ_y of selected parametric model due to tension load at 0.9t

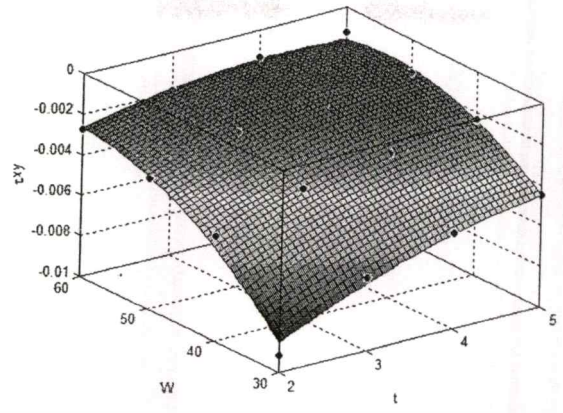

Figure B-1.6 τ_{xy} of selected parametric model due to tension load at 0.9t

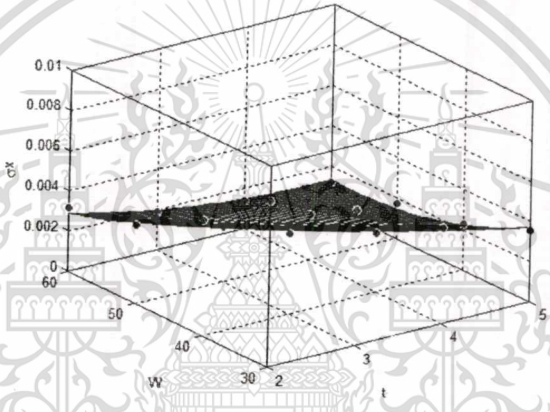

Figure B-1.7 σ_x of selected parametric model due to tension load at 1.4t

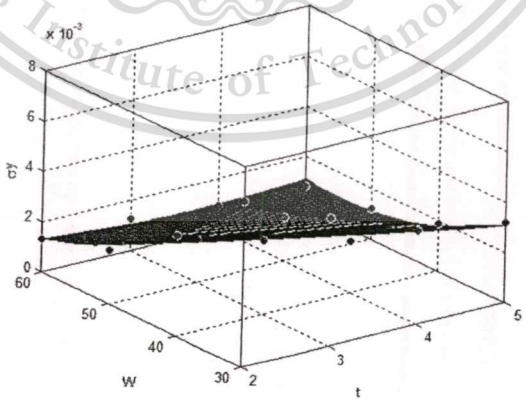

Figure B-1.8 σ_y of selected parametric model due to tension load at 1.4t

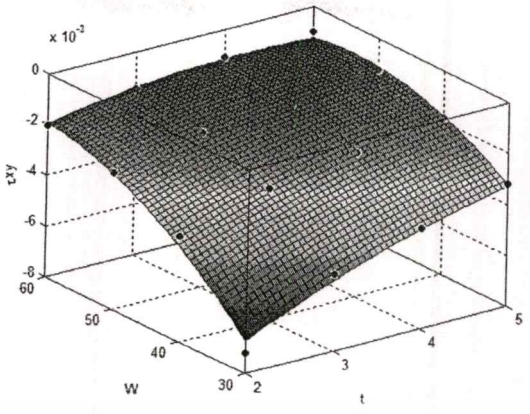

Figure B-1.9 τ_{xy} of selected parametric model due to tension load at 1.4t

Appendix B-2: σ_x, σ_y, and τ_{xy} of selected parametric model due to 1 unit bending load

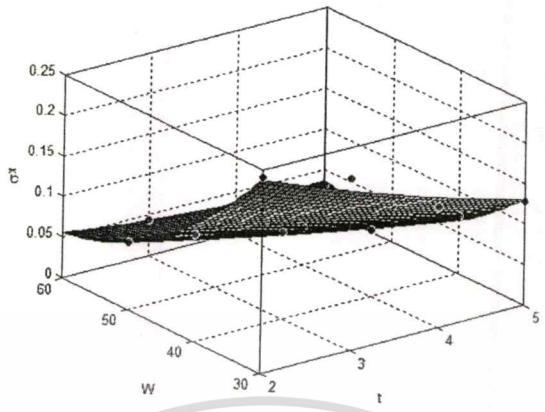

Figure B-2.1 σ_x of selected parametric model due to bending load at 0.4t

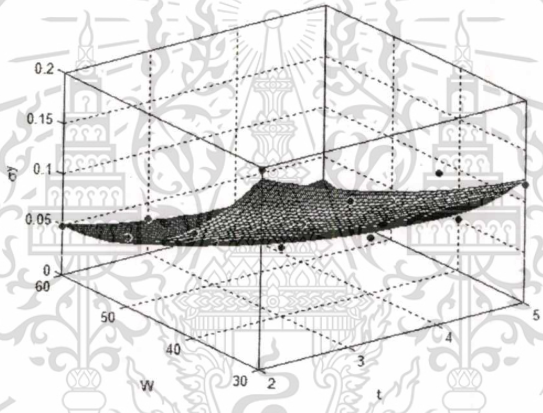

Figure B-2.2 σ_y of selected parametric model due to bending load at 0.4t

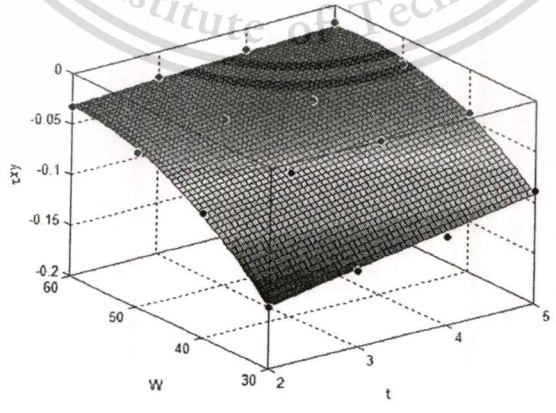

Figure B-2.3 τ_{xy} of selected parametric model due to bending load at 0.4t

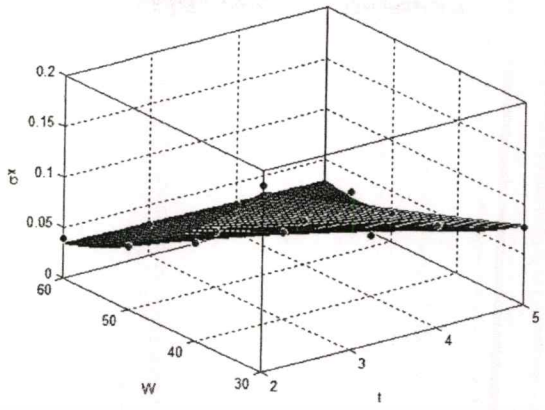

Figure B-2.4 σ_x of selected parametric model due to bending load at 0.9t

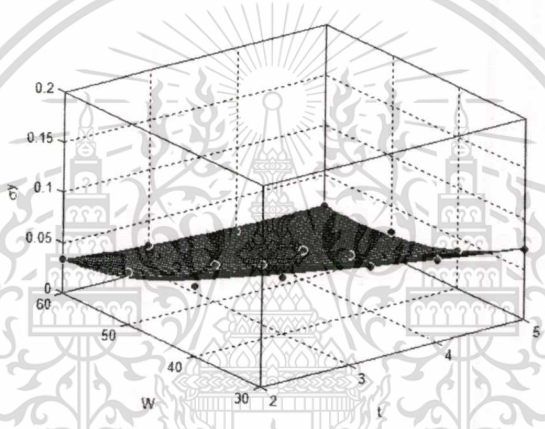

Figure B-2.5 σ_y of selected parametric model due to bending load at 0.9t

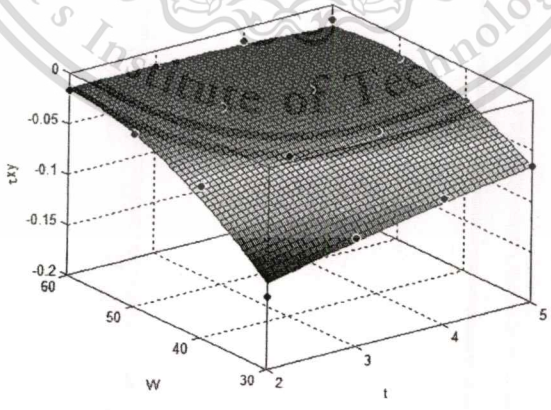

Figure B-2.6 τ_{xy} of selected parametric model due to bending load at 0.9t

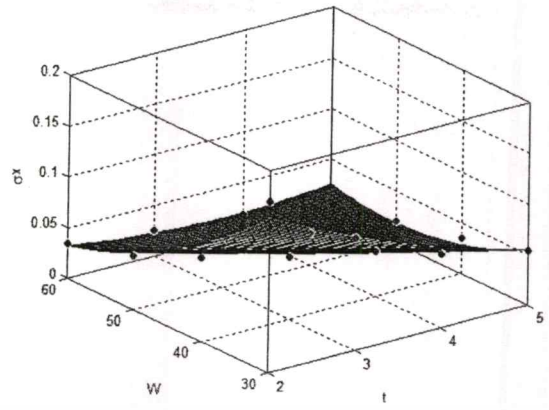

Figure B-2.7 σ_x of selected parametric model due to bending load at 1.4t

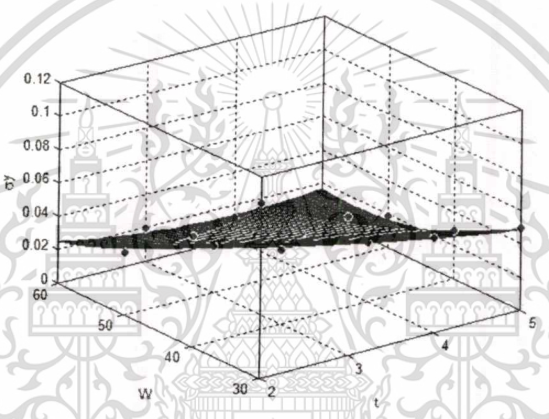

Figure B-2.8 σ_y of selected parametric model due to bending load at 1.4t

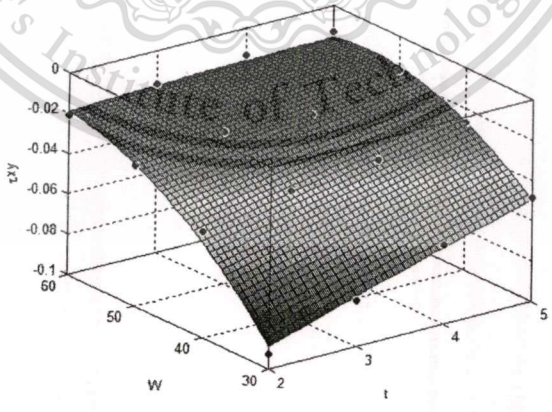

Figure B-2.9 τ_{xy} of selected parametric model due to bending load at 1.4t

Appendix B-3: σ_x, σ_y, and τ_{xy} of selected parametric model due to 1 unit moment load

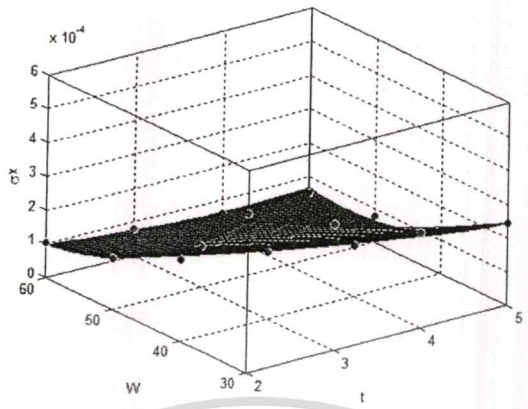

Figure B-3.1 σ_x of selected parametric model due to moment load at 0.4t

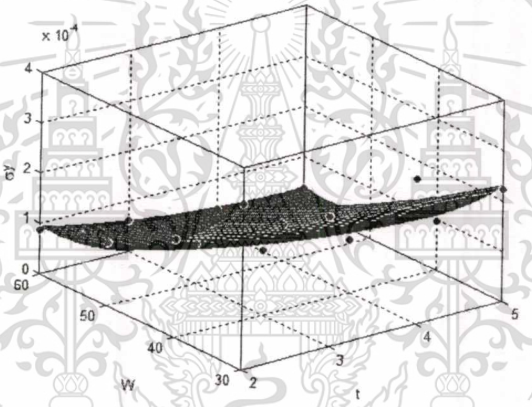

Figure B-3.2 σ_y of selected parametric model due to moment load at 0.4t

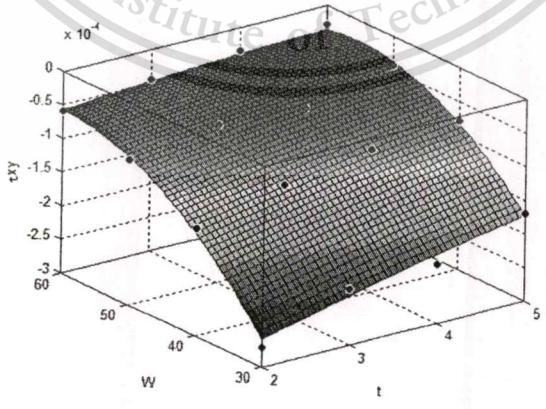

Figure B-3.3 τ_{xy} of selected parametric model due to moment load at 0.4t

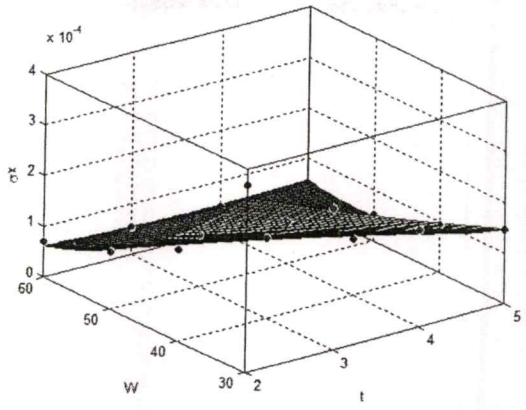

Figure B-3.4 σ_x of selected parametric model due to moment load at 0.9t

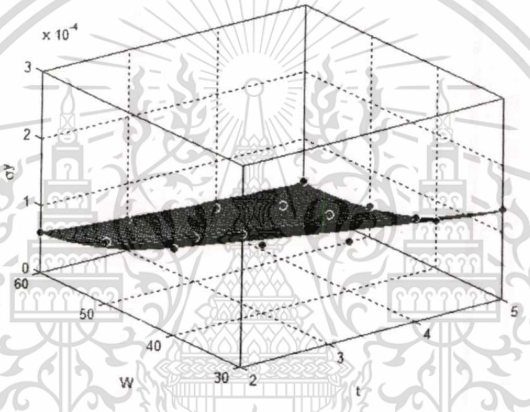

Figure B-3.5 σ_y of selected parametric model due to moment load at 0.9t

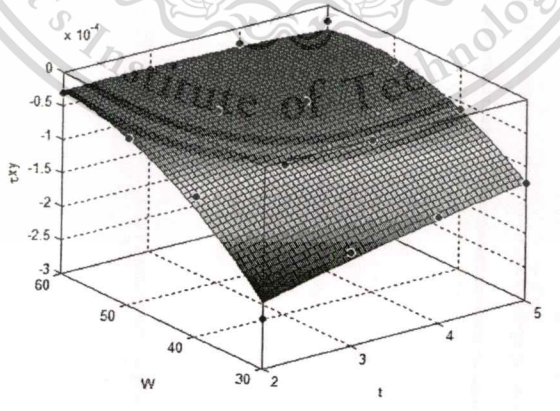

Figure B-3.6 τ_{xy} of s selected parametric model due to moment load at 0.9t

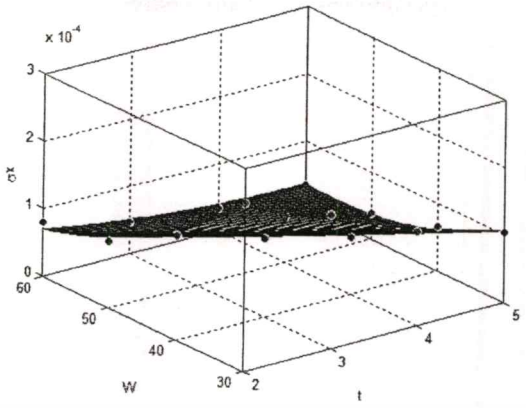

Figure B-3.7 σ_x of selected parametric model due to moment load at 1.4t

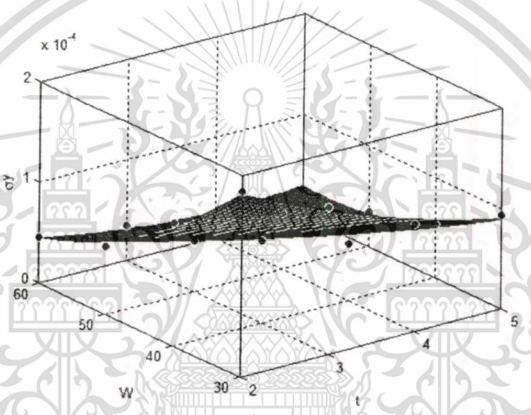

Figure B-3.8 σ_y of selected parametric model due to moment load at 1.4t

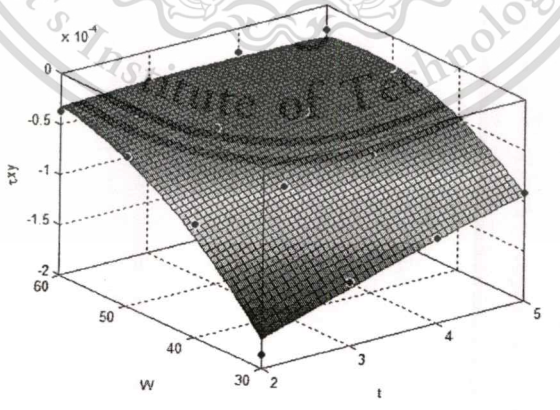

Figure B-3.9 τ_{xy} of selected parametric model due to moment load at 1.4t

Appendix B-4: Stress correction factors of selected parametric model due to unit tension load

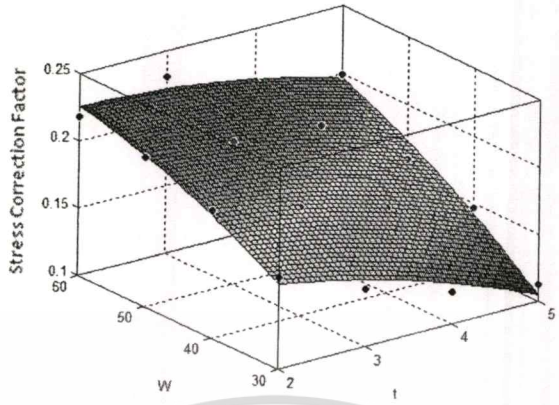

Figure B-4.1 Stress correction factor in x direction due to tension load at 0.4t

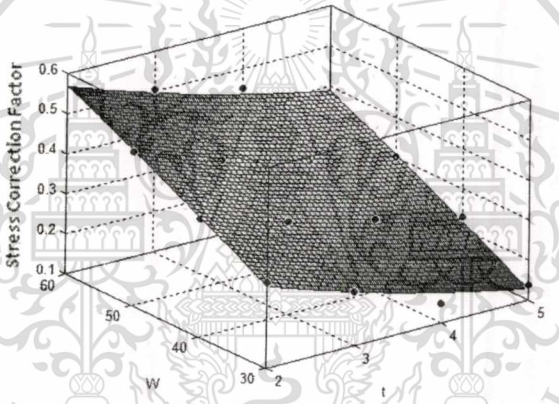

Figure B-4.2 Stress correction factor in y direction due to tension load at 0.4t

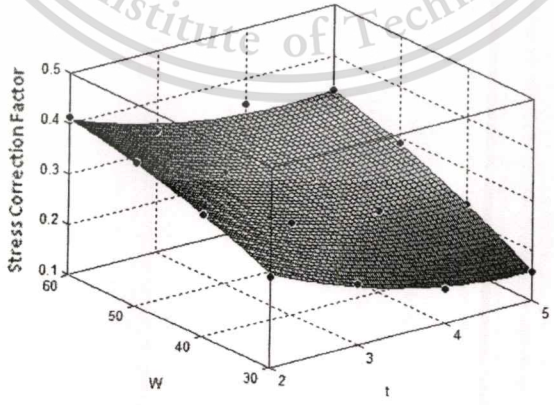

Figure B-4.3 Stress correction factor in xy plane due to tension load at 0.4t

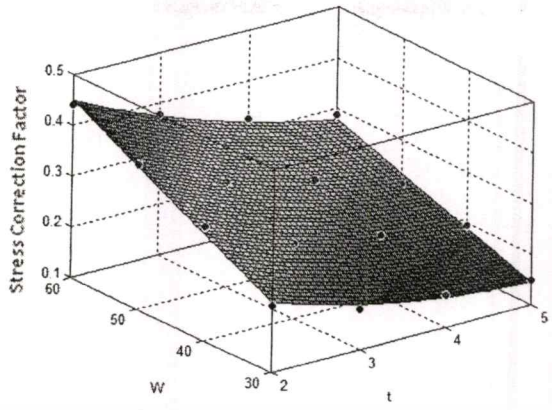

Figure B-4.4 Stress correction factor in x direction due to tension load at 0.9t

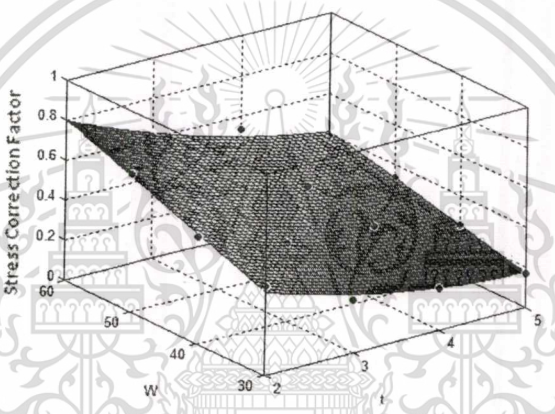

Figure B-4.5 Stress correction factor in y direction due to tension load at 0.9t

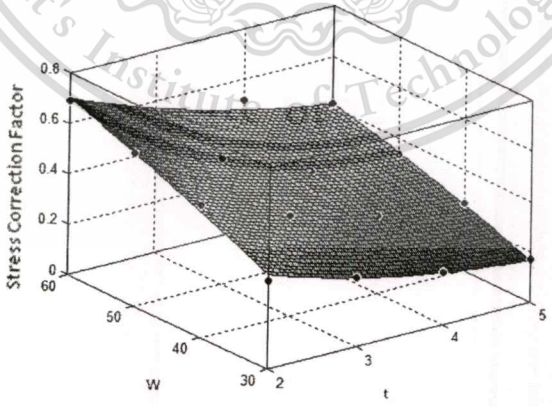

Figure B-4.6 Stress correction factor in xy plane due to tension load at 0.9t

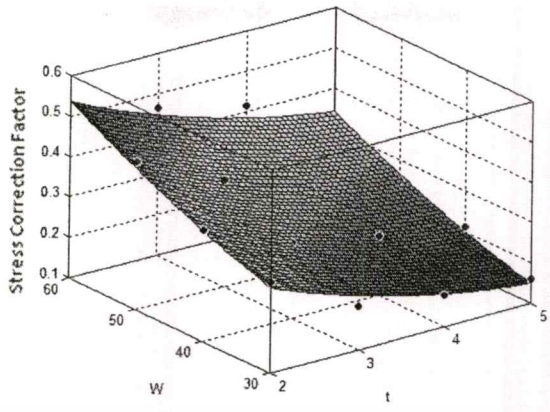

Figure B-4.7 Stress correction factor in x direction due to tension load at 1.4t

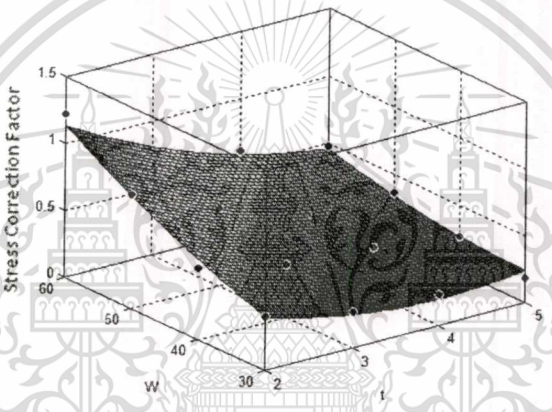

Figure B-4.8 Stress correction factor in y direction due to tension load at 1.4t

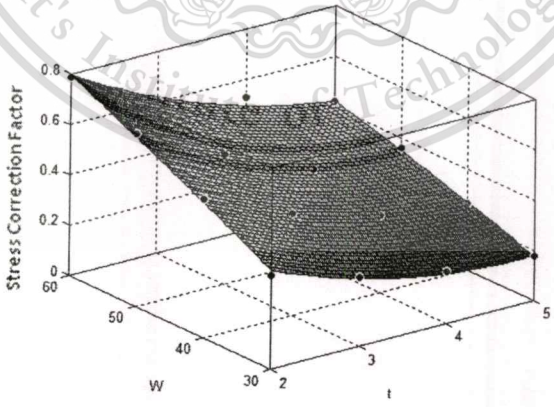

Figure B-4.9 Stress correction factor in xy plane due to tension load at 1.4t

Appendix B-5: Stress correction factors of selected parametric model due to 1 unit bending load

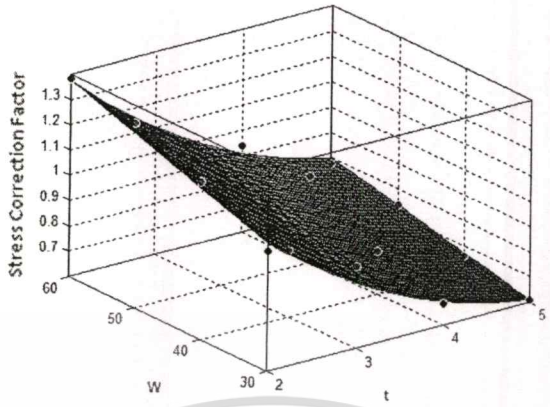

Figure B-5.1 Stress correction factor in x direction due to bending load at 0.4t

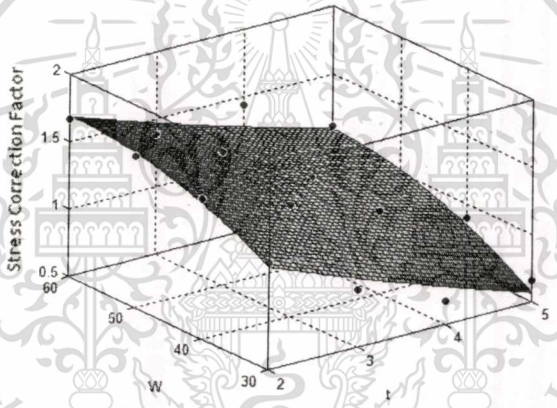

Figure B-5.2 Stress correction factor in y direction due to bending load at 0.4t

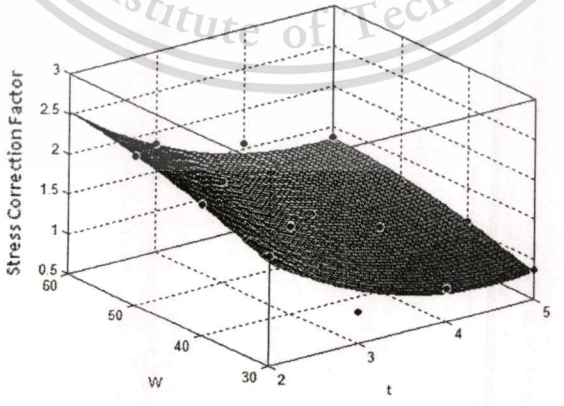

Figure B-5.3 Stress correction factor in xy plane due to bending load at 0.4t

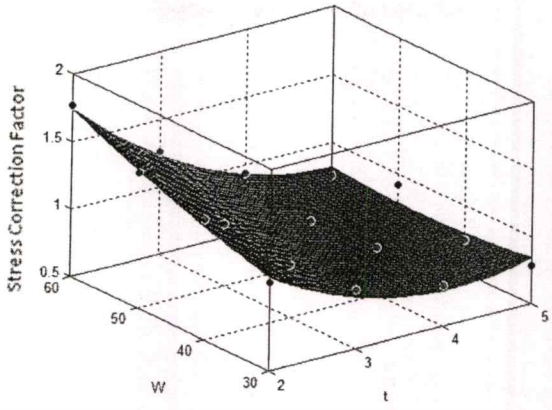

Figure B-5.4 Stress correction factor in x direction due to bending load at 0.9t

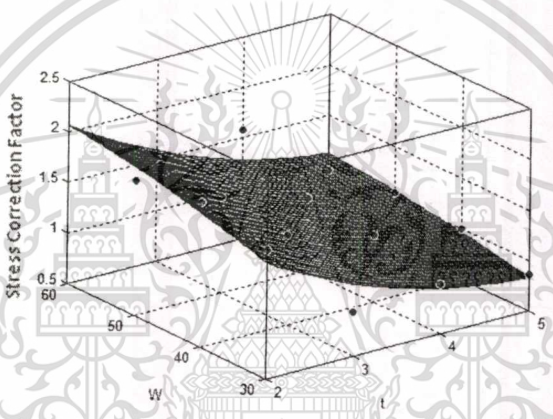

Figure B-5.5 Stress correction factor in y direction due to bending load at 0.9t

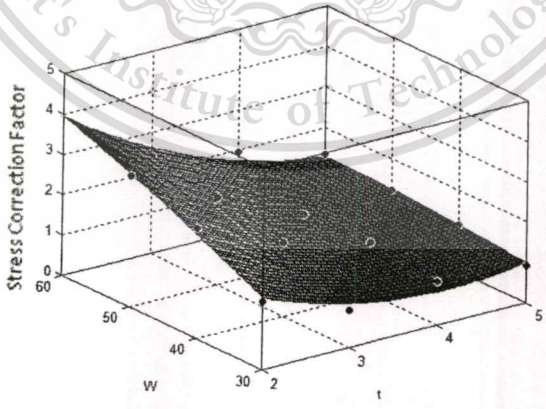

Figure B-5.6 Stress correction factor in xy plane due to bending load at 0.9t

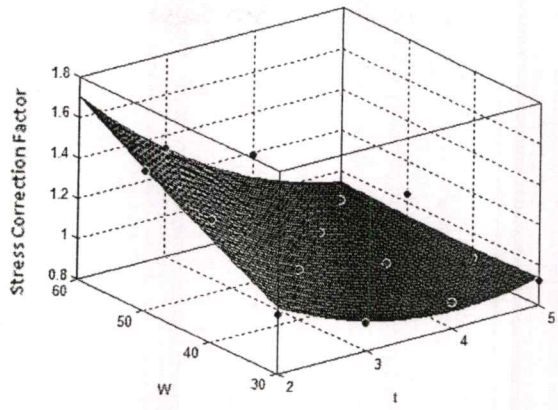

Figure B-5.7 Stress correction factor in x direction due to bending load at 1.4t

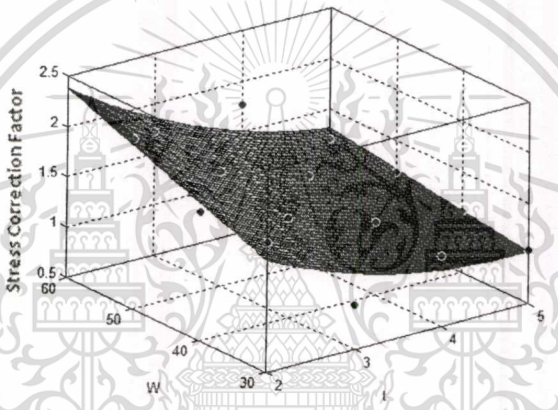

Figure B-5.8 Stress correction factor in y direction due to bending load at 1.4t

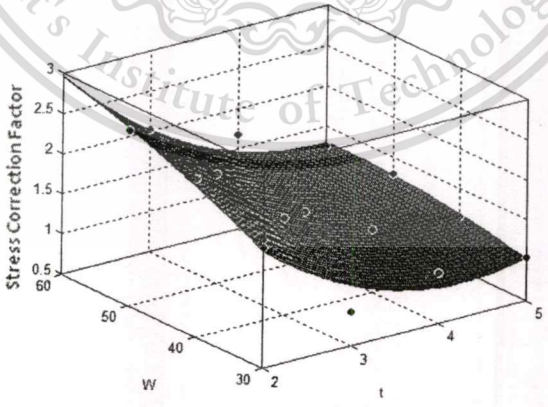

Figure B-5.9 Stress correction factor in xy plane due to bending load at 1.4t

Appendix B-6: Stress correction factors of selected parametric model due to 1 unit moment load

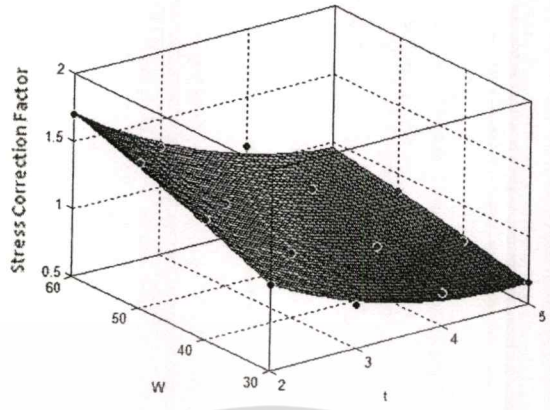

Figure B-6.1 Stress correction factor in x direction due to moment load at 0.4t

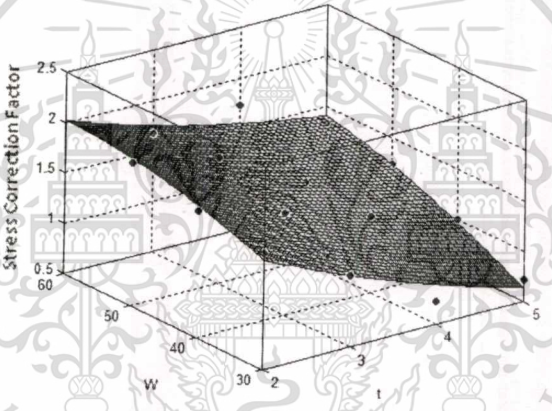

Figure B-6.2 Stress correction factor in y direction due to moment load at 0.4t

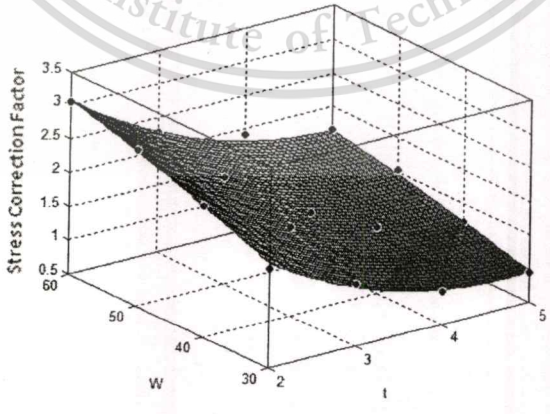

Figure B-6.3 Stress correction factor in xy plane due to moment load at 0.4t

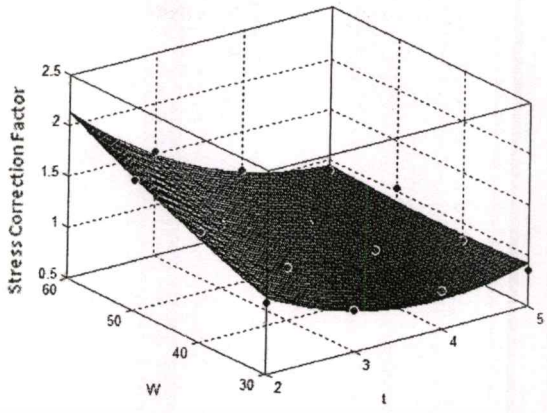

Figure B-6.4 Stress correction factor in x direction due to moment load at 0.9t

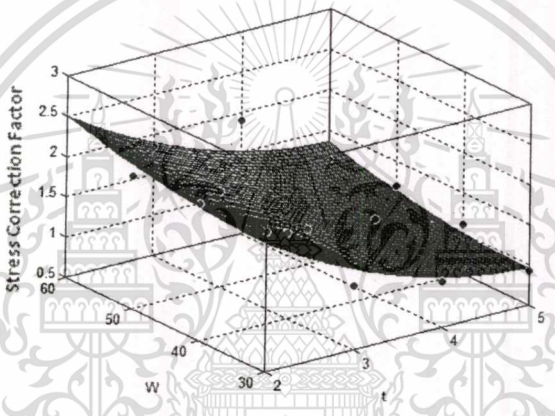

Figure B-6.5 Stress correction factor in y direction due to moment load at 0.9t

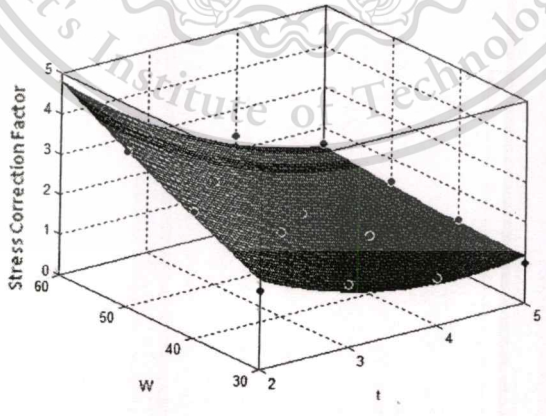

Figure B-6.6 Stress correction factor in xy plane due to moment load at 0.9t

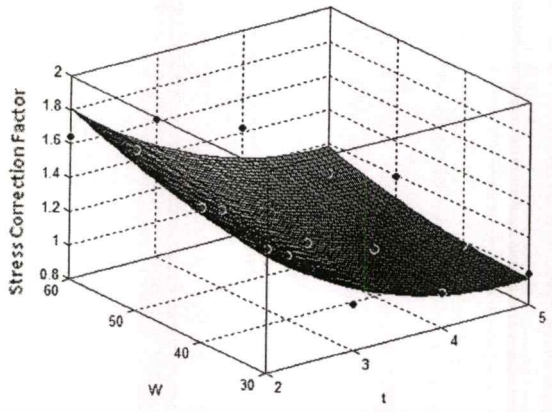

Figure B-6.7 Stress correction factor in x direction due to moment load at 1.4t

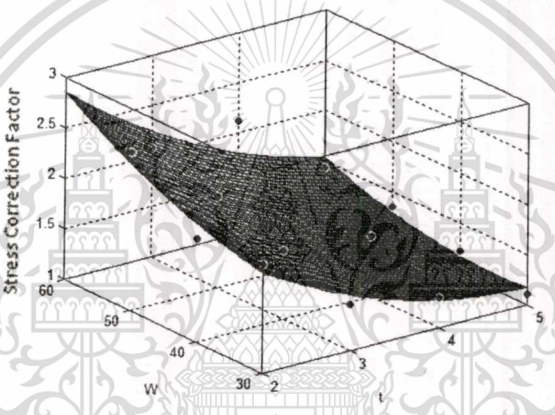

Figure B-6.8 Stress correction factor in y direction due to moment load at 1.4t

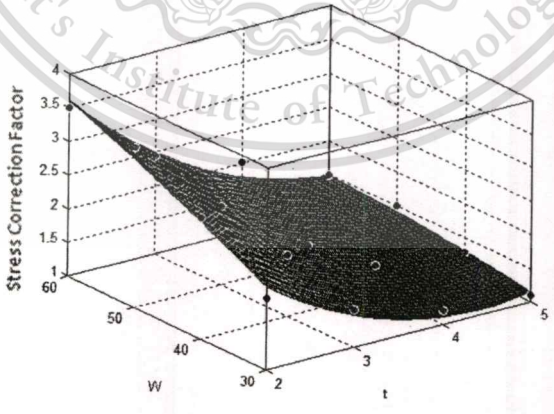

Figure B-6.9 Stress correction factor in xy plane due to moment load at 1.4t

BIOGRAPHY

Name: Mr. Thanakorn Vichiensamuth

Date of Birth: July 31, 1987

Place of Birth: Bangkok, Thailand

Education:

2005-2008 B. Eng. in Mechanical Engineering, Department of Mechanical Engineering, King Mongkut's Institute of Technology Ladkrabang (KMITL)

2009-2013 M. Eng. in Automotive Engineering (International program), International College, King Mongkut's Institute of Technology Ladkrabang (KMITL)

Honour and Scholarship:

2009-2013 Full scholarship for study in the master degree from National Science and Technology Development Agency (NSTDA)

Publications:

1. T. Vichiensamuth, M. Pimsarn, K. Takahashi, T. Tantanawat "A Simplified model of a Reinforced Square Hollow Section (SHS) T-Joint for Stress Evaluation in Bus Superstructure" **2013 International Conference on Manufacturing, Optimization, Industrial and Material Engineering** , Bandung, Indonesia, March 9-10, 2013.